

1 Scenario set-up and the new CMIP6-based climate-related forcings provided within the
2 third round of the Inter-Sectoral Model Intercomparison Project (ISIMIP3b, group I and II)

3
4 Katja Frieler^{1,2}, Stefan Lange¹, Jacob Schewe¹, Matthias Mengel¹, Simon Treu^{1,2}, Christian Otto¹, Jan
5 Volkholz¹, Christopher P.O. Reyer¹, Stefanie Heinicke¹, Colin Jones³, Julia L. Blanchard⁴, Cheryl S. Harrison⁵,
6 Colleen M. Petrik⁶, Tyler D. Eddy⁷, Kelly Ortega-Cisneros⁸, Camilla Novaglio⁴, Ryan Heneghan⁹, Derek P.
7 Tittensor¹⁰, Olivier Maury¹¹, Matthias Büchner¹, Thomas Vogt¹, Dánnell Quesada-Chacón¹, Kerry
8 Emanuel¹², Chia-Ying Lee¹³, Suzana J. Camargo^{13,14}, Linn Hamester¹, Jonas Jägermeyr^{14,15,1}, Sam Rabin^{16,a,b},
9 Jochen Klar¹, Iliusi D. Vega del Valle¹, Lisa Novak¹, Inga J. Sauer¹, Gitta Lasslop¹⁷, Sarah Chadburn¹⁸, Eleanor
10 Burke¹⁹, Angela Gallego-Sala²⁰, Noah Smith²¹, Jinfeng Chang²², Stijn Hantson²³, Chantelle Burton¹⁹, Anne
11 Gädeke¹, Fang Li²⁴, Simon N Gosling²⁵, Hannes Müller Schmied^{17,26}, Fred Hattermann¹, Thomas Hickler¹⁷,
12 Rafael Marcé²⁷, Don Pierson²⁸, Wim Thiery²⁹, Daniel Mercado-Bettín²⁷, Robert Ladwig³⁰, Ana I. Ayala²⁸,
13 Matthew Forrest¹⁷, Michel Bechtold³¹, Robert Reinecke³², Inge de Graaf³³, Jed O. Kaplan³⁴, Alexander
14 Koch³⁵, Matthieu Lengaigne¹¹, Rohini Kumar³⁶, Maryna Stokal³⁷

15
16
17 Affiliations:

18 ¹Potsdam Institute for Climate Impact Research, 14473 Potsdam, Germany

19 ²University of Potsdam, Institute for Environmental Science and Geography, 14476 Potsdam, Germany

20 ³National Centre for Atmospheric Science and School of Earth and Environment, University of Leeds,
21 Leeds, LS29JT, UK

22 ⁴Institute for Marine and Antarctic Studies, University of Tasmania, Hobart, Tasmania, Australia

23 ⁵Department of Ocean and Coastal Science and Center for Computation and Technology, Louisiana State
24 University, Baton Rouge, Louisiana, USA

25 ⁶Scripps Institution of Oceanography, University of California San Diego, CA, USA

26 ⁷Centre for Fisheries Ecosystems Research, Fisheries & Marine Institute, Memorial University, St. John's,
27 NL, Canada

28 ⁸Marine and Antarctic Research for Innovation and Sustainability, Department of Biological Sciences,
29 University of Cape Town, Rondebosch, Cape Town, 7701, South Africa

30 ⁹School of Environment and Science, Griffith University, Brisbane, Queensland, Australia

31 ¹⁰Department of Biology, Dalhousie University, Halifax, Nova Scotia, Canada, B3H 4R2

32 ¹¹IRD, Univ Montpellier, CNRS, Ifremer, INRAE, MARBEC, Sète, France

33 ¹²Lorenz Center, Massachusetts Institute of Technology, Cambridge, MA, USA

34 ¹³Lamont-Doherty Earth Observatory, Columbia University, Palisades, New York, USA

35 ¹⁴Columbia Climate School, Columbia University, New York, NY 10025, USA

36 ¹⁵NASA Goddard Institute for Space Studies, New York, NY 10025, USA

37 ¹⁶Climate and Global Dynamics Laboratory, National Center for Atmospheric Research Boulder, CO 80302,
38 USA

39 ¹⁷Senckenberg Leibniz Biodiversity and Climate Research Centre (SBIK-F), Frankfurt am Main, Germany.

40 ¹⁸Department of Mathematics, University of Exeter, Exeter UK

41 ¹⁹Met Office Hadley Centre, Fitzroy Road, Exeter, UK

- 42 ²⁰Geography Department, University of Exeter, Exeter, UK
- 43 ²¹College of Engineering, Mathematics and Physical Sciences, University of Exeter, Exeter EX4 4QF, UK.
- 44 ²²College of Environmental and Resource Sciences, Zhejiang University, Hangzhou, China
- 45 ²³Faculty of Natural Sciences, Universidad del Rosario, Bogotá, Colombia
- 46 ²⁴International Center for Climate and Environment Sciences, Institute of Atmospheric Physics, Chinese
47 Academy of Sciences, Beijing, China
- 48 ²⁵School of Geography, University of Nottingham, Nottingham, UK
- 49 ²⁶Institute of Physical Geography, Goethe University Frankfurt, Frankfurt am Main, Germany
- 50 ²⁷Blanes Centre for Advanced Studies (CEAB-CSIC), Blanes, Spain
- 51 ²⁸Department of Ecology and Genetics, Uppsala University, Norbyvägen 18 D, 752 36 Uppsala, Sweden
- 52 ²⁹Vrije Universiteit Brussel, Department of Water and Climate, Brussels, Belgium
- 53 ³⁰Department of Ecoscience, Aarhus University, C.F. Møllers Allé 3, 8000 Aarhus C, Denmark
- 54 ³¹KU Leuven, Department of Earth and Environmental Sciences, Leuven, Belgium
- 55 ³²Johannes Gutenberg-University Mainz, Mainz, Germany
- 56 ³³Earth Systems and Global Change Group, Wageningen University and Research, Wageningen, The
57 Netherlands
- 58 ³⁴Department of Earth Sciences and Institute for Climate and Carbon Neutrality, The University of Hong
59 Kong, Hong Kong
- 60 ³⁵Simon Fraser University, Burnaby, British Columbia, CA
- 61 ³⁶Department of Computational Hydrosystems, Helmholtz Centre for Environmental Research—UFZ,
62 Leipzig 04318, Germany
- 63 ³⁷Wageningen University & Research, Wageningen, Netherlands
- 64 ^aformerly at: Institute of Meteorology and Climate Research / Atmospheric Environmental Research,
65 Karlsruhe Institute of Technology, Garmisch-Partenkirchen, Germany
- 66 ^bformerly at: Department of Environmental Sciences, Rutgers University, New Brunswick, New Jersey, USA
- 67
- 68 *Correspondence to:* Katja Frieler (katja.frieler@pik-potsdam.de)
- 69

70 **Abstract.** This paper describes the climate-related forcings (CRFs) provided within the ‘b’ part of the third
71 simulation round of the Inter-Sectoral Impact Model Intercomparison Project (ISIMIP3b). While ISIMIP3a
72 comprises historical impact models simulations forced by observational CRF and direct human forcings
73 (DHF), the ISIMIP3b CRFs are based on climate model simulations generated within the sixth phase of the
74 Coupled Model Intercomparison Project (CMIP6). In a first set of experiments (ISIMIP3b, group I) the
75 CMIP6-based CRFs for the historical period are combined with historical observation-based DHF also
76 considered in ISIMIP3a (e.g. land use patterns, water and agricultural management, and fishing efforts).
77 These group I simulations allow for the quantification of impacts of historical climate change by
78 comparison to simulations where the observational DHF are combined with simulated pre-industrial CRFs.
79 In addition, the impacts of observed changes in CRFs can be compared to the impacts of simulated
80 changes in CRFs by comparing the ISIMIP3a simulations to the ISIMIP3b, group I simulations. The second
81 group of experiments (ISIMIP3b, group II) comprises future projections assuming constant observational
82 direct human forcings at 2015 levels to estimate the impact of climate change given today’s direct human

83 influences for the low emission scenario SSP1-2.6, the high and the very high emission scenarios SSP3-7.0,
84 SSP5-8.5, respectively. The very high emissions scenarios and the assumption of fixed present day direct
85 human forcings particularly allow for testing the scalability of impacts in terms of global temperature
86 change. The provided CRFs comprise atmospheric CO₂ and CH₄ concentrations, atmospheric and oceanic
87 climate data, coastal water levels, tropical cyclone tracks and their associated wind speed and
88 precipitation fields. In addition to the CRFs data, this paper describes the experiments belonging to group
89 I and II and the rationale behind them. Another set of future projections accounting for changing DHFs
90 (ISIMIP3b, group III) is in preparation and will be described in another paper.

91
92

93 **Introduction**

94 This is the second paper of a series of three papers describing the experiments of the third simulation
95 round of the Inter-Sectoral Impact Model Intercomparison Project ISIMIP (isimip.org). The project
96 provides a common scenario framework for cross-sectorally consistent climate impact simulations.
97 Currently, operational simulation protocols exist for the following sectors: Agriculture, Biomes, Energy,
98 Fire, Food security and nutrition, Groundwater, Labour, Lakes global, Lakes regional, Fisheries and marine
99 ecosystems global, Fisheries and marine ecosystems local, Peatland, Permafrost, Water global, Water
100 regional. Additional protocols for Coastal systems, Regional forests, Temperature-related mortality,
101 health indicators, Terrestrial biodiversity and Water quality sectors are under development. In its third
102 round it covers i) model evaluation and climate impact attribution experiments based on observation-
103 based climate and direct human forcings (DHF) (ISIMIP3a, first paper, (Frieler et al., 2023)), ii) climate
104 impact simulations driven by simulated climate-related forcings (CRF) based the sixth phase of the
105 Coupled Climate Model Intercomparison Project (CMIP6) assuming ISIMIP3a observational DHF in the
106 historical period and fixed 2015 DHF for the future simulations (ISIMIP3b, group I+II, this paper), and iii)
107 an upcoming set of CMIP6-based future projections where DHF vary according to given Shared
108 Socioeconomic Pathways (SSPs) (no adaptation scenarios) and in response to climate change impacts
109 (adaptation scenarios) (ISIMIP3b, group III). So while this paper only describes the ISIMIP3b CRF, the third
110 paper will only address the DHFs that are still under development while the CRF of the group III simulations
111 will be identical to the future CRF described here.

112

113 Similar to the Coupled Model Intercomparison Project (CMIP) (Eyring et al., 2016) all simulations will be
114 freely available (<https://data.isimip.org/>) to allow for follow-up analysis. The consistent design of the
115 simulations does not only allow for the comparison of climate impact simulations within each sector, but
116 also enables the bottom-up integration of impacts across sectors. Thus, it provides a unique basis for the
117 estimation of the effects of climate change on, e.g., the economy, displacement and migration, health, or
118 water quality resolving the mechanisms along different impact channels and fully exploiting the process-
119 understanding represented in the biophysical impact models.

120

121 Compared to ISIMIP2b, the ISIMIP3b CRF represent the following updates: i) climate forcing data based
122 on phase 6 of the Coupled Model Intercomparison Project (CMIP6) (Eyring et al., 2016) and post-processed
123 by an improved bias adjustment and statistical downscaling method (see section 3.2), and ii) large

124 ensembles of potential realisations of tropical cyclone tracks, wind and precipitation fields derived from
125 two different modelling approaches assuming CMIP6 boundary conditions, while in ISIMIP2b only one
126 approach was used and precipitation fields were not included. In addition, we plan to provide coastal
127 water levels at high temporal resolution (upcoming). The approach to generate the data is also described
128 here.

129
130 The development of the ISIMIP3b protocol was coordinated by the ISIMIP-Cross-Sectoral Science Team
131 (CSST) at the Potsdam Institute for Climate Impact Research (PIK) along the same decision process as for
132 ISIMIP3a (Frieler et al., 2024a).

133
134 This paper is accompanied by a simulation protocol (*ISIMIP3b Simulation Protocol*, 2023) providing all
135 technical details such as file and variable naming conventions, as well as sector-specific output variables
136 to be reported by the participating modelling teams. This paper refers to the protocol version of December
137 21st, 2023. However, as the protocol may still be updated due to addition of new variables, correction of
138 errors, or the inclusion of new sectors, contributors to ISIMIP should always refer to protocol.isimip.org
139 for the most up to date reference for planned impact model simulations.

140
141 The ISMIP3a and ISIMIP3b protocols have been jointly developed and participation in ISIMIP3 requires
142 contribution to both ISIMIP3a and ISIMIP3b, using the same impact model versions in order to allow for
143 the evaluation of the impact models future projections in ISIMIP3b.

144
145 In the following, we describe the rationale behind the individual scenario set-ups (section 1). We then
146 introduce the individual climate-related forcing data sets in the second section covering atmospheric
147 climate data including lightning and tropical cyclones tracks, wind and precipitation fields; ocean data;
148 coastal water levels; and atmospheric CO₂ as well as CH₄ concentrations.

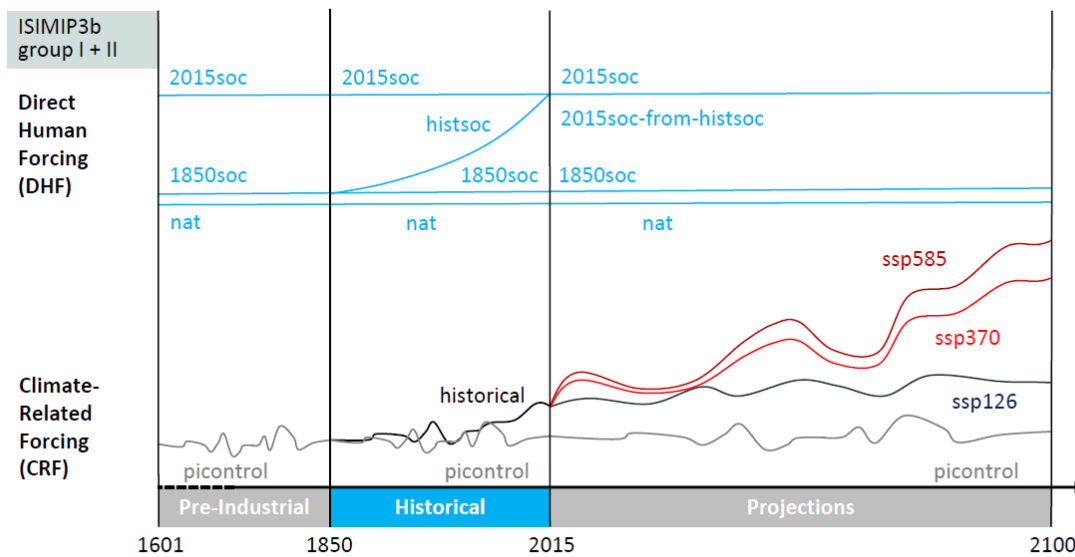
150 **1 Experiments and underlying rationale**

151
152 The selection of the scenarios is a community-driven process constrained by the availability of climate
153 model simulations (multi-GCM ensemble per scenario) and socio-economic background information (such
154 as land use patterns, populations and GDP data etc. additionally required as ‘Direct Human Forcing’ for
155 the ISIMIP3b, group III impact model simulations that will be introduced in an upcoming paper). These
156 criteria have made CMIP6-ScenarioMIP the reference point for the selection (O’Neill et al., 2016). The
157 selection of ISIMIP3b scenarios (see **Figure 1**) from the four ScenarioMIP Tier 1 scenarios was additionally
158 driven by the aim to capture a wide range of possible futures from low to high emission scenarios and to
159 provide of a long baseline simulation assuming pre-industrial climate conditions that allows for a robust
160 estimation of reference return levels of extreme events. This is why the original selection comprised the
161 pre-industrial baseline (‘picontrol’), the historical simulations (‘historical’), SSP1-2.6 representing the ‘low
162 end of the range of future forcing pathways in the IAM literature’ (O’Neill et al., 2016), and SSP5-8.5
163 representing the ‘high end of the range of future pathways in the IAM literature’ (O’Neill et al., 2016).
164 Given recent mitigation efforts, some estimates of recoverable coal reserves, and decreasing prices for

165 renewable energies the emissions underlying SSP5-8.5 have been criticised for being unplausibly high
166 (Hausfather & Peters, 2020). Based on these discussions, the ‘medium to high end of the range of future
167 forcing pathway’ SSP3-7.0 (O’Neill et al., 2016) has been added to the ISIMIP3b scenario set-up. While this
168 scenario is described as ‘average no climate protection policy’ by (Hausfather & Peters, 2020), we highlight
169 that we explicitly not describe it as a ‘business as usual scenario’ and that this was not the framing within
170 ScenarioMIP either. Instead SSP3-7.0 is based on rather extreme assumptions about land use changes and
171 aerosol emissions e.g. leading to a scaling of precipitation with global mean temperature that diverges
172 from the scaling identified in the other scenarios (Shiogama et al., 2023). In addition, SSP5-8.5 is explicitly
173 kept in the ISIMIP3b ensemble as its particularly strong warming signal allows testing to what degree the
174 simulated impacts of climate may scale with global mean temperature, which could allow for a translation
175 of impacts to other emission scenarios. In addition, even under lower emission scenarios, global warming
176 levels as the ones reached under SSP5-8.5 in 2100 will eventually be reached later in time as long as
177 emissions are not reduced to zero. These impacts of high warming levels would not be captured when
178 only considering lower emission scenarios ending in 2100.

179
180 All ISIMIP experiments are determined by the underlying set of CRFs and DHF, where each package of CRF
181 and DHF has a specific label that will then be included in the output file names to allow for an identification
182 of the experiments they belong to. The individual experiments are defined by the combination of both
183 types of forcing data sets, where the associated specifiers are indicated in brackets in the subheadings
184 naming the experiments (CRF specifier + DHF specifier). The different combinations of the default sets of
185 ISIMIP3b CRFs (‘picontrol’, ‘historical’, ‘ssp126’, ‘ssp370’, and ‘ssp585’) and DHF (‘histsoc’, ‘2015soc’,
186 ‘1901soc’, ‘1850soc’, ‘nat’, and ‘2015soc-from-histsoc’) are sketched in **Figure 1** and described in more
187 detail below.

188
189 The CRF data described in this paper are mandatory; i.e. if impact models consider this forcing, the
190 specified dataset must be used; if an alternative input data set is used instead, the run cannot be
191 considered an ISIMIP3b, group I + II simulation. The DHF for the historical period is identical to the
192 ISIMIP3a DHF listed in **Table 1** of (Frieler et al., 2024a) where we also indicate whether the data set is
193 mandatory or optional. Optional forcing data could be used but is not mandatory. In addition, the protocol
194 includes a set of sensitivity experiments that are described as deviations from the default runs and labelled
195 by the baseline CRF and DHF settings and a third specifier indicating the deviation from this default setting.
196 The ISIMIP3b group I+II sensitivity runs include experiments with fixed levels of atmospheric CO₂
197 concentrations (‘2015co2’), high levels in CO₂ concentrations in combination with low levels of climate
198 change (‘ssp585co2’), and runs with lightning data that vary in response to climate change (‘varlightning’),
199 while lightning is fixed at present day levels in the default runs. These sensitivity experiment runs are not
200 depicted in **Figure 1** but listed in **Table 2**.



203
204
205
206
207
208
209

Figure 1: Illustration of the default ISIMIP3b forcing data sets. Each ISIMIP3b experiment is defined by a combination of a CRF data set with a DHF data set. The considered combinations are listed in **Table 2** and the underlying rationale is described in section **1.1** and **1.2**. **Table 1** lists all data sets defining the considered CRFs while the DHFs are based on the same datasets as in ISIMIP3a. Potentially required spin-up procedures are not included in the Figure, but described in section **1.1**.

The ISMIP3b simulations are divided into two groups. Group I comprises the simulations from 1601 - 1849 (pre-industrial) and 1850 - 2014 (historical) assuming simulated pre-industrial and historical CRFs and different constant ('nat', '1850soc', and '2015soc') or varying ('histsoc') levels of DHF based on the same observational data used in ISIMIP3a (see **Figure 1**). Group II comprises the future projections assuming constant 2015 levels of DHF (see **Figure 1**) including a baseline with pre-industrial CRF (grey line in the future projections part of **Figure 1**). All experiments are introduced in more detail below (section **1.1** for group I and **1.2** for group II).

In contrast to ISIMIP3a, the CRFs provided for ISIMIP3b currently only comprise atmospheric (see section **2.1**) and oceanic climate data (see section **2.4**), tropical cyclone tracks with associated wind and precipitation fields (see section **2.2**), and CO₂ and methane concentration (see section **2.5**). We do not yet provide associated coastal water levels (see section **2.2.3** for planned work). Impact simulations that rely on the missing forcings cannot be generated within ISIMIP3b yet, but we are currently developing their setup and will provide the forcings as soon as possible. The ISIMIP3b atmospheric and oceanic climate data is derived from five different General Circulation Models (GCMs) generated within the Coupled Model Intercomparison project, phase 6 (CMIP6).

Table 1: Climate-Related Forcing datasets for ISIMIP3b.

Forcing	Status	Source, description
---------	--------	---------------------

Climate-related forcings ('picontrol', 'historical', 'ssp126', 'ssp370', 'ssp585')		
Atmospheric forcings ('picontrol', 'historical', 'ssp585', 'ssp370', 'ssp126')		
Gridded atmospheric climate forcing	mandatory	Bias-adjusted data (pre-industrial climate, historical climate, and future projections for the SSP1-2.6, SSP3-7.0, and SSP5-8.5 scenarios) generated by GFDL-ESM4, IPSL-CM6A-LR, MPI-ESM1-2-HR, MRI-ESM2-0, and UKESM1-0-LL within CMIP6 (Lange & Büchner, 2021), see section 2.1
Local atmospheric climate forcing for lakes	mandatory	Atmospheric data extracted from the data sets above for 72 lakes that have been identified within the lake sector as locations (grid cell of the ISIMIP 0.5° grid, ISIMIP3 local lake sites) where models can be calibrated based on observed temperature profiles and hypsometry within ISIMIP3b (depth and area) (Lange and Büchner 2021)
Tropical cyclone tracks with wind and precipitation fields	mandatory	<p>Samples of synthetic tropical cyclone tracks derived from the five CMIP6 GCMs considered within ISIMIP generated by two different statistical downscaling approaches, see section 2.2.</p> <p>MIT approach (Emanuel et al., 2008, 2025):</p> <ul style="list-style-type: none"> • pre-industrial climate from IPSL-CM6A-LR, MPI-ESM1-2-HR and MRI-ESM2-0 (all 1850-2014), and from UKESM1-0-LL (1950-2100) • historical climate from IPSL-CM6A-LR, MPI-ESM1-2-HR, UKESM1-0-LL and GFDL-ESM4 (all 1850-2014), and from MRI-ESM2-0 (1950-2014). • Future climate: ssp126 (2061-2100), ssp370 (2015-2100) and ssp585 (2015-2100) from IPSL-CM6A-LR, MPI-ESM1-2-HR, MRI-ESM2-0, UKESM1-0-LL, and ssp585 (2061-2100) from GFDL-ESM4. <p>Two different configurations (SD and CRH, see section 2.2) of the Columbia HAZard model (CHAZ, Lee et al., 2018, 2025):</p> <ul style="list-style-type: none"> • historical climate (1850-2014) from GFDL-ESM4, IPSL-CM6A-LR, MPI-ESM1-2-HR, MRI-ESM2-0, and UKESM1-0-LL • future climate (2015-2100): ssp126, ssp370, ssp585 from GFDL-ESM4, IPSL-CM6A-LR, MPI-ESM1-2-HR, MRI-ESM2-0, and UKESM1-0-L <p>For tracks generated by the MIT approach, we also provide wind and precipitation fields (Quesada-Chacón et al., 2025)</p>

Lightning	mandatory	Flash Rate Monthly Climatology not changing with climate change (Cecil, 2006)
Oceanic forcings ('picontrol', 'historical', 'ssp585', 'ssp370', 'ssp126')		
Oceanic climate forcing	mandatory	Uncorrected data (pre-industrial climate, historical climate, and future projections for the SSP1-2.6, SSP3-7.0, and SSP5-8.5 scenarios) generated by GFDL-ESM4, IPSL-CM6A-LR, MPI-ESM1-2-HR, and UKESM1-0-LL within CMIP6 (Büchner 2024), see section 2.4
Coastal water levels		
Coastal water levels	mandatory	In section 2.3 we describe a method to generate relative sea level projections that smoothly extend tide gauge observations into the future building on a Bayesian model (Perrette & Mengel, 2025). For ISIMIP3, we plan to extend the framework to all coastlines and directly use ISIMIP GCM output for the global thermodynamic and local stereodynamic components, adjusting the gridded simulations to associated observations to ensure a consistent transition from the historical period. Ice sheet and glacier contributions are incorporated through spatial fingerprints, while unresolved vertical land motion processes are estimated from residuals at tide gauges and extrapolated where no observations are available. We are also developing an approach to extend the sea level projections to daily maximum water levels derived from the ISIMIP3 atmospheric forcings (daily mean Surface Air Pressure and daily mean Near-Surface Wind Speed).
Atmospheric composition or fluxes		
Atmospheric CO ₂ concentration	mandatory	(Büchner & Reyer, 2022) based on the following sources: 1850-2005: (Meinshausen et al., 2011); 2006-2014: Global annual CO ₂ from NOAA Global Monthly Mean CO ₂ (Lan et al., 2023); 2015-2100: (Meinshausen et al., 2020)
Atmospheric CH ₄ concentration	mandatory	(Büchner & Reyer, 2022) based on the following sources: 1850-2014:(Meinshausen et al., 2017); 2015-2100: (Meinshausen et al., 2020)
Climate-Related Forcings for the sensitivity experiment 'varlightning', using above forcing data except for:		
Lightning data ('varlightning')		

Varying lightning according to climate change	mandatory	Lightning data has been generated for the ssp126, ssp370, and ssp850 climate projections from UKESM1-0-LL (Kaplan et al., 2023)
Climate-Related Forcings for the ‘de-biased’ sensitivity experiment		
Global oceanic forcings		
Oceanic forcings based on de-biased atmospheric forcings	mandatory	In section 2.4.2 we describe an approach to de-bias the oceanic forcings based on the ocean biogeochemistry model NEMO-PISCES forced by a de-biased version of the IPSL-CM6A-LR-based atmospheric forcing as an option to fulfil the demand for de-biased ocean data we would like to follow.
Regional oceanic forcings		
De-biased oceanic forcing based on observed oceanic data for individual variables and regions	mandatory	The regional models of the fisheries and marine ecosystem sector have applied regional bias-adjustments within their impact simulations that are described in section 2.4.3 and that make these simulations part of the ‘de-biased’ sensitivity experiment in the sector (see Table 2) while the default experiments are based on the raw oceanic forcings.

228

229

230 **1.1 ISIMIP3b, group I: Climate-model based impact model simulations for the period** 231 **from 1601 to 2015**

232

233 The group I experiments cover the years 1601-1849 with pre-industrial CRFs (‘picontrol’) and fixed 1850
234 direct human forcings (‘1850soc’) described in the grey column 3 of the ISIMIP3b scenario **Table 2** as well
235 as the subsequent years 1850-2014 considering pre-industrial and historical CRF(‘picontrol’ or ‘historical’)
236 and different assumptions about DHF (‘histsoc’, ‘2015soc’, ‘1850soc’, and ‘nat’) as described in the grey
237 column 4 of **Table 2**. The reasoning behind the individual experiments are introduced below.

238

239 **Pre-industrial reference simulations (picontrol + histsoc, picontrol + 2015soc, picontrol + 2015soc-from-**
240 **histsoc, picontrol + 1850soc, picontrol + nat; default):** To estimate the impacts of historical and future
241 changes in the CRFs, the protocol includes reference simulations based on pre-industrial CRFs and DHF
242 identical to those considered in the climate change scenario runs. In order to allow for the fitting of
243 extreme value distributions such as Gumble or Generalized Extreme Value (GEV) distributions to e.g.
244 annual maximum discharge to estimate reference 100 year return levels, the runs are designed to include
245 the generation of large samples (at least 250 years) of impact distributions distribution based on stable
246 pre-industrial CRFs (picontrol) and constant DHFs (see ‘picontrol + 1850soc’, ‘picontrol + 2015soc’, and
247 ‘picontrol + nat’ experiments in **Table 2**).

248 In addition, the protocol includes a reference experiment for the historical period (1850-2014) with DHF
249 changing over time (histsoc) and 1850-2014 pre-industrial CRF (picontrol), while fixed 2015 DHF is
250 considered afterwards (2015-2100) ('picontrol + 2015soc-from-histsoc'). This run may be different from
251 the 'picontrol + 2015soc' simulation for this time window because of the lagged effects of increasing DHF
252 from 1850 to 2014. The 'histsoc' DHF is identical to ISIMIP3a (Frieler et al., 2024a).

253 The complete pre-industrial reference runs are divided in two parts. Only the first parts from the start
254 until 2014 belong to group I (grey fields in **Table 2**), while the second parts covering the period 2015-2100
255 belong to group II (red parts of **Table 2**).

256
257 Comparing these reference simulations to the scenario experiments using historical CRFs (historical +
258 histsoc, historical + 2015soc, historical + 1850soc, historical + nat; default (see below)) allows for the
259 estimation of the effects of simulated historical climate change conditional on the assumed DHF. The
260 historical CRF ('historical') starts from the pre-industrial climate simulation in 1850, i.e. the 'picontrol' and
261 'historical' versions of the experiments have a common starting point. As some impact indicators may
262 have 'internal' trends not necessarily forced by external drivers (e.g. re-growth of forests), the comparison
263 of the 1850-2014 impact simulations forced by the 'historical' CRF to parallel simulations using the
264 'picontrol' CRF is more appropriate to estimate the effects of historical climate change than comparing an
265 early period of the historical impact simulation to the end of the historical period.

266 For models requiring a spin-up, the 'picontrol' CRFs should be used in combinations with DHF i) at 1850
267 levels to spin-up for the '1850soc' and 'histsoc' experiments, ii) at 2015 levels to initialise the '2015soc'
268 experiment, and iii) set to zero to start the 'nat' experiments. For the spin-up the 'picontrol' CRF should
269 be copied as often as needed. The 'picontrol + 1850soc' run from 1601-1849 is part of the regular
270 experiments that should be reported and hence the spin-up has to be finished before this pre-industrial
271 period.

272 To allow for a quantification of the impacts of the anthropogenic CRFs, we also support historical
273 reference simulation assuming only natural CRF ('hist-nat' simulations generated within the Detection and
274 Attribution Model Intercomparison Project (DAMIP) as sub-MIP of CMIP6, (Gillett et al., 2016) by providing
275 the associated bias-adjusted CRF as secondary climate input data (Lange et al., 2023). However, associated
276 simulations are not an official part of ISIMIP3b and not described in the associated protocol.

277
278 **Standard historical simulations based on historical climate-related forcing and observed changes in**
279 **direct human forcing (historical + histsoc; default):** The historical simulations (1850-2014) are forced by
280 historical ('historical') CRFs and DHFs evolving according to observations (ISIMIP3a 'histsoc' DHF). The
281 ISIMIP3b 'historical + histsoc' experiment is comparable to the default 'obsclim + histsoc' run used in
282 ISIMIP3a but based on simulated CRFs. The simulated climate is different from the observed realisation
283 due to differences in the internal variability of the observed and simulated historical climate and potential
284 deficits in the climate model simulations. A comparison between the default ISIMIP3b 'historical + histsoc'
285 impact model simulations to the associated ISIMIP3a results allows for a quantification of the effects of
286 the discrepancies between the observed and simulated CRFs on the considered impact indicators. This
287 experiment can be initialised from the spin-up of the associated pre-industrial reference simulation in
288 case a spin-up is needed.

289
290
291
292
293
294
295
296
297
298
299
300
301
302
303
304
305
306
307
308
309
310
311
312
313
314
315
316
317
318
319
320
321
322
323
324
325
326
327
328
329

Simulations with historical climate-related forcing and fixed 2015 direct human forcing (historical + 2015soc; default): This historical experiment is similar to the standard historical experiment except that it is forced by fixed 2015 DHF. It is introduced into the ‘first priority’ scenario-set-up to generate an ensemble of historical cross-sectorally consistent impact simulations that is as large as possible by not excluding impact models that are not able to handle varying DHF. If a spin-up is needed the experiment can be initialised from the spin-up of the associated pre-industrial reference simulation (picontrol + 2015soc, default) described at the beginning of this section.

Simulations with historical climate-related forcing and fixed 1850 direct human forcing (historical + 1850soc; default): This historical experiment is also similar to the standard historical experiment but it is forced by the fixed 1850 DHFs. It corresponds to the ‘obsclim + 1901soc’ simulation of ISIMIP3a. Here in ISIMIP3b we consider the year 1850 instead of 1901 used in ISIMIP3a as this is the year where the ‘historical’ climate simulations with observed natural and human forcings start, i.e. a branch from the pre-industrial climate simulations assuming constant pre-industrial forcings (‘picontrol’). If a spin-up is required it does not have to be newly generated as it is identical to the spin-up for the default ‘picontrol + 1850soc’, ‘picontrol + histsoc’, and ‘historical + histsoc’ experiments and described in the beginning of this section.

Simulations with historical climate-related forcing and no direct human forcings (historical + nat; default): Considering no DHF (nature run) allows quantifying the effect of the simulated historical climate change conditional on otherwise natural conditions, i.e. no direct human influences on land use, water management etc.. This experiment is introduced as a companion experiment to the ‘obsclim + nat’ simulations of ISIMIP3a. The comparison with the three historical simulations with constant DHF allows testing to what degree the impact of climate change on the simulated natural or human systems is conditional on the underlying DHF. This experiment is only included for the biomes and fisheries and marine ecosystems fisheries sectors as models from other sectors usually need some basic information such as vegetation patterns that are not available for natural-only conditions. The biomes models generate their own natural-only vegetation patterns based on their dynamic representation of vegetation. A spin-up does not have to be newly generated but is identical to the spin-up for the ‘picontrol + nat’ experiment described above.

‘De-biased’ sensitivity simulations within the marine ecosystems and fisheries sector (FishMIP) with de-biased historical oceanic forcings and no or histsoc direct human forcings (historical + nat, historical + histsoc; de-biased): So far, the default oceanic forcing is not bias-adjusted as globally the observational data are too sparse to be used in a similar empirical way as for the bias-adjustment of the atmospheric forcing. However, the biases in the forcing are expected to also induce biases in the historical and future impact simulations. To quantify these effects and to test a suggested bias-adjustment method based on comprehensive ocean-biogeochimistry model simulations forced by bias-adjusted atmospheric forcings we include a sensitivity experiment where the default CRF is replaced by input data generated by a dynamical de-biasing approach (Lengaigne et al., 2025) using the NEMO-PISCES physical-biogeochimical

330 ocean model (Madec, 2015), which is the oceanic component of the IPSL-CM6A-LR climate model. Thus,
331 the forcing data will first be generated for IPSL-CM6A-LR, but later extended to other ISIMIP-GCMs as
332 described in subsection 2.4.2.

333 In contrast, the oceanic forcing for the regional component of the marine ecosystems and fisheries sector
334 have been bias-adjusted by regional observational oceanic data as described in subsection 2.4.3. In this
335 case most models only use the bias-adjusted inputs and not the raw ones. Nevertheless the experiments
336 are labeled as ‘de-biased’ sensitivity experiments to ensure a consistent naming across scales.
337

338 **1.2 ISIMIP3b, group II: Climate-model based future impact model simulations with** 339 **constant 2015 direct human forcings**

340
341 The ISIMIP3b, group II simulations comprise a set of future impact projections (2015-2100) using fixed
342 levels of DHF as considered in the historical simulations (‘2015soc’, ‘1850soc’, and ‘nat’) or reached at the
343 end (2014) of the historical period in the ‘historical + histsoc’ runs (‘2015soc-from-histsoc’). These runs
344 are described in the red cells of **Table 2**.
345

346 **Pre-industrial reference simulations (picontrol + 2015soc, picontrol + 2015soc-from-histsoc, picontrol +**
347 **1850soc, picontrol + nat; default):** These simulations are included into the ISIMIP3, group II part of the
348 protocol to allow for the estimation of the effect of climate change by comparing the future impact
349 projections to simulations assuming the same background DHF but pre-industrial levels of CRF (see
350 description of baseline simulations in section 1.1).
351

352 **Future impact projections assuming SSP-RCP-based climate-related forcings starting from ‘historical +**
353 **histsoc’ simulations (ssp126 + 2015soc-from-histsoc, ssp370 + 2015soc-from-histsoc, ssp585 + 2015soc-**
354 **from-histsoc; default):** These runs are a continuation of the group I ‘historical + histsoc’ simulations
355 assuming fixed 2015 DHF for the future. Note that this experiment is different from the experiment with
356 fixed 2015 DHF for the future starting from the ‘historical + 2015soc’ group I experiment (see description
357 below).
358

359 These experiments have been introduced to describe the impacts of different scenarios of changes in the
360 climate-related systems on today’s natural systems and societies, i.e. assuming present day population
361 levels and distributions, land use patterns, water, and agricultural management measures etc.. In many
362 cases, the projected changes in natural and human systems can be interpreted as the pure effect of the
363 prescribed changes in the climate-related systems. However, they could also partly result from lagged
364 effects of the historical changes in DHFs (‘histsoc’), CRF (‘historical’), or natural temporal trends induced
365 e.g. by re-growth of forests. To be able to separate natural trends from the effects of changing CRFs, these
366 simulations can be compared to reference impact simulations with pre-industrial CRF forced with the
367 same DHF (‘picontrol + 2015soc-from-histsoc’, see description in group I section).
368

369 **Future impact projections assuming SSP-RCP-based climate-related forcings starting from historical**
370 **simulations with constant 2015 direct human forcings (ssp126 + 2015soc, ssp370 + 2015soc, ssp585 +**

371 **2015soc; default):** These experiments continue the ‘historical + 2015soc’ experiments from ISIMIP3b,
372 group I using DHF held constant at 2015 levels for the historical period. Although the DHF in the future
373 period is identical to the future simulations described above, the difference in historical forcing may affect
374 the impact simulations in the future period. These simulations are also considered first priority as some
375 of the impact models may not be able to handle varying DHF and therefore can only perform these
376 experiments. Models participating in the ‘2015soc-from-histsoc’ experiments described above are also
377 asked to complete the ‘2015soc’ runs to generate an as large as possible ensemble of consistent impact
378 model simulations.

380 **Future impact projections assuming SSP-RCP-based climate-related forcings starting from historical**
381 **simulations assuming constant 1850 direct human forcings (ssp126 + 1850soc, ssp370 + 1850soc, ssp585**
382 **+ 1850soc; default):** These experiments continue the default ‘historical + 1850soc’ experiments
383 considered in ISIMIP3b, group I. They are included to estimate the impact of changes in the climate-
384 related systems conditional on 1850 levels of DHF that can be compared to the impact conditional on
385 today’s levels of DHF (‘2015soc’).

387 **Future impact projections assuming SSP-RCP-based climate-related forcings starting from historical**
388 **simulations assuming no direct human forcings (ssp126 + nat, ssp370 + nat, ssp585 + nat; default):** These
389 experiments continue the default ‘historical + nat’ experiments in ISIMIP3b, group I. They are included to
390 estimate the effect of changes in the climate-related systems (here climate change itself and increasing
391 CO₂ concentrations) assuming no DHF.

393 **CO₂ sensitivity simulations (ssp126 + 2015soc-from-histsoc, ssp370 + 2015soc-from-histsoc, ssp585 +**
394 **2015soc-from-histsoc, ssp585 + 2015soc, ssp585 + 1850soc, ssp585 + nat; 2015co2):** To separate the
395 effects of increasing atmospheric CO₂ concentrations from the effects of other changes in the climate-
396 related systems, the ISIMIP3b protocol includes sensitivity experiments where atmospheric CO₂
397 concentrations are held constant at 2015 levels. For SSP1-2.6 and SSP3-7.0, they are only introduced as
398 deviations from the default ‘2015soc-from-histsoc’ experiments while for SSP5-8.5 the effect can also be
399 quantified conditional on all levels of direct human influences considered in the previous experiments.

400 **Future lightning sensitivity simulations (ssp126 + 2015soc-from-histsoc, ssp370 + 2015soc-from-histsoc,**
401 **ssp585 + 2015soc-from-histsoc; varlightning):** To study the effects of future changes in lightning flash
402 rates as opposed to using a stationary lightning climatology, the ISIMIP3b protocol includes sensitivity
403 experiments where future lightning flash rates change along the RCPs. The future lightning data sensitivity
404 experiment is introduced as a deviation from the default ‘2015soc-from-histsoc’ experiment and only for
405 one climate model (UK-ESM). This sensitivity experiment has been introduced for the fire sector.

406 **Climate sensitivity simulations under high levels of CO₂ (ssp126 + 2015soc-from-histsoc, ssp585co2):** To
407 study the effects of high atmospheric CO₂ concentration without accompanying changes in climate, the
408 ISIMIP3b protocol includes a sensitivity experiment where the atmospheric CO₂ concentration are
409 prescribed according to RCP8.5, while the other CRF, in particular the atmospheric forcings are from SSP1-

410 2.6. The future climate sensitivity experiment is introduced as a deviation from the default ‘ssp126 +
 411 2015soc-from-histsoc’ experiment. This sensitivity experiment has been introduced for the peat sector.

412 **‘De-biased’ sensitivity simulations within the marine ecosystems and fisheries sector (FishMIP) with de-**
 413 **biased oceanic forcings and no or 2015soc direct human forcings for reference simulations based on**
 414 **pre-industrial oceanic forcing (picontrol + nat, picontrol + 2015soc-from-histsoc; de-biased) and the**
 415 **associated simulations accounting for different levels of climate change (ssp126 + nat, ssp370 + nat,**
 416 **ssp858 + nat, ssp126 + 2015soc-from-histsoc, ssp370 + 2015soc-from-histsoc, ssp585 + 2015soc-from-**
 417 **histsoc):** These simulations represent the future extensions of the ‘de-biased’ group I simulations
 418 described above. They are designed to test the dynamical bias-adjustment suggested for the global
 419 oceanic forcings under different levels of climate change (ssp126, ssp370, ssp585). The regional impact
 420 projections within the sector are also based on de-biased oceanic forcings and are therefore also labeled
 421 as ‘de-biased’ sensitivity experiments to ensure a consistent labeling across scales.
 422

423 **Table 2: ISIMIP3b climate-model based experiments.** The table provides a comprehensive list of all
 424 ISIMIP3b, group I (grey) and group II (red) experiments defined by the assumed climate-related forcings
 425 (CRF) and direct human forcings (DHF). Here the climate-related forcings are only described by the climate
 426 (oceanic and atmospheric) and CO₂ forcings as we do not provide coastal water levels yet.

Experiment	Short description	Period: Pre-industrial 1601-1849	Period: Historical 1850-2014	Period: Future 2015-2100
pre-industrial control 2015soc-from-histsoc	CRF: No changes in the climate-related systems, CO ₂ and CH ₄ fixed at 1850 levels	picontrol	picontrol	picontrol
1st priority	DHF: Varying management before 2015, then fixed at 2015 levels thereafter	1850soc	histsoc	2015soc-from-histsoc
pre-industrial control 2015soc	CRF: No changes in the climate-related systems, CO ₂ and CH ₄ fixed at 1850 levels	Does not have to be simulated as the following periods already provide 251 simulation years	picontrol	picontrol

1st priority		assuming stable baseline CRF and DHF.		
	DHF: Fixed at 2015 levels for all periods	s	2015soc	2015soc
pre-industrial control 1850soc	CRF: No changes in the climate-related systems, CO ₂ and CH ₄ fixed at 1850 levels	Does not have to be simulated as the following periods already provide 251 simulation years assuming stable baseline CRF and DHF.	picontrol	picontrol
2nd priority	DHF: Fixed at 1850 levels for all periods		1850soc	1850soc
pre-industrial control nat	CRF: No changes in the climate-related systems, CO ₂ and CH ₄ fixed at 1850 levels	Does not have to be simulated as the following periods already provide 251 simulation years assuming stable baseline CRF and DHF.	picontrol	picontrol
2nd priority	DHF: No direct human influences		nat	nat
RCP2.6 2015soc-from-histsoc 1st priority	CRF: Simulated historical changes in climate-related systems, CO ₂ and CH ₄ concentrations as observed in the historical period, then simulated SSP1-2.6 changes in the climate-related systems	Identical to picontrol + 1850soc run described above	historical	ssp126
	DHF: Varying management before 2015, then fixed at 2015 levels thereafter		histsoc	2015soc-from-histsoc

RCP2.6 2015soc 1st priority	CRF: Simulated historical changes in climate-related systems, CO ₂ and CH ₄ concentrations as observed in the historical period, then simulated SSP1-2.6 changes in the climate-related systems	Identical to “picontrol + 2015soc” run	historical	ssp126
	DHF: Fixed at 2015 levels for all periods		2015soc	2015soc
RCP2.6 1850soc 2nd priority	CRF: Simulated historical changes in climate-related systems, CO ₂ and CH ₄ concentrations as observed in the historical period, then simulated SSP1-2.6 changes in the climate-related systems	Identical to “picontrol + 1850soc” run	historical	ssp126
	DHF: Fixed at 1850 levels for all periods		1850soc	1850soc
RCP2.6 nat 2nd priority	CRF: Simulated historical changes in climate-related systems, CO ₂ and CH ₄ concentrations as observed in the historical period, then simulated SSP1-2.6 changes in the climate-related systems	Identical to “picontrol + nat” run	historical	ssp126
	DHF: No direct human influences		nat	nat

CO₂ sensitivity RCP2.6 2015soc-from-histsoc 2nd priority	CRF: Simulated historical changes in climate-related systems, CO ₂ and CH ₄ concentrations as observed in the historical period, then simulated SSP1-2.6 changes in the climate-related systems but fixed 2015 CO ₂ concentrations	Identical to “picontrol + 1850soc” run	"histsoc" version of the historical period of the RCP2.6 experiment, as described above	ssp126 Sensitivity experiment: 2015co2
	DHF: Varying management before 2015, then fixed at 2015 levels thereafter			
RCP7.0 2015soc-from-histsoc 1st priority	CRF: Simulated historical changes in climate-related systems, CO ₂ and CH ₄ concentrations as observed in the historical period, then simulated SSP3-7.0 changes in the climate-related systems	Identical to “picontrol + 1850soc” run	"histsoc" version of the historical period of the RCP2.6 experiment	ssp370
	DHF: Varying management before 2015, then fixed at 2015 levels thereafter			
RCP7.0 2015soc 1st priority	CRF: Simulated historical changes in climate-related systems, CO ₂ and CH ₄ concentrations as observed in the historical period, then simulated SSP3-7.0 changes in the	Identical to “picontrol + 2015soc” run	Identical to "historical + 2015soc" run described above	ssp370

	climate-related systems			
	DHF: Fixed at 2015 levels for all periods			2015soc
RCP7.0 1850soc 2nd priority	CRF: Simulated historical changes in climate-related systems, CO ₂ and CH ₄ concentrations as observed in the historical period, then simulated SSP3-7.0 changes in the climate-related systems	Identical to “picontrol + 1850soc” run	Identical to "historical + 1850soc" run described above	ssp370
	DHF: Fixed at 1850 levels for all periods			1850soc
RCP7.0 nat 2nd priority	CRF: Simulated historical changes in climate-related systems, CO ₂ and CH ₄ concentrations as observed in the historical period, then simulated SSP3-7.0 changes in the climate-related systems	Identical to “picontrol + nat” run	Identical to "historical + nat" run described above	ssp370
	DHF: No direct human influences			nat

CO₂ sensitivity RCP7 2015soc-from-histsoc 2nd priority	CRF: Simulated historical changes in climate-related systems, CO ₂ and CH ₄ concentrations as observed in the historical period, then simulated SSP3-7.0 changes in the climate-related systems but CO ₂ concentrations fixed at 2015 levels	Identical to “picontrol + 1850soc” run	Identical to "historical + histsoc" run described above	ssp370 Sensitivity experiment: 2015co2
	DHF: Varying management before 2015, then fixed at 2015 levels thereafter			
RCP8.5 2015soc-from-histsoc 1st priority	CRF: Simulated historical changes in climate-related systems, CO ₂ and CH ₄ concentrations as observed in the historical period, then simulated SSP5-8.5 changes in the climate-related systems	Identical to “picontrol + 1850soc” run	Identical to "historical + histsoc" run described above	ssp585
	DHF: Varying management before 2015, then fixed at 2015 levels thereafter			
RCP8.5 2015soc 1st priority	CRF: Simulated historical changes in climate-related systems, CO ₂ and CH ₄ concentrations as observed in the historical period, then simulated SSP5-8.5	Identical to “picontrol + 2015soc” run	Identical to "historical + 2015soc" run described above	ssp585

	changes in the climate-related systems			
	DHF: Fixed at 2015 levels for all periods			2015soc
RCP8.5 1850soc 2nd priority	CRF: Simulated historical changes in climate-related systems, CO ₂ and CH ₄ concentrations as observed in the historical period, then simulated SSP5-8.5 changes in the climate-related systems	Identical to “picontrol + 1850soc” run	Identical to "historical + 1850soc" run described above	ssp585
	DHF: Fixed at 1850 levels for all periods			1850soc
RCP8.5 nat 2nd priority	CRF: Simulated historical changes in climate-related systems, CO ₂ and CH ₄ concentrations as observed in the historical period, then simulated SSP5-8.5 changes in the climate-related systems	Identical to “picontrol + nat” run	Identical to "historical + nat" run	ssp585
	DHF: No direct human influences			nat
CO₂ sensitivity RCP8.5	CRF: Simulated historical changes in climate-related systems, CO ₂ and CH ₄ concentrations as	Identical to “picontrol + 1850soc” run	Identical to "historical + histsoc" run	ssp585 Sensitivity experiment: 2015co2

<p>2015soc-from-histsoc</p> <p>1st priority</p>	<p>observed in the historical period, then simulated SSP5-8.5 changes in the climate-related systems but CO₂ concentrations fixed at 2015 levels</p>			
	<p>DHF: Varying management before 2015, then fixed at 2015 levels thereafter</p>			<p>2015soc-from-histsoc</p>
<p>CO₂ sensitivity RCP8.5</p> <p>2015soc</p> <p>1st priority</p>	<p>CRF: Simulated historical changes in climate-related systems, CO₂ and CH₄ concentrations as observed in the historical period, then simulated SSP5-8.5 changes in the climate-related systems, but CO₂ concentrations fixed at 2015 levels</p>	<p>Identical to "picontrol + 2015soc" run</p>	<p>Identical to "historical + 2015soc" run</p>	<p>ssp585</p> <p>Sensitivity experiment: 2015co2</p>
	<p>DHF: Fixed at 2015 levels for all periods</p>			<p>2015soc</p>
<p>CO₂ sensitivity RCP8.5</p> <p>1850soc</p> <p>2nd priority</p>	<p>CRF: Simulated historical changes in climate-related systems, CO₂ and CH₄ concentrations as observed in the historical period, then simulated SSP5-8.5 changes in the climate-related systems, but CO₂ concentrations fixed at 2015 levels</p>	<p>Identical to "picontrol + 1850soc" run</p>	<p>Identical to "historical + 1850soc" run</p>	<p>ssp585</p> <p>Sensitivity experiment: 2015co2</p>

	DHF: Fixed at 1850 levels for all periods			1850soc
CO₂ sensitivity RCP8.5 nat 1st priority	CRF: Simulated historical changes in climate-related systems, CO ₂ and CH ₄ concentrations as observed in the historical period, then simulated SSP5-8.5 changes in the climate-related systems, but CO ₂ concentrations fixed at 2015 levels	Identical to "picontrol + nat" run	Identical to "historical + nat" run	ssp585 Sensitivity experiment: 2015co2
	DHF: No direct human influences			nat
Lightning sensitivity RCP2.6 2015soc-from-histsoc 2nd priority	CRF: Simulated historical changes in climate-related systems, CO ₂ and CH ₄ concentrations as observed in the historical period, then simulated SSP1-2.6 changes in the climate-related systems including future lightning which in the default case is considered fixed at climatological levels	Identical to "picontrol + 1850soc" run	Identical to "historical + histsoc" run	ssp126 Sensitivity experiment: varlightning
	DHF: Varying management before 2015, then fixed at 2015 levels thereafter			2015soc-from-histsoc

Lightning sensitivity RCP7.0 2015soc-from-histsoc 2nd priority	CRF: Simulated historical changes in climate-related systems, CO ₂ and CH ₄ concentrations as observed in the historical period, then simulated SSP3-7.0 changes in the climate-related systems including future lightning which in the default case is considered fixed at climatological levels	Identical to "picontrol + 1850soc" run	Identical to "historical + histsoc" run	ssp370 Sensitivity experiment: varlightning
	DHF: Varying management before 2015, then fixed at 2015 levels thereafter			2015soc-from-histsoc
Lightning sensitivity RCP8.5 2015soc-from-histsoc 2nd priority	CRF: Simulated historical changes in climate-related systems, CO ₂ and CH ₄ concentrations as observed in the historical period, then simulated SSP5-8.5 changes in the climate-related systems including future lightning which in the default case is considered fixed at climatological levels	Identical to "picontrol + 1850soc" run	Identical to "historical + histsoc" run	ssp585 Sensitivity experiment: varlightning
	DHF: Varying management before 2015, then fixed at 2015 levels thereafter			2015soc-from-histsoc

Climate sensitivity, RCP2.6 with RCP8.5 CO₂ 2015soc-from-histsoc 2nd priority	CRF: Simulated historical changes in climate-related systems, CO ₂ and CH ₄ concentrations as observed in the historical period, then CO ₂ evolves according to SSP5-8.5 while all other CRFs change according to default SSP1-2.6 forcing data	Identical to "picontrol + 1850soc" run	Identical to "historical + histsoc" run	ssp126 Sensitivity experiment: ssp585co2
	DHF: Varying management before 2015, then fixed at 2015 levels thereafter			2015soc-from-histsoc
Bias sensitivity, de-biased oceanic data for pre-industrial control nat 2nd priority	CRF: De-biased pre-industrial oceanic forcing, CO ₂ fixed at 1850 levels	Not covered	picontrol	picontrol Sensitivity experiment: de-biased
	DHF: no direct human influences			nat
Bias sensitivity, de-biased oceanic data for SSP1-2.6 nat 2nd priority	CRF: De-biased simulated historical oceanic forcing, then de-biased simulated SSP1-2.6 oceanic forcing	Not covered	historical	ssp126 Sensitivity experiment: de-biased
	DHF: no direct human influences			nat
	CRF: De-biased simulated historical oceanic forcing, then de-biased simulated	Not covered	historical	ssp370 Sensitivity experiment: de-biased

Bias sensitivity, de-biased oceanic data for SSP3-7.0	SSP3-7.0 oceanic forcing			
nat 2nd priority	DHF: no direct human influences	Not covered	nat	nat
Bias sensitivity, de-biased oceanic data for SSP5-8.5	CRF: De-biased simulated historical oceanic forcing, then de-biased simulated SSP5-8.5 oceanic forcing	Not covered	historical	ssp585 Sensitivity experiment: de-biased
nat 2nd priority	DHF: No direct human influences	Not covered	nat	nat
Bias sensitivity, de-biased oceanic data for pre-industrial control	CRF: De-biased pre-industrial oceanic forcing, CO ₂ fixed at 1850 levels	Not covered	picontrol	picontrol Sensitivity experiment: de-biased
2015soc-from-histsoc 2nd priority	DHF: Varying direct human influences before 2015, then fixed at 2015 levels thereafter	Not covered	histsoc	2015soc-from-histsoc
Bias sensitivity, de-biased oceanic data for SSP1-2.6	CRF: De-biased simulated historical oceanic forcing, then de-biased simulated SSP1-2.6 oceanic forcing	Not covered	historical	ssp126 Sensitivity experiment: de-biased
2015soc-from-histsoc 2nd priority	DHF: Varying direct human influences before 2015, then fixed at 2015 levels thereafter	Not covered	histsoc	2015soc-from-histsoc

Bias sensitivity, de-biased oceanic data for SSP3-7.0 2015soc-from-histsoc 2nd priority	CRF: De-biased simulated historical oceanic forcing, then de-biased simulated SSP3-7.0 oceanic forcing	Not covered	historical	ssp370 Sensitivity experiment: de-biased
	DHF: Varying direct human influences before 2015, then fixed at 2015 levels thereafter	Not covered	histsoc	2015soc-from-histsoc
Bias sensitivity, de-biased oceanic data for SSP5-8.5 2015soc-from-histsoc 2nd priority	CRF: De-biased simulated historical oceanic forcing, then de-biased simulated SSP5-8.5 oceanic forcing	Not covered	historical	ssp585 Sensitivity experiment: de-biased
	DHF: Varying direct human influences before 2015, then fixed at 2015 levels thereafter	Not covered	histsoc	2015soc-from-histsoc

427

428

429

430 2 Climate-related forcing data

431

432 2.1 Bias-adjusted and statistically downscaled atmospheric climate forcing

433

434 For ISIMIP3b we provide the daily atmospheric forcings for the same variables as in ISIMIP3a on the
435 default 0.5° grid (see **Table 3**). These variables are from the output of CMIP6 climate model simulations,
436 selected and processed as described below. We use the climate simulations from the piconrol (for pre-
437 industrial conditions), historical (for historical conditions), ssp126, ssp370, and ssp585 (for future
438 conditions under the scenarios SSP1-2.6, SSP3-7.0, and SSP5-8.5, respectively) CMIP6 experiments.

439

440

441 **Table 3:** Climate-related atmospheric forcing data provided within ISIMIP3b. The upper limits of
442 precipitation (pr) and snowfall (prsn) correspond to 600 mm day-1 and 300 mm day-1, respectively, while
443 the lower and upper limits of Near-Surface Air Temperature (tas), Daily Maximum Near-Surface Air Temperature

444 (tasmax) and Daily Minimum Near-Surface Air Temperature (tasmin) correspond to -90°C and $+70^{\circ}\text{C}$,
 445 respectively.

Variable	Variable specifier	Unit (maximum range, inner bounds if considered)	Resolution	Datasets
Near-Surface Relative Humidity	hurs	% ([1, 100], [0.01, 99.99])	0.5° grid, daily	Bias-adjusted and downscaled from GFDL-ESM4, IPSL-CM6A-LR, MPI-ESM1-2-HR, MRI-ESM2-0, and UKESM1-0-LL simulations generated for CMIP6.
Near-Surface Specific Humidity	huss	kg kg ⁻¹ ([0.0000001, 0.1])	0.5° grid, daily	Derived from bias-adjusted and downscaled hurs, ps, and tas from GFDL-ESM4, IPSL-CM6A-LR, MPI-ESM1-2-HR, MRI-ESM2-0, and UKESM1-0-LL simulations generated for CMIP6.
Precipitation (including snowfall)	pr	kg m ⁻² s ⁻¹ ([0, 600/86400], [0.1/86400, ∞])	0.5° grid, daily	Bias-adjusted and downscaled from GFDL-ESM4, IPSL-CM6A-LR, MPI-ESM1-2-HR, MRI-ESM2-0, and UKESM1-0-LL simulations generated for CMIP6.
Snowfall	prsn	kg m ⁻² s ⁻¹ ([0, 300/86400]) Maximum range and inner bounds of unitless snowfall ratio (prsnratio = prsn/pr): ([0,1], [0.0001,0.9999])	0.5° grid, daily	Derived from bias-adjusted and downscaled pr and prsnratio from GFDL-ESM4, IPSL-CM6A-LR, MPI-ESM1-2-HR, MRI-ESM2-0, and UKESM1-0-LL simulations generated for CMIP6.
Surface Air Pressure	ps	Pa ([480, 110000])	0.5° grid, daily	Bias-adjusted and downscaled from GFDL-ESM4, IPSL-CM6A-LR, MPI-ESM1-2-HR, MRI-ESM2-0, and UKESM1-0-LL simulations generated for CMIP6.
Surface Downwelling Longwave Radiation	rlds	W m ⁻² ([40, 600])	0.5° grid, daily	Bias-adjusted and downscaled from GFDL-ESM4, IPSL-CM6A-LR, MPI-ESM1-2-HR, MRI-ESM2-0, and UKESM1-0-LL simulations generated for CMIP6.

Surface Downwelling Shortwave Radiation	rsds	W m ⁻² ([0, 500]) Maximum range and inner bounds of normalized rsds used during bias adjustment: ([0,1], [0.0001, 0.9999])	0.5° grid, daily	Bias-adjusted and downscaled from GFDL-ESM4, IPSL-CM6A-LR, MPI-ESM1-2-HR, MRI-ESM2-0, and UKESM1-0-LL simulations generated for CMIP6.
Near-Surface Wind Speed	sfcwind	m s ⁻¹ ([0.1, 50], [0.01,∞[)	0.5° grid, daily	Bias-adjusted and downscaled from GFDL-ESM4, IPSL-CM6A-LR, MPI-ESM1-2-HR, MRI-ESM2-0, and UKESM1-0-LL simulations generated for CMIP6.
Near-Surface Air Temperature	tas	K ([183.15, 343.15])	0.5° grid, daily	Bias-adjusted and downscaled from GFDL-ESM4, IPSL-CM6A-LR, MPI-ESM1-2-HR, MRI-ESM2-0, and UKESM1-0-LL simulations generated for CMIP6.
Daily Maximum Near-Surface Air Temperature	tasmax	K ([183.15, 343.15]) Maximum range and inner bounds considered for tasrange: ([0.01, ∞[, [0.01,∞[) Maximum range and inner bounds considered for unitless tasskew: ([0,1], [0.0001,0.9999])	0.5° grid, daily	Derived from bias-adjusted and downscaled tasrange = tasmax - tasmin and tasskew = (tas - tasmin) / (tasmax - tasmin) from GFDL-ESM4, IPSL-CM6A-LR, MPI-ESM1-2-HR, MRI-ESM2-0, and UKESM1-0-LL simulations generated for CMIP6.
Daily Minimum Near-Surface Air Temperature	tasmin	K ([183.15, 343.15]) Maximum range and inner bounds considered for tasrange: ([0.01, ∞[, [0.01,∞[) Maximum range and inner bounds considered for unitless tasskew: ([0,1], [0.0001,0.9999])	0.5° grid, daily	Derived from bias-adjusted and downscaled tasrange = tasmax - tasmin and tasskew = (tas - tasmin) / (tasmax - tasmin) from GFDL-ESM4, IPSL-CM6A-LR, MPI-ESM1-2-HR, MRI-ESM2-0, and UKESM1-0-LL simulations generated for CMIP6.

447 For the pre-industrial conditions, 500 years of picontrol output data are used and harmonised across
 448 GCMs with respect to the time range they cover. This is possible because picontrol data only carry nominal
 449 year labels. We shift the GCM-specific picontrol time ranges listed in **Table 4** to 1601–2100. For the
 450 historical and future climate conditions, we provide input data for 1850–2014 and 2015–2100,
 451 respectively, in line with the time ranges covered by the corresponding CMIP6 experiments. The common
 452 time axis is important as the use of the input data should be harmonised across all sectors. In particular,
 453 the year-by-year combination of the pre-industrial CRF with the historical DHF should be done in the same
 454 way across all sectors and models.

455
 456 **Selection of climate models.** To limit the number of mandatory impact simulations and hence lower the
 457 barrier to participation in ISIMIP3b, we provide climate input data for only five selected CMIP6 climate
 458 models. The basic characteristics of the five GCMs are listed in **Table 4**. The models were selected based
 459 on data availability at the selection time (late 2019 to early 2020), performance in the historical period,
 460 structural independence, process representation and equilibrium climate sensitivity (ECS).

461
 462 To be included in ISIMIP3b, a GCM had to provide daily data for all variables listed in **Table 3** except for
 463 near-surface specific humidity (huss) (which was derived from near-surface relative humidity (hurs), surface air
 464 pressure (ps) and near-surface air temperature (tas), see below), ps if sea level pressure (psl) was available,
 465 so a proxy for ps could be computed based on psl and tas, and near-surface wind speed (sfcwind) if zonal
 466 and meridional near-surface wind components (uas, vas) were available, so a proxy for sfcwind could be
 467 computed based on uas and vas. Those daily data had to cover 500 picontrol years and all years of the
 468 historical, SSP1-2.6, SSP3-7.0, and SSP5-8.5. In addition, we favoured GCMs that provided the additional
 469 input data needed for the tropical cyclone modelling (**Table 5**) and the fisheries and marine ecosystems
 470 sector (FishMIP; **Table 10**).

471
 472 **Table 4:** Characteristics of CMIP6 climate models used in ISIMIP3b. Columns show (from left to right) the
 473 climate model acronym, the horizontal grid size (longitude x latitude) of the original atmospheric output
 474 data, the ensemble member used, the nominal time range covered by the picontrol data used, the
 475 equilibrium climate sensitivity (ECS) according to (Meehl et al., 2020), and the main model reference paper
 476 and the CMIP6 simulation data publications used. For definitions of climate model acronyms and
 477 modelling groups see (Durack, n.d.).

GCM	Grid size	Member	picontrol	ECS	References
GFDL-ESM4	288 x 180	r1i1p1f1	0001–0500	2.6°C	(Dunne et al., 2020; John et al., 2018; Krasting et al., 2018)
IPSL-CM6A-LR	144 x 143	r1i1p1f1	1870–2369	4.6°C	(Boucher et al., 2018, 2019, 2020)
MPI-ESM1-2-HR	384 x 192	r1i1p1f1	1850–2349	3.0°C	(Jungclaus et al., 2019; Mauritsen et al., 2019; Schupfner et al., 2019)

495 **Figure 2:** Relative space-time root-mean-square deviation (RMSD) calculated from the climatological seasonal cycle
496 of the CMIP6 historical simulations (1980–1999) compared to observational datasets, for various CMIP6 GCMs
497 (columns) and climate variables (rows), similar to Fig. 6 of (Bock et al., 2020). A relative performance is displayed,
498 with blue shading being better and red shading worse than the median RMSD of all model results of the CMIP6
499 ensemble. A diagonal split of a grid square shows the relative error with respect to the reference data set (lower
500 right triangle) and an alternative data set (upper left triangle), as listed in Table 5 of (Bock et al., 2020). White boxes
501 are used when data are not available for a given model and variable. Models selected for ISIMIP3b are highlighted
502 in red. Variables are (from top to bottom): Surface Downwelling Shortwave Radiation (rsds), Surface Upwelling
503 Shortwave Radiation (rsus), Surface Downwelling Longwave Radiation (rlds), Surface Upwelling Longwave Radiation
504 (rlus), Soil Moisture (sm), Ambient Fine Aerosol Optical Depth at 550 nm (od550lt1aer), Ambient Aerosol Absorption
505 Optical Thickness at 550 nm (abs550aer), Ambient Aerosol Optical Depth at 870 nm (od870aer), Ambient Aerosol
506 Optical Thickness at 550 nm (od550aer), Shortwave Cloud Radiative Effect (swcre), Longwave Cloud Radiative Effect
507 (lwcre), Top-of-Atmosphere Outgoing Shortwave Radiation (rsut), Top-of-Atmosphere Outgoing Longwave
508 Radiation (rlut), Total Cloud Cover Percentage (clt), Precipitation (pr), Surface Temperature (ts), Near-Surface Air
509 Temperature (tas), Specific Humidity at 400 hPa (hus400), Sea Level Pressure (psl), Geopotential Height at 500 hPa
510 (zg500), Northward Wind at 200 hPa (va200), Northward Wind at 850 hPa (va850), Eastward Wind at 200 hPa
511 (ua200), Eastward Wind at 850 hPa (ua850), Air Temperature at 200 hPa (ta200), and Air Temperature at 850 hPa
512 (ta850). Produced with ESMValTool v2.0 (Andela et al., 2020b, 2020a; Righi et al., 2020).

513

514 The five GCMs are structurally independent in terms of their ocean and atmosphere model components.
515 Furthermore, all of them have a coupled climate and carbon cycle and in some cases, fully interactive
516 chemistry and aerosol components. We favoured models that applied prognostic couplings between
517 processes and model domains wherever possible to maximise the coverage of simulated feedbacks.

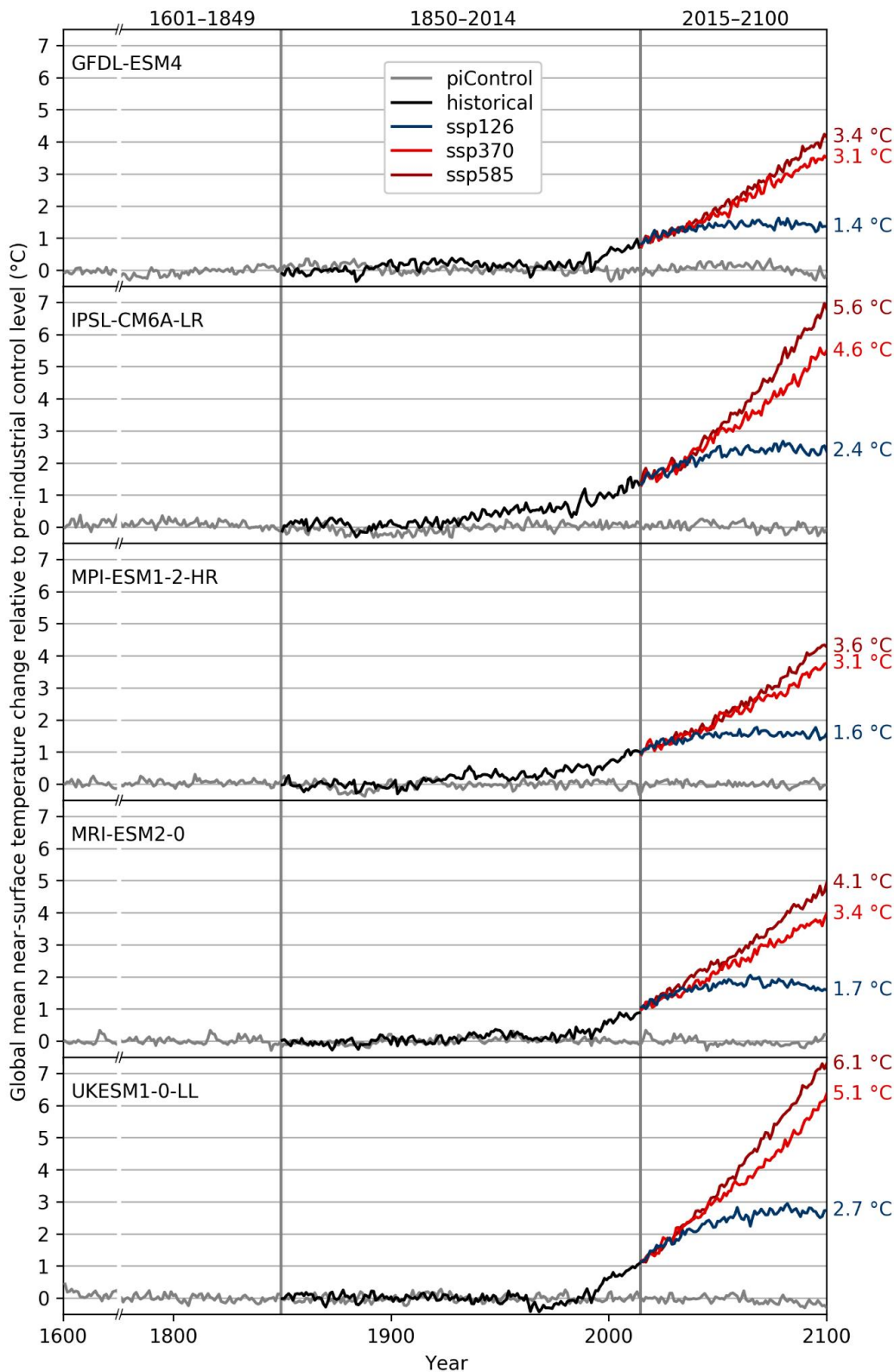
518

519 The five GCMs provide a good representation of both the mean and the range of the full CMIP6 multi-
520 model ensemble ECS. According to (Meehl et al., 2020), the CMIP6 multi-model mean ECS is 3.7°C, which
521 is precisely met by the mean ECS of the five ISIMIP3b GCMs. The transient climate response (TCR) of 2.0°C
522 is also precisely met. This provides an improvement over ISIMIP2b, in the sense of the selected GCM
523 subset reflecting the statistics of the larger CMIP ensemble. In ISIMIP2b the mean ECS for the full CMIP5
524 was 3.2°C compared with a mean ECS of 3.72°C for the four ISMIP2b GCMs (see Table S1 and S2 in
525 (Jägermeyr et al., 2021)). The ISIMIP3b ensemble includes three models with below-average ECS (GFDL-
526 ESM4, MPI-ESM1-2-HR, MRI-ESM2-0) and two models with above-average ECS (IPSL-CM6A-LR, UKESM1-
527 0-LL) (see **Table 4**). In line with their ECS values, we find GFDL-ESM4 and UKESM1-0-LL to project the
528 weakest and strongest global warming, respectively, under any future scenario considered (see **Figure 3**).
529 Under SSP5-8.5, the global mean near-surface temperature in 2100 is about 3°C larger in UKESM1-0-LL
530 than in GFDL-ESM4. Under SSP1-2.6, the projections are about 1.5°C apart. The ensemble mean warming
531 of the ISIMIP3b CMIP6 models is significantly higher than the warming of the ISIMIP2b CMIP5 models,
532 across global land area by an average of 0.3°C, but over the main breadbasket cropland regions by more
533 than 0.5°C between 1983–2013 and 2069–2099, under both SSP1-2.6 and SSP5-8.5 (Table S1 in (Jägermeyr
534 et al., 2021)). This is in line with the higher median ECS in CMIP6 compared to CMIP5; indeed, some CMIP6
535 models have an ECS above the assessed likely (2.5°C to 4°C) and very likely (2°C to 5°C) ranges in the IPCC's
536 sixth assessment report (AR6) (Forster et al., 2021). The reasons for these higher estimates of ECS are
537 complex, with cloud feedback processes playing an important role (Zelinka et al., 2020). While the

538 plausibility of the very high ECS estimates has been questioned, recent studies indicate CMIP6 models
539 with high ECS tend to simulate cloud properties better than low ECS models (Bock & Lauer, 2024); also,
540 unaccounted natural variability may have biased the IPCC's assessed ranges somewhat low (Liang et al.,
541 2024; Watanabe et al., 2024).

542

543 The ISIMIP3b ensemble reflects the spread in ECS of the overall CMIP6 ensemble, with two models above
544 the AR6 likely range and one of these (UKESM1-0-LL) above the very likely range. The strong warming
545 response of these models should be kept in mind when conducting ISIMIP3b-based impacts studies.
546 However, depending on the region and variable of interest, the high ECS does not necessarily have any
547 bearing on the magnitude or realism of projected regional impacts, and any further selection of models
548 should not be based solely on ECS but on the models' suitability for the impacts variables in question
549 (Swaminathan et al., 2024). In many applications, results can be harmonized by describing the simulated
550 impacts in terms of global mean temperature changes instead of time for the different emission scenarios.
551



552
553
554
555
556
557

Figure 3: Time series of annual global mean near-surface temperature change relative to pre-industrial levels (1601–1849 average) as simulated with GFDL-ESM4, IPSL-CM6A-LR, MPI-ESM1-2-HR, MRI-ESM2-0 and UKESM1-0-LL (from top to bottom). Colour coding indicates the underlying CMIP6 experiments (grey: pre-industrial control, black: historical, blue: SSP1-2.6, light red: SSP3-7.0, dark red: SSP5-8.5) with corresponding time periods given at the top. Numbers to the right of the plot represent end-of-century warming levels under the different future

scenarios, expressed as the global multi-year mean near-surface temperature change from 1601–1849 to 2070–2100.

Bias adjustment and statistical downscaling. To make the GCM-based climate forcing usable for the impact modellers we apply a bias adjustment ensuring that the GCM simulations match the observed distribution of climate data over the historical reference period (1979–2014). In addition to the bias adjustment a statistical downscaling to our standard 0.5° grid is included in the pre-processing of the surface and near-surface atmospheric variables (see **Table 3**). The method used for the bias adjustment and statistical downscaling (BASD) in ISIMIP3b is version 2.5 of ISIMIP3BASD (Lange, 2019b, 2021a).

ISIMP3BASD has several advantages compared to the method used for bias adjustment and statistical downscaling in ISIMIP2b (Frieler et al., 2017; Lange, 2017, 2018). First, it clearly separates the adjustment of biases in climate model output at 1° or 2° resolution, whatever is closest to the original output data, from the statistical downscaling to the target resolution of 0.5°. Compared to ISIMIP2b, where climate model output was first spatially interpolated to the target resolution and then bias-adjusted, the new approach avoids the associated underestimation of the spatial variability at the target resolution (Lange, 2019b). Second, the new quantile mapping method preserves trends in each quantile of the distribution of the daily data and adjusts biases in distribution quantiles of the daily data more accurately than the ISIMIP2b bias adjustment methods (Lange, 2019b).

For trend preservation, we first produce pseudo-future observations by shifting the historically observed daily data by the simulated future climate change. Here, the signal of climate change is the difference or the ratio between the inverse empirical cumulative distribution function of the historical period and the respective distribution functions of each 36-year period of the future. Using the difference ensures additive trend preservation and using the ratio ensures multiplicative trend preservation under bias adjustment. We apply additive trend preservation for near-surface air temperature (tas), sea level pressure (psl, see **Table 3**), and surface downwelling longwave radiation (rlds). We apply primarily multiplicative trend preservation for precipitation including snowfall (pr), near-surface wind speed (sfcWind), and the range (tasrange = tasmax - tasmin) between the daily maximum and minimum near-surface air temperatures (tasmax and tasmin, respectively) that can transition smoothly to additive trend preservation for data with large negative biases in the historical period (Lange, 2019b). In a second step, the future simulations are mapped onto the pseudo-future observations by quantile mapping. Both steps, the generation of the pseudo future observations and the quantile mapping of the future simulations onto the pseudo observations, are applied for each day of the year separately. The distributions include data from the 31 days around the considered day and all years of the reference or future period, respectively. This means a sample size of 31x36 values for each day of the year. Through this approach the bias adjustment implicitly also adjusts the multi-year mean annual cycle and a mix of year-to-year and day-to-day variability (Haerter et al., 2011).

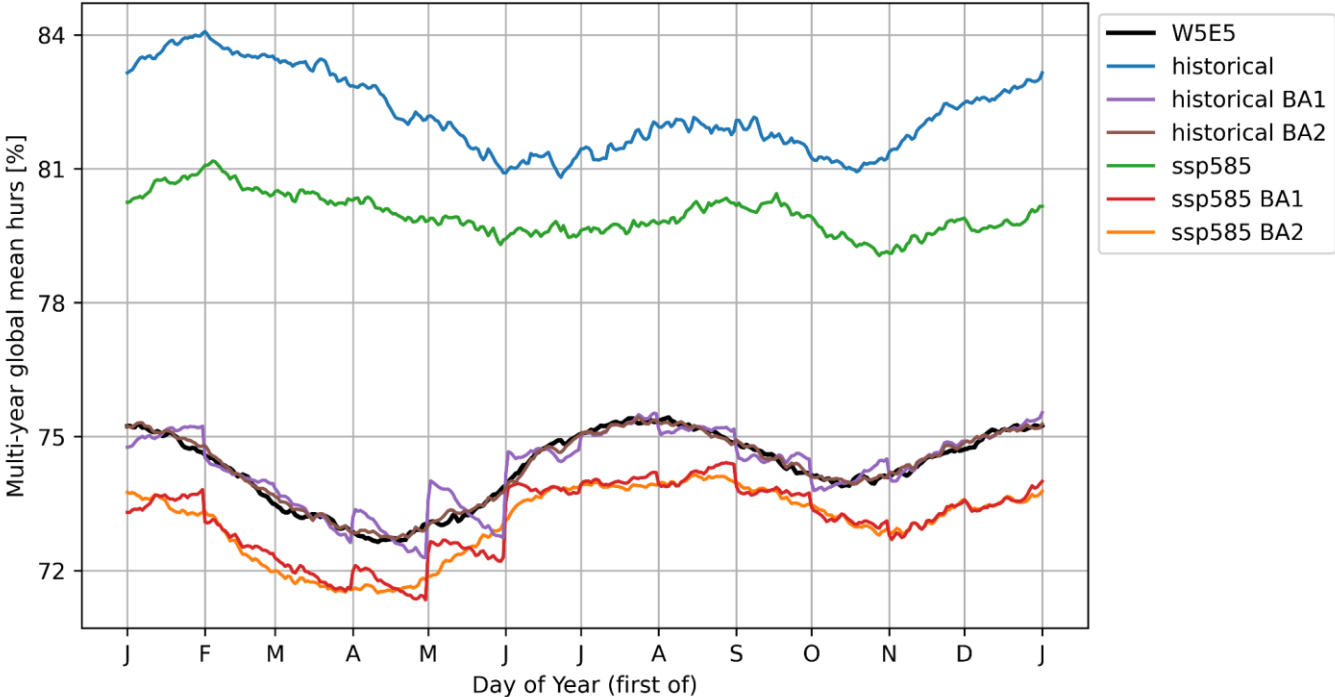
In addition, the method adjusts the frequency of daily data falling outside of the inner bounds specified in **Table 3** (e.g. the dry day frequency, i.e. the number of days with precipitation below 0.1 mm day⁻¹).

599
600
601
602
603
604
605
606
607
608
609
610
611
612
613
614
615
616
617
618
619
620
621
622
623

Four variables were adjusted and downscaled indirectly: near-surface specific humidity (huss) was derived from adjusted and downscaled near-surface relative humidity (hurs), surface air pressure (ps), and near-surface air temperature (tas) using the equations of (Buck, 1981) as described in (Weedon et al., 2010), snowfall (prsn) was derived from adjusted and downscaled precipitation including snow (pr) and the snowfall ratio (prsnratio = prsn / pr), and daily maximum and daily minimum near-surface air temperatures (tasmax and tasmin, respectively) were derived from adjusted and downscaled tas, and the tasrange = tasmax - tasmin and skewness of the daily temperature cycle tasskew = (tas - tasmin) / (tasmax - tasmin).

The basic characteristics of ISIMIP3BASD (version 1.0) are described in Lange (2019b). However, the method finally used to generate the forcing data now provided within ISIMIP3b (ISIMIP3BASD version 2.5) deviates from the original version in some aspects. In the following we describe the most important updates of the procedure relative to the one described in Lange (2019b). For a complete list of differences between the two versions of the BASD method and the full history of which feature was added in which update, see the CHANGELOG included in the archive of code version 2.5 (Lange, 2021a).

In Lange (2019b) the bias-adjustment was applied on a monthly basis, i.e. the pseudo-future observations and the quantile mapping described above was applied to all daily January data, February data and so forth. This approach can introduce discontinuities at the transition from one month to another (see **Figure 4**). That is why for ISIMIP3b the adjustment is done in the running window mode with steps of one day and a window width of 31 days as described above. This approach resolves the discontinuity issue (see **Figure 4**), as suggested by (hemeßl et al. (2012) Thrasher et al. , 2012) (Gennaretti et al., 2015) and (Grenier, 2018).



624

625 Figure 4: Global multi-year daily mean near-surface relative humidity for UKESM1-0-LL historical (1979-
626 2014) and SSP5-8.5 (2065-2100), with uncorrected historical simulated data in blue, uncorrected future
627 simulated data in green, historical bias-adjusted data in purple and brown, future bias-adjusted data in red and
628 orange, and observational reference data in black. The bias is effectively reduced throughout all days of the year
629 (brown line closely matching the black line) when ISIMIP3BASD v2.5 is applied in running-window mode in steps of
630 one day (BA2). In contrast, a month-by-month application, which was the only option in ISIMIP3BASD v1.0,
631 generates discontinuities at each turn of the month (BA1).
632

633 Since ps , $rlds$ and tas can show significant trends within the 36-year training and application periods
634 ISIMIP3BASD v1.0 includes a detrending of these variables within these intervals before the pseudo future
635 observations and the transfer functions are estimated and applied. Afterwards the trend is added back
636 again. This is done to prevent the confusion of trends with interannual variability during quantile mapping
637 (Lange, 2019b; Maraun, 2013). In contrast to v1.0, in v2.5, applied to generate the ISIMIP3b forcing data,
638 the detrending is only applied if the trend is significantly different from zero at the 5% level.
639

640 We also changed the method used to generate future pseudo-observations of bounded variables
641 (equations (8) and (9) of (Lange, 2019b)), in order to stabilise results in some edge cases. If, e.g., the
642 historically observed relative dry-day frequency was 0.0 while the simulated frequency was 0.8 for the
643 historical period and 0.9 for some future period, then, according to equation (9) of (Lange, 2019b), the
644 future pseudo-observed frequency would be equal to $1 - (1 - 0.0)(1 - 0.9)/(1 - 0.8) = 0.5$. As this is
645 considered unrealistic we apply a revised version of equation (9) of (Lange, 2019b) that reads
646

$$\begin{aligned}
647 \quad P^{obs}_{fut} = \{ \\
648 \quad P^{sim}_{fut} \text{ if } P^{sim}_{hist} = P^{obs}_{hist}, \\
649 \quad 0 + (P^{obs}_{hist} - 0)(P^{sim}_{fut} - 0)/(P^{sim}_{hist} - 0) \text{ if } P^{sim}_{fut} \leq P^{sim}_{hist} > P^{obs}_{hist}, \\
650 \quad 1 - (1 - P^{obs}_{hist})(1 - P^{sim}_{fut})/(1 - P^{sim}_{hist}) \text{ if } P^{sim}_{fut} \geq P^{sim}_{hist} < P^{obs}_{hist}, \\
651 \quad P^{obs}_{hist} + P^{sim}_{fut} - P^{sim}_{hist} \text{ otherwise.} \tag{1}
\end{aligned}$$

652
653 In this revised relation, the otherwise case applies if $P^{sim}_{fut} < P^{sim}_{hist} < P^{obs}_{hist}$ or $P^{sim}_{fut} >$
654 $P^{sim}_{hist} > P^{obs}_{hist}$. Hence it applies to the aforementioned edge case, where it produces a less extreme
655 future pseudo-observed relative frequency of $0.0 + 0.9 - 0.8 = 0.1$. Equation (8) of (Lange, 2019b) was
656 revised analogously to equation (9).
657

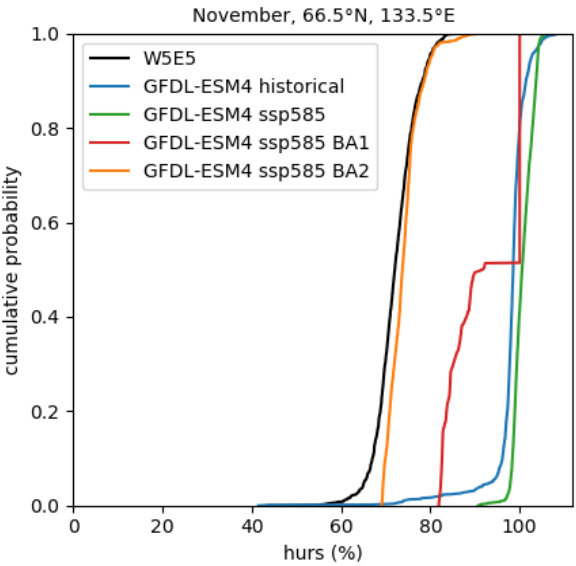
658 Furthermore, we refined the method used to generate future pseudo-observations (step 5 of the bias
659 adjustment algorithm of (Lange, 2019b)) for all variables with at least one bound: In v1.0, the future
660 pseudo observations were generated by transferring simulated trends in all distribution quantiles to the
661 observational reference data. That included trends in, e.g., precipitation quantiles below the wet-day
662 threshold. However, in some cases, the trend transfer turned many dry days into wet days, with a
663 profound impact on the shape of the distribution of future pseudo-observed wet-day precipitation. As a
664 result, simulated trends in wet-day precipitation intensity were not well preserved. In v2.5, trend transfers

665 are restricted to values within threshold. This particularly improves the preservation of trends in wet-day
666 precipitation intensities.

667

668 We also modified the bias adjustment method for Near-Surface Relative Humidity (hurs) because
669 ISIMIP3BASD v1.0 turned out to produce unrealistic distributions of hurs under climate change if there
670 are too many cases of supersaturation ($\text{hurs} \geq 100\%$) in the simulated data. This is the case for several of
671 the CMIP6 GCMs selected for ISIMIP3b, particularly in high-latitude winter: While no supersaturations are
672 found in the observational reference data, the GCM simulates many supersaturations in the historical
673 reference period and even more so in a future period, under SSP5-8.5 (see **Figure 5**). ISIMIP3BASD v1.0
674 preserves this projected trend and hence produces future bias-adjusted hurs data with many
675 supersaturations. In v2.5, this trend is no longer preserved. Instead, the supersaturation probability is
676 fixed at the observed level, which is zero or very close to zero in all seasons and grid cells for W5E5. Future
677 pseudo observations of hurs are generated by applying the revised (see above) equation (8) of (Lange,
678 2019b) to all hurs values after capping them at 100%. The new approach was motivated by findings from
679 (Ruosteenoja et al., 2017, 2018). They analysed hurs data from CMIP5 and showed that (i)
680 supersaturations in those data are mostly spurious, resulting from, e.g., inconsistencies in the
681 interpolation of temperature and specific humidity to the near-surface level, and (ii) climatological mean
682 value trends of hurs become more consistent with trends in relative humidity from the lowest model level
683 if hurs is capped at 100% before trends are calculated.

684



685

686

687 **Figure 5:** Empirical cumulative distribution functions of near-surface relative humidity in high-latitude winter
688 (November, 66.5°N, 133.5°E) for GFDL-ESM4 historical (1979-2014) and SSP5-8.5 (2065-2100), with historical
689 simulated data in blue, future simulated data in green, future bias-adjusted data in red and orange, and
690 observational reference data in black. The simulated climate change signal is well preserved with ISIMIP3BASD v2.5
691 using a fixed supersaturation ($\text{hurs} \geq 100\%$) probability and equation (1) applied to all hurs values after capping
692 them at 100% to generate future pseudo observations (orange, BA2). In contrast, the simulated climate change
693 signal is not well preserved if the supersaturation probability is allowed to change and equations (8) and (9) of
694 (Lange, 2019b) are used to generate future pseudo observations of hurs (red, BA1).

695
696
697
698
699
700
701
702
703
704
705
706
707
708
709
710
711
712
713
714
715
716
717
718
719
720
721
722
723
724
725
726
727
728
729
730
731
732
733
734
735

In addition, while ISIMIP3BASD v1.0 applies parametric quantile mapping to all climate variables, we used a nonparametric approach for the bias adjustment of near-surface relative humidity (hurs), the snowfall ratio (prsnratio), surface downwelling shortwave radiation (rsds), and the skewness of the daily temperature (tasskew) since the parametric quantile mapping method previously used for those variables suffered from occasionally unstable beta distribution fits.

Moreover, the parametric quantile mapping described in (Lange, 2019b) does not only adjust biases in quantiles of the simulated daily data but also adjusts biases in the likelihood of individual events, as in (Switanek et al., 2017). To avoid overfitting artifacts we did not adjust event likelihoods for ISIMIP3b.

Finally, the diurnal temperature range (tasrange) was ultimately bias-adjusted using a Weibull distribution, not a Rice distribution as described in (Lange, 2019b) because the Weibull distribution fits the data better in most cases, in particular in the upper tail.

For further details of the application of ISIMIP3BASD v2.5 for ISIMIP3b, including the exact Python commands and application periods used per CMIP6 experiment, see the ISIMIP3b bias adjustment fact sheet (Lange, 2021b).

In addition, we use a new observational target dataset. Instead of using the EWEMBI dataset (E2OBS, WFDEI and ERAI data merged and bias-corrected for ISIMIP; (Lange, 2019a) in ISIMIP3b we adjust the climate forcing data to version 2.0 of the W5E5 dataset (WFDE5 over land merged with ERA5 over the ocean; (Lange et al., 2021). The data cover the entire globe at 0.5° horizontal and daily temporal resolution from 1979 to 2019. W5E5 v2.0 is derived by applying version 2.0 of the WATCH Forcing Data methodology (WFDE5; (Cucchi et al., 2020) to ERA5 reanalysis data (Hersbach et al., 2020) and precipitation data from version 2.3 of the Global Precipitation Climatology Project (GPCP; (Adler et al., 2003)).

The statistical downscaling method did not change between v1.0 and v2.5 of ISIMIP3BASD, i.e. for ISIMIP3b we use the approach described (Lange, 2019b). This method adds the spatiotemporal variability that is missing at the low spatial resolution at which the bias adjustment is done (1° or 2°, depending on the GCM), compared to the target resolution of the downscaling (0.5°). The method is a modified version of the MBCn algorithm from (Cannon, 2018), which in turn is a stochastic, multivariate, non-parametric quantile mapping method. We use it to transfer the statistical relationship between low-resolution and high-resolution W5E5 data to the GCM output that was previously bias-adjusted using low-resolution W5E5 data. In comparison to the approach used in ISIMIP2b (a spatial interpolation to the target resolution followed by a bias adjustment at that resolution), the approach used in ISIMIP3b is less prone to inflate temporal variability and deflate spatial variability, i.e. the ISIMIP3b approach produces more realistic spatiotemporal variability patterns at the target resolution (Lange, 2019b).

2.2 Tropical cyclones

736
737

Table 5: Information about tropical cyclone tracks and windfields provided as climate-related forcing data within ISIMIP3b.

Variable	Variable specifier	Unit	Resolution	Datasets
Time associated with a given location of the storm centre	time	hours since 1950-01-01 00:00	along-track, 2-hourly (MIT model) 6-hourly (CHAZ model)	MIT (Emanuel et al., 2008) and CHAZ (Lee et al., 2018)
Latitudinal coordinate of storm centre	lat	degrees north	along-track, 2-hourly (MIT model) 6-hourly (CHAZ model)	MIT (Emanuel et al., 2008) and CHAZ (Lee et al., 2018)
Longitudinal coordinate of storm centre	lon	degrees east	along-track, 2-hourly (MIT model) 6-hourly (CHAZ model)	MIT (Emanuel et al., 2008) and CHAZ (Lee et al., 2018)
Central pressure	pres	hPa	along-track, 2-hourly	MIT (Emanuel et al., 2008)
Maximum 1-minute sustained wind speed	windspat ialmax	ms ⁻¹	along-track, 2-hourly (MIT model) 6-hourly (CHAZ model)	MIT (Emanuel et al., 2008) and CHAZ (Lee et al., 2018)
Radius of maximum wind speeds	rmw	km	along-track, 2-hourly	MIT (Emanuel et al., 2008)
Wind speed on the 850 hPa pressure level	ua850 va850	ms ⁻¹	along-track, 2-hourly (MIT model) 6-hourly (CHAZ model)	MIT (Emanuel et al., 2008) and CHAZ (Lee et al., 2018)
Temperature on the 600 hPa pressure level	ta600	K	along-track, 2-hourly (MIT model) 6-hourly (CHAZ model)	MIT (Emanuel et al., 2008) and CHAZ (Lee et al., 2018)
Frequency of TC occurrence	freqyear	count per year	annual	MIT (Emanuel et al., 2008)
Gridded lifetime maximum 1-minute sustained wind speed	windlifet imemax	ms ⁻¹	Per storm on a 300 arc-seconds (~10 km) grid	Wind fields calculated with Holland and Emanuel-Rotunno wind profiles (Holland, 1980, 2008) for MIT synthetic tracks
Maximum 24-hourly rainfall total during	maxrain	mm	per storm on a 300 arc-seconds (~10 km) grid	Maximum 24-hourly rainfall (Zhu et al., 2013) calculated for Holland and Emanuel-

the whole storm duration				Rotunno wind profiles for MIT synthetic tracks
--------------------------	--	--	--	--

738

739 We provide large ensembles of potential realisations of TC tracks and intensities that are consistent with
740 the large-scale atmospheric and oceanic conditions simulated by four of the five ISIMIP3b GCMs (see
741 **Table 6**) and for a selection of scenarios considered in ISIMIP3b (see **Table 1**). The tracks are generated
742 by two different statistical-dynamical approaches, the **MIT approach** and the **CHAZ approach** detailed
743 below forced by data from the ISIMIP3b GCMs listed in **Table 6**. For the MIT, approach, we provide gridded
744 wind (maximum 1-minute sustained wind speeds during the whole duration of the TC) and rainfall
745 (maximum 24-hourly amounts of rain during the whole duration of the TC) fields at a spatial resolution of
746 300 arc-seconds (approximately 10 km) using the same approaches also applied to the historically
747 observed tracks ((Frieler et al., 2024), section **3.2**).

748 Both methods to generate the TC tracks consist of a genesis, a track, and an intensity module:

749 **MIT approach.** Within MIT (Emanuel et al., 2008), the time-evolving state of the atmosphere and ocean
750 surface given by the GCMs is randomly (uniformly distributed in time and space) seeded by weak proto-
751 cyclones (genesis module). The seed disturbances are assumed to move with the GCM-provided large-
752 scale flow in which they are embedded, plus a westward and poleward component owing to planetary
753 curvature and rotation (track module). Their intensity is calculated using the Coupled Hurricane Intensity
754 Prediction System (CHIPS; (Emanuel et al., 2004), a simple axisymmetric hurricane model coupled to a
755 reduced upper ocean model to account for the effects of upper ocean mixing of cold water to the surface
756 (intensity module). Applied to the synthetically generated tracks, this model simulates which of the
757 seeded proto-cyclones develop into TCs, reaching maximum 1-minute sustained wind speeds of at least
758 35 knots, or dissipate due to unfavourable environments. The probabilistic seeding of proto-cyclones is
759 repeated until the desired number of storms per year is reached (in our case, 1500). For each year, the
760 share of proto-cyclones that dissipated in the process is used to derive an estimate of annual TC
761 occurrences (**freqyear**). Extensive comparisons to historical events (Emanuel et al., 2008) have revealed
762 that the statistical properties of the simulated events are consistent with historical TC genesis.

763 For each year of the ISIMIP3b period 1850—2100 (except for GFDL-ESM4, where tracks were only
764 generated for 1850-2014 and 2061-2100, and MRI-ESM2-0 for 1950-2100, see **Table 1**), 1500 tracks were
765 generated, globally. Depending on the application, a simple subsampling (Meiler et al., 2022) or a more
766 advanced bias-correction and emulation procedure (Geiger et al., 2021) might be necessary to extract
767 properly-sized sets of potential realisations from the MIT ensembles.

768 The “ISIMIP3b tropical cyclone tracks MIT” dataset shall only be used for noncommercial purposes,
769 including teaching and research at universities, colleges and other educational institutions, research at
770 non-profit research institutions, and personal non-profit purposes. It is accessible through the ISIMIP data
771 portal after agreeing to the corresponding license.

772 For using the tracks for commercial purposes, including but not restricted to consulting activities, software
773 or data products, and a commercial entity participating in research projects, please contact Kerry Emanuel
774 (MIT, email: emanuel@mit.edu) for an appropriate license.

775 **CHAZ approach.** CHAZ (Lee et al., 2018) seed disturbances are also initialised randomly, but, in contrast
776 to the MIT model, the global seeding rate and the local probabilities are derived from two versions of a
777 TC genesis index (TCGI, (Tippett et al., 2011) (genesis module) and intended to represent the
778 environmental conditions instead of being adjusted to produce a prescribed number of TCs. It is noted
779 that CHAZ's projection of global and basin-wide TC annual frequency is sensitive to the choice of the
780 particular variable used to represent moisture in its genesis module. Simulations using column relative
781 humidity (CRH) as the moisture variable tend to project an overall increase in global TC frequency, while
782 those using saturation deficit (SD) show a decrease (Camargo et al., 2014), (Lee et al., 2020). Both
783 parameters describe how far the atmosphere is from saturation, and they have very similar spatial
784 patterns in the present climate, so historical data cannot be used to determine which variable is the best
785 choice to represent the climate. These two configurations reflect the uncertainty of TC frequency
786 projections (Sobel et al., 2021). Here we provide CHAZ downscaling using both choices of moisture
787 variable to account for this uncertainty.

788 Similar to MIT, CHAZ then moves the synthetic storms by advection of the environmental steering flow
789 plus a beta drift (track module). The evolution of synthetic storm intensity is calculated using the
790 surrounding atmospheric conditions through an empirical multiple linear regression model plus a
791 stochastic component (intensity module, (Lee et al., 2015, 2016)). The stochastic component accounts for
792 internal storm dynamics that do not depend explicitly on the environment. While, in MIT, TC occurrence
793 frequency is provided as an additional variable, in CHAZ, this information is implicitly contained in the
794 number of TCs that were seeded by the genesis module and that reached TC strength according to the
795 intensity module.

796 For ISIMIP3b, 20 different CHAZ realisations of the genesis and subsequent tracks are generated with 40
797 ensemble members each from the intensity module for the historical period and for all RCP-SSP
798 combinations considered within ISIMIP3b. For each of the 20 realisations, we compute wind and rain fields
799 for the first ensemble member from the intensity ensemble. The design of 20 realisations allows CHAZ to
800 generate similar numbers (~1800) of synthetic storms per year per GCM as the MIT models over the
801 historical period. The exact number of storms per year in CHAZ varies by GCM, by scenario, by the choice
802 of humidity variables in CHAZ's genesis component (Lee et al., 2020). On average, CHAZ generates 1817,
803 1802, 1820, 1810, 1842 storms per year for GFDL-ESM4, IPSL-CM6A-LR, MPI-ESM1-2-HR, MRI-ESM2-0,
804 and UKESM1-0-LL, respectively. The CHAZ model has been shown to capture the statistical properties of
805 the observed storms when forced by a global reanalysis data (Lee et al., 2018). Its CMIP6 downscaling
806 results are reported in (Fosu et al., 2024). (Sobel et al., 2019) used both models to study cyclone risk at
807 Mumbai, India and showed that MIT and CHAZ generate comparable return periods (frequency of
808 exceedance) of maximum wind speeds at landfall. However, a frequency bias-correction might still be
809 necessary, depending on the application (Meiler et al., 2022).

810 The "ISIMIP3b tropical cyclone tracks (CHAZ)" dataset shall only be used for non-commercial purposes,
811 including teaching and research at universities, colleges and other educational institutions, research at

812 non-profit research institutions, and personal non-profit purposes. It is accessible through the ISIMIP data
 813 portal after agreeing to the corresponding license.

814 For using the tracks for commercial purposes, including but not restricted to consulting activities, software
 815 or data products, and a commercial entity participating in research projects, please contact Chia-Ying Lee
 816 (Columbia University, email: cl3225@columbia.edu) for an appropriate license.

817

818 **Table 6:** Climate input data interpolated to 2° horizontal resolution and provided without bias adjustment
 819 for tropical cyclone modelling with MIT and CHAZ.

Variable	Variable specifier	Unit	Resolution	Datasets
Sea Water Potential Temperature	thetao	°C	2° grid, model specific levels (m from surface to 200m depth), monthly	GFDL-ESM4, IPSL-CM6A-LR, MPI-ESM1-2-HR, MRI-ESM2-0, and UKESM1-0-LL simulations generated for CMIP6.
Sea Surface Temperature	tos	°C	2° grid over the ocean, monthly	GFDL-ESM4, IPSL-CM6A-LR, MPI-ESM1-2-HR, MRI-ESM2-0, and UKESM1-0-LL simulations generated for CMIP6.
Surface Temperature	ts	K	2° grid covering land and ocean areas, monthly	GFDL-ESM4, IPSL-CM6A-LR, MPI-ESM1-2-HR, MRI-ESM2-0, and UKESM1-0-LL simulations generated for CMIP6. ts may differ from tos in regions of sea ice where tos refers to temperatures under the ice while ts refers to temperatures at the surface.
Air Temperature	ta	K	2° grid; 15 pressure levels (from 1000 to 30 hPa), monthly	GFDL-ESM4, IPSL-CM6A-LR, MPI-ESM1-2-HR, MRI-ESM2-0, and UKESM1-0-LL simulations generated for CMIP6.
Specific Humidity	hus	kg kg-1	2° grid; 15 pressure levels (from 1000 to 30 hPa), monthly	GFDL-ESM4, IPSL-CM6A-LR, MPI-ESM1-2-HR, MRI-ESM2-0, and UKESM1-0-LL simulations generated for CMIP6.
Relative Humidity at 600 hPa	hur	%	2° grid, monthly	GFDL-ESM4, IPSL-CM6A-LR, MPI-ESM1-2-HR, MRI-ESM2-0, and UKESM1-0-LL simulations generated for CMIP6.
Precipitable water (water)	prw	kg m-2	2° grid, monthly	GFDL-ESM4, IPSL-CM6A-LR, MPI-ESM1-2-HR, MRI-ESM2-0, and

vapour content vertically integrated through the atmospheric column)				UKESM1-0-LL simulations generated for CMIP6.
Sea Level Pressure	psl	Pa	2° grid, monthly	GFDL-ESM4, IPSL-CM6A-LR, MPI-ESM1-2-HR, MRI-ESM2-0, and UKESM1-0-LL simulations generated for CMIP6.
Eastward Wind	ua	m s ⁻¹	2° grid; 200, 250, 850 hPa; monthly	GFDL-ESM4, IPSL-CM6A-LR, MPI-ESM1-2-HR, MRI-ESM2-0, and UKESM1-0-LL simulations generated for CMIP6.
Northward Wind	va	m s ⁻¹	2° grid; 200, 250, 850 hPa; monthly	GFDL-ESM4, IPSL-CM6A-LR, MPI-ESM1-2-HR, MRI-ESM2-0, and UKESM1-0-LL simulations generated for CMIP6.
Eastward Wind	ua	m s ⁻¹	2° grid; 250, 850 hPa; daily	GFDL-ESM4, IPSL-CM6A-LR, MPI-ESM1-2-HR, MRI-ESM2-0, and UKESM1-0-LL simulations generated for CMIP6.
Northward Wind	va	m s ⁻¹	2° grid; 250, 850 hPa; daily	GFDL-ESM4, IPSL-CM6A-LR, MPI-ESM1-2-HR, MRI-ESM2-0, and UKESM1-0-LL simulations generated for CMIP6.

820

821 2.3 Coastal water levels

822

823

Table 7: Coastal water level specifications

Variable	Variable specifier	Unit	Resolution	Datasets
Coastal water levels	cwl	m	custom coastal grid Hourly or daily maxima	planned

824

825

826

827

We do not yet provide coastal water levels as forcing data for ISIMIP3b. However, we plan to generate time series of coastal water levels from 1900 to 2100 at hourly resolution or for daily maxima. The data

828 set and method will be described in a separate manuscript. Similar to the hourly water level dataset of
829 ISIMIP3a (see section 3.3 of (Frieler et al., 2024) and (Treu et al., 2023)), we will combine longer-term
830 annual sea level change with estimates of short-term coastal water level variation. Concerning the long-
831 term sea level change component, we go beyond the ISIMIP2b approach (Frieler et al., 2017) and use tide
832 gauge, satellite, vertical land motion and global climate model data to constrain a model with observations
833 and IPCC AR6 projections in a Bayesian setting building on (Perrette & Mengel, 2025). The (Perrette &
834 Mengel, 2025) model allows for smooth projections of relative sea level from observational time series
835 collected at tide gauge stations with an explicit representation of the different components of sea level
836 rise . To become usable for ISIMIP3 we will a) extend the approach to all coastlines and b) use GCM output
837 directly for the global thermosteric and local sterodynamic components (Gregory et al., 2019) of sea level
838 rise, which are modeled by the GCMs. Extension to all coastlines is possible for the ice sheet, glacier and
839 sterodynamic components as they rely on spatial fingerprints or GCM output. Processes driving vertical
840 land motion that are not related to large scale climate processes are however more difficult to model.
841 They are estimated from data as residual vertical land motion in (Perrette & Mengel, 2025). As we do not
842 have data at all coastlines we will extrapolate in time and space the historical rates from tide gauge sites
843 or apply zero rates for this component. Using the explicit component structure of the model, we replace
844 the global thermosteric and the local sterodynamic parts by the output from ISIMIP GCMs. To that end,
845 we reference the gridded sterodynamic simulation data with observations of that component so that they
846 smoothly emerge from the historical period. We do not adjust variability or trends of the GCM data. The
847 method will provide relative sea level projections (including vertical land motion), which can be directly
848 used in coastal impact studies. We plan to estimate the short-term coastal water level variation by a
849 machine-learning approach that is trained to reproduce simulations of the Global Tide and Surge Model
850 (GTSM) driven by ERA5 reanalysis data (Muis et al., 2020) or simulations from HighResMIP (Muis et al.,
851 2023). We are currently testing the dependency of the short-term water level variation on available
852 atmospheric information at GCM resolution. If the predictive power is high enough we will use the findings
853 to provide computationally efficient water level projections specific for the ISIMIP GCMs.

855 2.4 Ocean data

856
857 In the default experiments, the ocean variables provided by the GCMs are not subject to bias-adjustment,
858 unlike the atmospheric forcing data (section 2.4.1). This is due to the absence of a comprehensive global
859 observational oceanic dataset to serve as a reference for the adjustment.

860 However, in order to mitigate potential biases in global impact model simulations stemming from biases
861 in raw oceanic forcing data, we provide a de-biased version to be used in a sensitivity experiment (see
862 **Table 2**). They will be derived from an ocean-biogeochemistry model forced by bias-adjusted monthly
863 atmospheric surface flux data from four of the five ISIMIP3b GCMs. The approach preserves the monthly
864 variability of the underlying GCM while the daily variability is added from an independent simulation (see
865 section 2.4.2).

866 For the regional impact model simulations, observational data for individual variables have either been
867 applied directly (if the required forcing was observed) to rectify biases in regional oceanic forcings by the
868 delta method or have first been translated into the required forcing variable by model simulations (see

869 section **2.4.3**). In the delta approach absolute simulated deviations from reference levels are added to the
 870 observed reference levels. The regional bias-adjustment is independent from the generation of the global
 871 de-biased forcing data.

872 In order to gauge the effects of these adjustments on the corresponding impact simulations, the protocol
 873 includes sensitivity experiments (**'de-biased'**) grounded on these adjusted CRF (see **Table 2**). The
 874 comparison of associated impact simulation to the default ones is expected to provide valuable insights
 875 into the effects of potential biases in the CRF. The 'de-biased' experiments are considered a starting point
 876 to develop methods to bias-adjust the oceanic forcings in further ISIMIP simulation rounds and make
 877 these simulations the default ones. Following the ISIMIP 'consistency framing' the bias-adjustment should
 878 also preserve the daily variability of the original GCM simulations to allow for a cross-sectoral integration
 879 on daily time scale. .

880 **2.4.1 Raw data without bias adjustment (default experiment)**

881 In ISIMIP3b, a set of physical and biogeochemical ocean variables nearly identical to that in ISIMIP3a is
 882 provided (see section **3.4, Table 8** of (Frieler et al., 2023) and **Table 8** below). These variables are obtained
 883 from the CMIP6 GCMs, which also supply the atmospheric forcing for ISIMIP3b, except for MRI-ESM2-0,
 884 which lacks bio-geochemical variables. In other models, only certain individual variables are missing (see
 885 **Table 8**). Obtaining both atmospheric and oceanic variables from the same set of GCMs ensures
 886 consistency between the fisheries and marine ecosystems sector and other ISIMIP sectors. The available
 887 variables in ISIMIP3b are interpolated from the native grids of the ocean models to a regular 1° grid. This
 888 resolution is comparatively lower than that of the ISIMIP3a ocean input data due to the generally reduced
 889 native resolution of CMIP6 GCM simulations compared to the ocean model used to generate the oceanic
 890 forcings based on observational atmospheric forcings for ISIMIP3a.

891
 892 **Table 8:** Oceanic climate-related forcing data provided within ISIMIP3b. Variables with suffixes -bot, -surf,
 893 and -vint were obtained from the seafloor, the top layer of the ocean, and vertical integration,
 894 respectively.

Variable	Variable specifier	Unit	Resolution	Datasets
Mass concentration of total phytoplankton expressed as chlorophyll	chl	kg m-3	1° grid, vertically resolved, monthly	GFDL-ESM4, IPSL-CM6A-LR, MPI-ESM1-2-HR, UKESM1-0-LL
Sea floor depth	deptho	m	1° grid, constant	GFDL-ESM4, IPSL-CM6A-LR, MPI-ESM1-2-HR, UKESM1-0-LL

Downward flux of particulate organic carbon	expc-bot	mol m ⁻² s ⁻¹	1° grid, monthly	GFDL-ESM4, IPSL-CM6A-LR, MPI-ESM1-2-HR, UKESM1-0-LL
Particulate organic carbon content	intpoc	kg m ⁻²	1° grid, monthly	GFDL-ESM4, MPI-ESM1-2-HR, UKESM1-0-LL
Net primary organic carbon production by all types of phytoplankton	intpp	mol m ⁻² s ⁻¹	1° grid, monthly	GFDL-ESM4, IPSL-CM6A-LR, MPI-ESM1-2-HR, UKESM1-0-LL
Net primary organic carbon production by diatoms	intppdiat	mol m ⁻² s ⁻¹	1° grid, monthly	GFDL-ESM4, IPSL-CM6A-LR, UKESM1-0-LL
Net Primary Organic Carbon Production by Other Phytoplankton	intppmisc	mol m ⁻² s ⁻¹	1° grid, monthly	GFDL-ESM4, IPSL-CM6A-LR, UKESM1-0-LL
Net Primary Mole Productivity of Carbon by Picophytoplankton	intpppico	mol m ⁻² s ⁻¹	1° grid, monthly	GFDL-ESM4
Net Primary Organic Carbon Production of Carbon by Diazotrophs	intppdiaz	mol m ⁻² s ⁻¹	1° grid, monthly	GFDL-ESM4, MPI-ESM1-2-HR
Mixed layer depth defined by delta rho = 0.125	mloststmax	m	1° grid, monthly	IPSL-CM6A-LR, MPI-ESM1-2-HR, UKESM1-0-LL
Dissolved oxygen concentration	o2, o2-bot, o2-surf	mol m ⁻³	1° grid, vertically resolved, ocean bottom and surface fields, monthly	GFDL-ESM4, IPSL-CM6A-LR, MPI-ESM1-2-HR, UKESM1-0-LL

pH	ph, ph-bot, ph-surf	1	1° grid, vertically resolved, ocean bottom and surface fields, monthly	GFDL-ESM4, IPSL-CM6A-LR, MPI-ESM1-2-HR, UKESM1-0-LL
Total phytoplankton carbon concentration	phyc, phyc-vint	mol m-3	1° grid, vertically resolved and vertically integrated, monthly	GFDL-ESM4, IPSL-CM6A-LR, MPI-ESM1-2-HR, UKESM1-0-LL
Concentration of diatoms expressed as carbon in sea water	phydiat, phydiat-vint	mol m-3	1° grid, vertically resolved and vertically integrated, monthly	GFDL-ESM4, IPSL-CM6A-LR, UKESM1-0-LL
Concentration of diazotrophs expressed as carbon in Sea Water	phydiaz, phydiaz-vint	mol m-3	1° grid, vertically resolved and vertically integrated, monthly	GFDL-ESM4, MPI-ESM1-2-HR
Mole Content of Miscellaneous Phytoplankton Expressed as Carbon in Sea Water	phymisc, phymisc-vint	mol m-2	1° grid, vertically resolved and vertically integrated, monthly	GFDL-ESM4, IPSL-CM6A-LR, MPI-ESM1-2-HR, UKESM1-0-LL
Mole Concentration of Picophytoplankton Expressed as Carbon in Sea Water	phypico, phypico-vint	mol m-3	1° grid, vertically resolved and vertically integrated, monthly	GFDL-ESM4
Net Downward Shortwave Radiation at Sea Water Surface	rsndts	W m-2	1° grid, monthly	GFDL-ESM4, IPSL-CM6A-LR, MPI-ESM1-2-HR
Sea Ice Area Fraction	siconc	%	1° grid, monthly	GFDL-ESM4, IPSL-CM6A-LR, MPI-ESM1-2-HR, UKESM1-0-LL

Sea water salinity	so, so-bot, so-surf	0.001	1° grid, vertically resolved, ocean bottom and surface fields, monthly	GFDL-ESM4, IPSL-CM6A-LR, MPI-ESM1-2-HR, UKESM1-0-LL
Sea water potential temperature	thetao	°C	1° grid, vertically resolved, monthly	GFDL-ESM4, IPSL-CM6A-LR, MPI-ESM1-2-HR, UKESM1-0-LL
Ocean model cell thickness	thkcello	m	1° grid, vertically resolved, monthly	GFDL-ESM4, IPSL-CM6A-LR, MPI-ESM1-2-HR, UKESM1-0-LL
Sea water potential temperature at sea floor (bottom)	tob	°C	1° grid, monthly	GFDL-ESM4, IPSL-CM6A-LR, MPI-ESM1-2-HR, UKESM1-0-LL
Sea surface temperature	tos	°C	1° grid, monthly	GFDL-ESM4, IPSL-CM6A-LR, MPI-ESM1-2-HR, UKESM1-0-LL
Sea water zonal velocity	uo	m s-1	1° grid, vertically resolved, monthly	IPSL-CM6A-LR, MPI-ESM1-2-HR, UKESM1-0-LL
Sea water meridional velocity	vo	m s-1	1° grid, vertically resolved, monthly	IPSL-CM6A-LR, MPI-ESM1-2-HR, UKESM1-0-LL
Concentration of mesozooplankton expressed as carbon in sea water	zmeso, zmeso-vint	mol m-3	1° grid, vertically resolved and vertically integrated, monthly	GFDL-ESM4, IPSL-CM6A-LR, UKESM1-0-LL
Concentration of microzooplankton expressed as carbon in sea water	zmicro, zmicro-vint	mol m-3	1° grid, vertically resolved and vertically integrated, monthly	GFDL-ESM4, IPSL-CM6A-LR, UKESM1-0-LL

Total Zooplankton Carbon Concentration	zooc, zooc-vint	mol m ⁻³	1° grid, vertically resolved and vertically integrated, monthly	GFDL-ESM4, IPSL-CM6A-LR, MPI-ESM1-2-HR, UKESM1-0-LL
--	------------------------	---------------------	---	---

895

896

2.4.2 Bias-adjusted global ocean forcings ('de-biased' sensitivity experiment)

897

898

899

900

901

902

903

904

905

906

907

908

909

910

911

912

913

914

915

916

917

918

919

920

GCMs have been shown to have limitations in accurately representing various aspects of the present climate system (Eyring et al., 2023), (Séférian et al., 2020), that are also expected to affect regional physical and biogeochemical oceanic projections (Li et al., 2016), (Tagliabue et al., 2021). In particular, biases in sea-surface temperature (SST, variable 'tos') and nutricline as well as thermocline depth influence oceanic primary productivity, which in turn has major influence on various marine ecosystem processes. Thus, reducing the substantial biases in GCMs' ocean variables through bias-adjustment is desirable. Typically, for bias-adjustment of atmospheric variables, statistical approaches are used where a transfer function is trained to map the simulated historical distribution of the relevant variables to the observed distribution and then applied to future simulations. Yet for oceanic variables, the scarcity of comprehensive sub-surface observational data globally does not allow for a similar, direct adjustment of the relevant variables. However, standalone ocean-biogeochemistry simulations, when driven by observation-based atmospheric reanalysis data, have been demonstrated to considerably alleviate SST-related biases and typically provide satisfactory simulations of the physical ocean and marine biogeochemistry for the historical period (e.g. (Tsuji et al., 2020), (Barrier et al., 2023)). Thus, an alternative process-oriented bias-adjustment approach has been developed that relies on a comprehensive ocean-biogeochemistry model that is forced by bias-adjusted atmospheric forcings. The adjustment of the ISIMIP3b oceanic forcings builds on such a dynamical de-biasing approach (Lengaigne et al., 2025), which relies on conducting forced oceanic simulations using the NEMO-PISCES physical-biogeochemical ocean model (Madec, 2015), which is the oceanic component of the IPSL-CM6A-LR climate model. The ocean model needs to be forced with high-frequency (3-hourly) surface momentum, heat and freshwater fluxes. Since from the CMIP6 pre-industrial, historical, and future scenario simulations used in ISIMIP3b these variables are only available at monthly resolution, additional steps are necessary to generate climatological high-frequency fluxes first. In the following, we first describe these preparatory steps, and then the de-biasing strategy, in more detail.

921

922

923

924

925

926

927

928

929

930

High-frequency surface flux forcing. Initially, a climatological simulation spanning the historical period from 1958 to 2022 is performed by forcing the ocean model NEMO-PISCES with a single repeating annual cycle representative of the 1990s' climate conditions sourced from the "Repeat Year Forcing" (RYF) from JRA55 reanalysis (Stewart et al., 2020). This simulation is driven using the CORE bulk formulae (Large W. G., 2004), incorporating all surface atmospheric variables at 3-hourly resolution from JRA55 RYF as inputs and storing 3-hourly momentum, heat and freshwater fluxes from this simulation. These 3-hourly JRA55 RYF fluxes are added to the monthly seasonal flux anomalies available from the ISIMIP3b climate models for the pre-industrial (picontrol), historical (historical) and future SSP1-2.6 (ssp126), SSP3-7.0 (ssp370), and SSP5-8.5 (ssp585) scenarios. In this way, 3-hourly surface flux forcings are created for all

931 ISIMIP3b scenarios. Notably, this procedure results in sub-monthly variability mirroring that of the JRA55
932 RYF, rather than the variability simulated by the coupled climate model. This means that any projected
933 changes in sub-monthly variability due to climate change are not integrated in the final de-biased product.
934 However, to date, marine ecosystem modellers have not analysed sub-monthly variability anyways (and
935 most marine ecosystem models are not suited to account for sub-monthly variability of forcings), making
936 this approach suitable.

937 Alternatively, de-biased ocean simulations including GCM-based sub-monthly variability could be
938 constructed by an alternative approach. In this scenario, 3-hourly surface atmospheric variables would be
939 extracted directly from each GCM simulation, rather than from JRA55 RYF forced oceanic simulations.
940 Forcing NEMO-PISCES with these variables using bulk formulae would once again produce the necessary
941 3-hourly surface fluxes, this time with variability consistent with the coupled GCM across all timescales.
942 This approach however requires running a separate ocean simulation for each GCM and scenario to derive
943 the surface fluxes, necessitating a much larger number of ocean model runs than the approach using
944 JRA55 RYF. In addition, the 3-hourly input from the GCMs is not available without gaps.

945

946 **De-biasing strategy.** The 3-hourly surface fluxes, constructed as described above, then serve as forcings
947 for another set of ocean model simulations. Notably, these simulations are not driven with bulk formulae
948 but directly with surface fluxes to enable an online implementation of the surface heat flux feedbacks
949 triggered by climate change into the forced ocean biogeochemistry model for historical and future
950 simulations (Lengaigne et al., 2025). For bias-adjustment, the part of the anomalous surface fluxes that
951 directly depends on climate change-induced SST warming is separated from the part that does not. Only
952 the latter part is used as a direct flux input to the ocean model, while the former is implemented within
953 NEMO-PISCES as an online relaxation to the warming signal from the debiased historical and future
954 simulations using a spatially and seasonally variable feedback damping coefficient. This SST feedback
955 coefficient, derived from observed surface variables, represents the Newtonian cooling negative feedback
956 related to latent heat fluxes through the Clausius-Clapeyron relationship and the negative feedback
957 related to upward long-wave radiation through Stefan's law (Zhang & Li, 2014) and the positive downward
958 longwave radiation feedback related to increasing temperature (Shakespeare & Roderick, 2022).
959 Application of this approach to the ocean model effectively reproduces the global SST changes simulated
960 by CMIP6 models, as demonstrated in (Lengaigne et al., 2025).

961 In this way, physical and biogeochemical ocean simulations are generated for picontrol and historical
962 climate forcings as well as for each of the future climate change scenarios, ensuring that the background
963 climatological state is constrained by the reanalysis, while still accounting for both interannual and long-
964 term climate variability simulated by the underlying GCM. Consequently, the resulting ocean-
965 biogeochemistry simulations considerably mitigate the strong present-day climatological biases identified
966 in the coupled models. Depending on data availability for the relevant monthly fluxes, this de-biasing
967 procedure can be applied to any climate model.

968 Additionally, to generate observation-based oceanic forcings for ISIMIP3a, a reference simulation is also
969 forced with the full JRA55 forcing (Tsujino et al., 2018) that includes observed inter-annual and decadal
970 variability. This oceanic forcing is expected to be a valuable additional CRF for impact model evaluation
971 within ISIMIP3a akin to the GFDL-MOM6-COBALT2 reanalysis-driven historical dataset used in ISIMIP3a

972 (Frieler et al., 2024a). The set of variables included in the de-biased dataset is a subset to the one in the
 973 raw GCM dataset (**Table 8**), detailed in **Table 9**.

974

975 **Table 9:** Bias-adjusted ocean data to be used by global impact models in the ‘de-biased’ sensitivity
 976 experiment in the fisheries and marine ecosystems sector

Variable	Variable specifier (variables in brackets are not directly available as model output but will have to be derived in post-processing)	Unit	Resolution	Forcing datasets
Mass concentration of total phytoplankton expressed as chlorophyll	chl	kg m ⁻³	1° grid, vertically resolved, monthly	JRA55+IPSL-CM6A-LR
Sea floor depth	deptho	m	1° grid, constant	JRA55+IPSL-CM6A-LR
Downward flux of particulate organic carbon	expc-bot	mol m ⁻² s ⁻¹	1° grid, monthly	JRA55+IPSL-CM6A-LR
Net primary organic carbon production by all types of phytoplankton	intpp	mol m ⁻² s ⁻¹	1° grid, monthly	JRA55+IPSL-CM6A-LR
Net primary organic carbon production by diatoms	intppdiat	mol m ⁻² s ⁻¹	1° grid, monthly	JRA55+IPSL-CM6A-LR
Net Primary Organic Carbon Production by Other Phytoplankton	intppmisc	mol m ⁻² s ⁻¹	1° grid, monthly	JRA55+IPSL-CM6A-LR
Mixed layer depth defined by delta rho = 0.125	mlotstmax	m	1° grid, monthly	JRA55+IPSL-CM6A-LR
Dissolved oxygen concentration	o2, (o2-bot), o2-surf	mol m ⁻³	1° grid, vertically resolved, ocean bottom and surface fields, monthly	JRA55+IPSL-CM6A-LR

pH	ph, (ph-bot), ph-surf	1	1° grid, vertically resolved, ocean bottom and surface fields, monthly	JRA55+IPSL-CM6A-LR
Total phytoplankton carbon concentration	phyc, (phyc-vint)	mol m-3	1° grid, vertically resolved and vertically integrated, monthly	JRA55+IPSL-CM6A-LR
Concentration of diatoms expressed as carbon in sea water	phydiat, (phydiat-vint)	mol m-3	1° grid, vertically resolved and vertically integrated, monthly	JRA55+IPSL-CM6A-LR
Mole Content of Miscellaneous Phytoplankton Expressed as Carbon in Sea Water	phymisc, (phymisc-vint)	mol m-2	1° grid, vertically resolved and vertically integrated, monthly	JRA55+IPSL-CM6A-LR
Net Downward Shortwave Radiation at Sea Water Surface	rsndts	W m-2	1° grid, monthly	JRA55+IPSL-CM6A-LR
Sea water salinity	so, (so-bot), so-surf	0.001	1° grid, vertically resolved, ocean bottom and surface fields, monthly	JRA55+IPSL-CM6A-LR
Sea water potential temperature	thetao	°C	1° grid, vertically resolved, monthly	JRA55+IPSL-CM6A-LR
Ocean model cell thickness	thkcello	m	1° grid, vertically resolved, monthly	JRA55+IPSL-CM6A-LR
Sea water potential temperature at sea floor (bottom)	(tob)	°C	1° grid, monthly	JRA55+IPSL-CM6A-LR
Sea surface temperature	tos	°C	1° grid, monthly	JRA55+IPSL-CM6A-LR
Sea water zonal velocity	uo	m s-1	1° grid, vertically resolved, monthly	JRA55+IPSL-CM6A-LR
Sea water meridional velocity	vo	m s-1	1° grid, vertically resolved, monthly	JRA55+IPSL-CM6A-LR

Concentration of mesozooplankton expressed as carbon in sea water	zmeso, (zmeso-vint)	mol m-3	1° grid, vertically resolved and vertically integrated, monthly	JRA55+IPSL-CM6A-LR
Concentration of microzooplankton expressed as carbon in sea water	zmicro, (zmicro-vint)	mol m-3	1° grid, vertically resolved and vertically integrated, monthly	JRA55+IPSL-CM6A-LR
Total Zooplankton Carbon Concentration	zooc, (zooc-vint)	mol m-3	1° grid, vertically resolved and vertically integrated, monthly	JRA55+IPSL-CM6A-LR

977

978 **2.4.3 Bias-adjusted regional ocean forcings ('de-biased' sensitivity experiment)**

979 Regional marine ecosystem models are most often calibrated to reproduce observed environmental
980 variables when driven by observed sea surface and bottom temperature, primary production
981 (phytoplankton production), and zooplankton biomass. However, that would still lead to biases in the
982 historical simulations if the impact model was forced by biased simulated input data instead of
983 observational data. To reduce this effect the GCM-based input data has been adjusted such that the
984 historical GCM simulations match observational data for certain regions (Eddy et al., 2025). The
985 adjustment is based on the delta approach where simulated and observational forcing data X_{sim} and X_{obs}
986 are averaged across a given historical reference period to determine the bias $\Delta = \text{mean}(X_{sim}) - \text{mean}$
987 (X_{obs}) that is then subtracted from the simulated forcing data. This method preserves the trend in the
988 forcing data and its internal variability. Some ocean forcing variables are not an exact match with variables
989 used in regional marine ecosystem models. For example, sea water potential temperature (θ_{sea}),
990 concentration of diatoms (phydiat-vint), or concentration of mesozooplankton (zmeso-vint) may first be
991 converted to other indicators that are then used as input for the regional marine ecosystem models. In
992 these cases the derived indicator is corrected using the delta method (see **Table 10**).

993 **Table 10:** Bias-adjusted ocean data to be used by regional impact models in the 'de-biased' sensitivity
994 experiment in the fisheries and marine ecosystems sector

Variable	Variable specifier	Unit	Resolution	Forcing datasets
Southern Benguela Current				

Net primary organic carbon production by all types of phytoplankton	intpp	mol m ⁻² s ⁻¹	1° grid, monthly	Corrected based on observed primary production for the southern Benguela current based on the delta method where the adjustment target is data from 1978 for the EwE model and 1990 for the Atlantis model
Sea water potential temperature	thetao	°C	1° grid, vertically resolved, monthly	Raw GCM temperature data converted to temperatures at 0-50, 50-100, 100-300 and 300-500 m according to the configuration for the southern Benguela Atlantis model, and 0-50 and 300-500 m for the EwE model.
Cook Strait				
Net primary organic carbon production by all types of phytoplankton	intpp	mol m ⁻² s ⁻¹	1° grid, monthly	Corrected based on observed primary production for Cook Strait using the delta method where observational target data is from 1950
East Bass Strait				
Net primary organic carbon production by all types of phytoplankton	intpp	mol m ⁻² s ⁻¹	1° grid, monthly	Corrected based on observed primary production for East Bass Strait using the delta method where observational target data is from 1994
East Bering Sea				
Concentration of diatoms expressed as carbon in sea water	phydiat-vint	mol m ⁻³	1/4° grid, vertically resolved and vertically integrated, monthly	Converted to phytoplankton size classes used in East Bering Sea mizer model then corrected using the delta method for the period 1982–1993
Concentration of diazotrophs expressed as carbon in sea water	phydiaz-vint	mol m ⁻³	1/4° grid, vertically resolved and vertically integrated, monthly	Converted to phytoplankton size classes used in East Bering Sea mizer model then corrected using the delta method for the period 1982–1993

Concentration of picoplankton expressed as carbon in sea water	phypico-vint	mol m-3	1/4° grid, vertically resolved and vertically integrated, monthly	Converted to phytoplankton size classes used in East Bering Sea mizer model then corrected using the delta method for the period 1982–1993
Concentration of mesozooplankton expressed as carbon in sea water	zmeso-vint	mol m-3	1/4° grid, vertically resolved and vertically integrated, monthly	Converted to zooplankton size classes used in East Bering Sea mizer model then corrected using the delta method for the period 1982–1993
Concentration of microzooplankton expressed as carbon in sea water	zmicro-vint	mol m-3	1/4° grid, vertically resolved and vertically integrated, monthly	Converted to zooplankton size classes used in East Bering Sea mizer model then corrected using the delta method for the period 1982–1993
Sea surface temperature	tos	°C	1/4° grid, monthly	Corrected based on configuration for the East Bering Sea mizer model using the delta method for the period 1982–1993
Hawai'i				
Concentration of diatoms expressed as carbon in sea water	phydiat-vint	mol m-3	1/4° grid, vertically resolved and vertically integrated, monthly	Converted to phytoplankton size classes used in Hawaii mizer model (Woodworth-Jefcoats, 2022) then corrected using the delta method
Concentration of diazotrophs expressed as carbon in sea water	phydiaz-vint	mol m-3	1/4° grid, vertically resolved and vertically integrated, monthly	Converted to phytoplankton size classes used in Hawaii mizer model then corrected using the delta method
Concentration of picoplankton expressed as carbon in sea water	phypico-vint	mol m-3	1/4° grid, vertically resolved and vertically integrated, monthly	Converted to phytoplankton size classes used in Hawaii mizer model then corrected using the delta method

Concentration of mesozooplankton expressed as carbon in sea water	zmeso-vint	mol m-3	1/4° grid, vertically resolved and vertically integrated, monthly	Converted to zooplankton size classes used in Hawaii mizer model then corrected using the delta method
Concentration of microzooplankton expressed as carbon in sea water	zmicro-vint	mol m-3	1/4° grid, vertically resolved and vertically integrated, monthly	Converted to zooplankton size classes used in Hawaii mizer model then corrected using the delta method
Sea water potential temperature	thetao	°C	1/4° grid, vertically resolved, monthly	Converted to temperature used in Hawaii Mizer model then corrected based on observed sea water potential temperature for Hawaii using the delta method from 1961–1980 with observed temperature data from the World Ocean Atlas

995

996

997

2.5 Future Lightning Data

998

For the ‘varlighting’ sensitivity experiment we provide temporally varying lightning density (strokes km⁻² day⁻¹) for the period 2015-2100 on monthly resolution (monthly mean of daily lightning stroke density) and the standard 0.5° global grid. This dataset may be used in a range of applications, for example, to understand the influence of lightning on wildfire ignition or atmospheric composition.

999

1000

1001

1002

The lightning density is derived from future climate simulations by UKESM1-0-LL and an empirical relationship between Convective Available Potential Energy (CAPE) and lightning strokes based on the WWLLN Global Lightning Climatology and time-series (WGLC) (Kaplan & Lau, 2021, 2022). Daily mean CAPE is calculated from non bias-adjusted air temperature, air pressure, and specific humidity on pressure levels from the surface to the top of the troposphere.

1003

1004

1005

1006

1007

The relationship between daily CAPE and daily lightning is estimated by linear regression of log-transformed CAPE derived from the GCM-calculated CAPE during the period of overlapping model output and observed daily lightning from WGLC (2015-2020) for each gridcell and month of the year. Where <10 observations of daily lightning were available over the calibration period, we used global mean regression parameters.

1008

1009

1010

1011

1012

The empirical relationships are applied to the daily CAPE data from the UKESM1-0-LL simulations for all three climate scenarios SSP1-2.6, SSP3-7.0, and SSP5-8.5. The associated lightning densities were monthly averaged. To maintain the spatial structure of lightning observed at present, lightning anomalies

1013

1014

1015 compared to the simulated 2015-2020 climatological reference were added to the observed present-day
 1016 lightning climatology from WGLC for 2015-2020. The ‘varlightning’ sensitivity experiment is assumed to
 1017 start from the default historical group I simulation, assuming the Flash Rate Monthly Climatology (Cecil,
 1018 2006), not changing with climate change.

1019
 1020

Table 11: Future lightning forcing data provided within ISIMIP3b.

Variable	Variable specifier	Unit	Resolution	Datasets
Monthly flash rate	lightning	km-2 d-1	0.5° grid, monthly	Derived from UKESM1-0-LL (SSP1-2.6, SSP3-7.0, and SSP5-8.5) using an empirical relationship between Convective Available Potential Energy (CAPE) and lightning densities (Kaplan et al., 2023).

1021
 1022
 1023

3 Conclusions

1024
 1025
 1026
 1027
 1028
 1029
 1030
 1031
 1032
 1033
 1034
 1035
 1036
 1037
 1038

This paper gives an overview over the ISIMIP3b, group I and II experiments and the provided climate-related forcing data sets. The simulations assuming fixed 2015 direct human forcings and a low (ssp126) and two high emission scenarios (ssp370 and ssp585) are designed to describe the impacts of different levels of climate change on present day natural and human systems. The set-up allows e.g. for testing to what degree the (bio-)physical impacts scale with global mean temperature change and could therefore be translated to other global warming pathways than the ones considered here. While a functional relationship between the considered impact indicator and global mean temperature change (or other climate variables) could be trained on ssp585 simulations because of the high warming levels reached, its performance could then be tested on ssp370 and ssp126. However, in such a setting it has to be taken into account that ssp370 is different from the other scenarios with regard to particularly high aerosol emissions and high decreases in forest areas going beyond the assumptions in the other models. So it has been shown that the increase of global mean precipitation with global warming is much weaker in SSP3-7.0 than in the other scenarios (Shiogama et al., 2023).

1039
 1040
 1041
 1042
 1043
 1044
 1045
 1046
 1047

This paper is intended to work as a catalogue where the climate impact modellers can find all relevant information about the climate-related forcings needed as reference for the impact model simulations generated within the CMIP6-based ISIMIP3b, group I (historical period) and group II (future projections). As a continuous process we would like to improve or complement these data sets wherever possible. So this paper can also be read as a call to either contribute by additional input data that allows other sectors to join the current simulation round or by methods that could be used to generate additional data sets for the next simulation round that will likely build on CMIP7 simulations. The following climate-related forcings have been identified as still missing and particularly critical to be added to a fourth simulation

1048 round of ISIMIP: i) temporally resolved lightning data accounting for changes in climate, ii) bias-adjusted
1049 oceanic forcing data, iii) projected coastal water levels in high temporal resolution accounting for
1050 extremes and representing the effects of long term sea level rise in line with the underlying global climate
1051 simulations, and v) ozone concentration fields in line with the GCM simulations. While a bias-adjustment
1052 of the oceanic forcings is already suggested in section 2.4.2, the approach does not preserve the daily
1053 variability of the raw oceanic forcings as it requires atmospheric surface flux only available in monthly
1054 resolution from the ISIMIP3b GCMs. To ensure the consistency on daily time scale, we have submitted an
1055 associated request for CMIP7 whose simulations will be used within the next round of ISIMIP. The
1056 generation of high resolution coastal water levels is ongoing research described in section 2.2.3. In
1057 particular the generation of the short term variability that will have to be added to the long term trends
1058 in water levels still has to be developed and prove to fulfill the demands. In addition, it would be great to
1059 also provide estimates of the extreme coastal water levels associated with the tropical cyclone tracks and
1060 wind fields we provide within ISIMIP3b (see section 2.2). There is a general demand for higher resolution
1061 CRF including both, the oceanic and the atmospheric components ideally accounting for heat island
1062 effects. As the ISIMIP CRF have to be globally consistent in the sense that they have to represent the daily
1063 variability of the underlying coarse resolution GCMs, we cannot use data from dynamical downscaling
1064 approaches using boundary conditions from different GCM runs as for example available through
1065 CORDEX. However, it seems to be appealing to harmonize the selection of the ISIMIP GCMs with a priority
1066 setting regarding the GCM-based boundary conditions within CORDEX.

1067
1068 The climate-related forcings described here are also provided as input for the new ISIMIP3b, group III
1069 simulations where the associated Direct Human Forcings (DHF) are not held constant at 2015 levels but
1070 are projected into the future in line with i) the population growth and economic development associated
1071 with the considered Shared Socioeconomic Pathways (SSPs) and mitigation measures required to reach
1072 the prescribed levels of climate forcings associated with the climate projections ('no adaptation'
1073 experiments) and ii) additionally accounting for the impacts of climate change ('adaptation' experiments).
1074 The collection of the associated DHF will be described in a separate paper.

1075
1076 **Code and data availability.** All generated ISIMIP3 climate-related forcing data described in this paper is
1077 publicly available at the [ISIMIP data repository](#). The repository is hosted by the Potsdam Institute for
1078 Climate Impact Research (PIK) e.V. which is part of the [TIB DOI Consortium](#) ensuring persistent, FAIR-
1079 compliant data publication, by committing to adhering to the [DataCite Consortium Agreement](#). This
1080 includes commitments to data persistence (§4 a.) as well as maintaining and updating metadata (§4 c.),
1081 which forbids "withdrawing content without posting a notification". In compliance with these rules a
1082 [system to document and trace back data issues](#) has been implemented in the repository to comply with
1083 this requirement. Additionally, should PIK be unable to continue hosting the ISIMIP repository, it will take
1084 responsibility for coordinating a timely transfer of the full repository and its DOI infrastructure to an
1085 appropriate, trusted archive or institutional partner to ensure uninterrupted access and citation
1086 continuity. DOIs are used to refer to datasets in a persistent way. Whenever a dataset is replaced a copy
1087 is kept on tape, and a new DOI is issued, while the old DOI is kept online with information on how to
1088 retrieve the archived data. Whenever we need to replace datasets, we will create a new version of the

1089 DOI, marked by a version number at the end. This ensures that every DOI references exactly the datasets,
1090 which were public at the time of registration. Detailed information can be found in the ISIMIP terms of
1091 use at <https://www.isimip.org/gettingstarted/terms-of-use/> (ISIMIP terms of use, 2023).

1092

1093

1094

1095 **Author contributions**

1096 KF lead the project and developed the concept with contributions from JS, MM, CO, CPOR, SH, JLB, CSH,
1097 CMP, TDE, KOC, CN, RH, DPT, OM, SJC, JJ, SR, GL, SC, EB, AGS, NS, JC, SH, CB, AG, FL, SNG, HMS, FH, TH,
1098 RM, DP, WT, DMB, RL, AIA, MF, MB, RR, and IDG. JV, MB, JK, IDVDV, LN, IJS supported the quality control
1099 and curation of the climate-related forcing data and the protocol development together with the sectoral
1100 ISIMIP coordinators listed as co-authors. SL developed the method and generated the downscaled and
1101 bias-adjusted atmospheric climate forcing data. MM and ST provided the description of the approach to
1102 generate the coastal water level data. ML provided the description of the method to bias-adjust the global
1103 oceanic forcings. TV, DQC, CYL, SJC, and KE provided TC data. JOK and AK provided the future lightning
1104 data. KF prepared the manuscript with contributions from all co-authors.

1105

1106 **Competing interests**

1107 At least one of the (co-)authors is a member of the editorial board of GMD

1108

1109 **Acknowledgements**

1110 This article is based upon work from COST Action CA19139 PROCLIAS (PROcess-based models for CLimate
1111 Impact Attribution across Sectors), supported by COST (European Cooperation in Science and Technology;
1112 <https://www.cost.eu>). SL received funding from the German Research Foundation (DFG, project number
1113 427397136). MB acknowledges funding from the BELSPO STEREO IV project SR/00/414. SC, AGS, MB and
1114 NS acknowledge funding through NERC NE/V01854X/1 (MOTHERSHIP). This research has received funding
1115 from the German Federal Ministry of Education and Research (BMBF) under the research projects QUIDIC
1116 (grant agreement no. 01LP1907A) and ISI-Access (16QK05), from the Horizon 2020 Framework
1117 Programme of the European Union under the project RECEIPT (grant agreement no. 820712) and from
1118 the Horizon Europe research and innovation programme under grant agreement No 101135481
1119 (COMPASS). C.-Y. L is supported by Palisades Geophysical Institute (PGI) Young Scientist Award. KOC
1120 acknowledges support from the National Research Foundation of South Africa (grant 136481) and the
1121 resources from the Cluster for High Performance Computing-CSIR. FL is supported by the National Key
1122 Research and Development Program of China (2022YFE0106500). DPT acknowledges funding from the
1123 Jarislowsky Foundation and NSERC. IDG acknowledges funding of the European Research Council (ERC
1124 Starting Grant, GROW-101041110).

1125

1126

1127

1128

1129 **References**

1130

- 1131 Adler, R. F., Huffman, G. J., Chang, A., Ferraro, R., Xie, P.-P., Janowiak, J., Rudolf, B., Schneider, U., Curtis,
1132 S., Bolvin, D., Gruber, A., Susskind, J., Arkin, P., & Nelkin, E. (2003). The Version-2 Global
1133 Precipitation Climatology Project (GPCP) Monthly Precipitation Analysis (1979–Present). *Journal of*
1134 *Hydrometeorology*, 4(6), 1147–1167. [https://doi.org/10.1175/1525-](https://doi.org/10.1175/1525-7541(2003)004<1147:TVGPCP>2.0.CO;2)
1135 [7541\(2003\)004<1147:TVGPCP>2.0.CO;2](https://doi.org/10.1175/1525-7541(2003)004<1147:TVGPCP>2.0.CO;2)
- 1136 Andela, B., Broetz, B., de Mora, L., Drost, N., Eyring, V., Koldunov, N., Lauer, A., Mueller, B., Predoi, V.,
1137 Righi, M., Schlund, M., Vegas-Regidor, J., Zimmermann, K., Adeniyi, K., Arnone, E., Bellprat, O., Berg,
1138 P., Bock, L., Caron, L.-P., ... Weigel, K. (2020b). *ESMValTool*.
1139 <https://doi.org/10.5281/zenodo.3970975>
- 1140 Andela, B., Broetz, B., Drost, N., Eyring, V., Koldunov, N., Lauer, A., Predoi, V., Righi, M., Schlund, M.,
1141 Zimmermann, K., Bock, L., Diblen, F., Dreyer, L., Earnshaw, P., Hassler, B., & Little, B. (2020a).
1142 *ESMValCore*. <https://doi.org/10.5281/zenodo.3952695>
- 1143 Barrier, N., Lengaigne, M., Rault, J., Person, R., Ethé, C., Aumont, O., & Maury, O. (2023). Mechanisms
1144 underlying the epipelagic ecosystem response to ENSO in the equatorial Pacific ocean. *Progress in*
1145 *Oceanography*, 213, 103002. <https://doi.org/10.1016/j.pocean.2023.103002>
- 1146 Bock, L., & Lauer, A. (2024). Cloud properties and their projected changes in CMIP models with low to
1147 high climate sensitivity. *Atmospheric Chemistry and Physics*, 24(3), 1587–1605.
1148 <https://doi.org/10.5194/acp-24-1587-2024>
- 1149 Bock, L., Lauer, A., Schlund, M., Barreiro, M., Bellouin, N., Jones, C., Meehl, G. A., Predoi, V., Roberts, M.
1150 J., & Eyring, V. (2020). Quantifying progress across different CMIP phases with the ESMValTool.
1151 *Journal of Geophysical Research*, 125(21). <https://doi.org/10.1029/2019jd032321>
- 1152 Boucher, O., Denvil, S., Levvasseur, G., Cozic, A., Caubel, A., Foujols, M.-A., Meurdesoif, Y., Cadule, P.,

1153 Devilliers, M., Dupont, E., & Lurton, T. (2019). *IPSL IPSL-CM6A-LR model output prepared for CMIP6*
1154 *ScenarioMIP* [Dataset]. Earth System Grid Federation. <https://doi.org/10.22033/ESGF/CMIP6.1532>

1155 Boucher, O., Denvil, S., Levavasseur, G., Cozic, A., Caubel, A., Foujols, M.-A., Meurdesoif, Y., Cadule, P.,
1156 Devilliers, M., Ghattas, J., Lebas, N., Lurton, T., Mellul, L., Musat, I., Mignot, J., & Cheruy, F. (2018).
1157 *IPSL IPSL-CM6A-LR model output prepared for CMIP6 CMIP* [Dataset]. Earth System Grid Federation.
1158 <https://doi.org/10.22033/ESGF/CMIP6.1534>

1159 Boucher, O., Servonnat, J., Albright, A. L., Aumont, O., Balkanski, Y., Bastrikov, V., Bekki, S., Bonnet, R.,
1160 Bony, S., Bopp, L., Braconnot, P., Brockmann, P., Cadule, P., Caubel, A., Cheruy, F., Codron, F., Cozic,
1161 A., Cugnet, D., D'Andrea, F., ... Vuichard, N. (2020). Presentation and evaluation of the IPSL-CM6A-
1162 LR climate model. *Journal of Advances in Modeling Earth Systems*, *12*(7).
1163 <https://doi.org/10.1029/2019ms002010>

1164 Büchner, M., & Reyer, C. (2022). *ISIMIP3b atmospheric composition input data* [Dataset]. ISIMIP
1165 Repository. <https://doi.org/10.48364/ISIMIP.482153.1>

1166 Buck, A. L. (1981). New Equations for Computing Vapor Pressure and Enhancement Factor. *Journal of*
1167 *Applied Meteorology and Climatology*, *20*(12), 1527–1532. [https://doi.org/10.1175/1520-0450\(1981\)020<1527:NEFCVP>2.0.CO;2](https://doi.org/10.1175/1520-0450(1981)020<1527:NEFCVP>2.0.CO;2)

1169 Camargo, S. J., Tippett, M. K., Sobel, A. H., Vecchi, G. A., & Zhao, M. (2014). Testing the Performance of
1170 Tropical Cyclone Genesis Indices in Future Climates Using the HiRAM Model. *Journal of Climate*,
1171 *27*(24), 9171–9196. <https://doi.org/10.1175/JCLI-D-13-00505.1>

1172 Cannon, A. J. (2018). Multivariate quantile mapping bias correction: an N-dimensional probability
1173 density function transform for climate model simulations of multiple variables. *Climate Dynamics*,
1174 *50*(1), 31–49. <https://doi.org/10.1007/s00382-017-3580-6>

1175 Cecil, D. (2006). *LIS/OTD 0.5 Degree High Resolution Monthly Climatology (HRMC)* [Dataset]. NASA
1176 Global Hydrometeorology Resource Center DAAC. <https://doi.org/10.5067/LIS/LIS-OTD/DATA303>

1177 Cucchi, M., Weedon, G. P., Amici, A., Bellouin, N., Lange, S., Müller Schmied, H., Hersbach, H., &
1178 Buontempo, C. (2020). WFDE5: bias-adjusted ERA5 reanalysis data for impact studies. *Earth System*
1179 *Science Data*, 12(3), 2097–2120. <https://doi.org/10.5194/essd-12-2097-2020>

1180 Dunne, J. P., Horowitz, L. W., Adcroft, A. J., Ginoux, P., Held, I. M., John, J. G., Krasting, J. P., Malyshev, S.,
1181 Naik, V., Paulot, F., Shevliakova, E., Stock, C. A., Zadeh, N., Balaji, V., Blanton, C., Dunne, K. A.,
1182 Dupuis, C., Durachta, J., Dussin, R., ... Zhao, M. (2020). The GFDL earth system model version 4.1
1183 (GFDL-ESM 4.1): Overall coupled model description and simulation characteristics. *Journal of*
1184 *Advances in Modeling Earth Systems*, 12(11). <https://doi.org/10.1029/2019ms002015>

1185 Durack, P. J. (n.d.). *CMIP6 source_id values*. Retrieved January 16, 2023, from [https://wcrp-](https://wcrp-cmip.github.io/CMIP6_CVs/docs/CMIP6_source_id.html)
1186 [cmip.github.io/CMIP6_CVs/docs/CMIP6_source_id.html](https://wcrp-cmip.github.io/CMIP6_CVs/docs/CMIP6_source_id.html)

1187 Eddy, T. D., Heneghan, R. F., Bryndum-Buchholz, A., Fulton, E. A., Harrison, C. S., Tittensor, D. P., Lotze,
1188 H. K., Ortega-Cisneros, K., Novaglio, C., Bianchi, D., Büchner, M., Bulman, C., Cheung, W. W. L.,
1189 Christensen, V., Coll, M., Everett, J. D., Fierro-Arcos, D., Galbraith, E. D., Gascuel, D., ... Blanchard, J.
1190 L. (2025). Global and regional marine ecosystem models reveal key uncertainties in climate change
1191 projections. *Earth's Future*, 13(3). <https://doi.org/10.1029/2024ef005537>

1192 Emanuel, K., DesAutels, C., Holloway, C., & Korty, R. (2004). Environmental Control of Tropical Cyclone
1193 Intensity. *Journal of the Atmospheric Sciences*, 61(7), 843–858. [https://doi.org/10.1175/1520-](https://doi.org/10.1175/1520-0469(2004)061<0843:ECOTCI>2.0.CO;2)
1194 [0469\(2004\)061<0843:ECOTCI>2.0.CO;2](https://doi.org/10.1175/1520-0469(2004)061<0843:ECOTCI>2.0.CO;2)

1195 Emanuel, K., Quesada-Chacón, D., Novak, L., & Otto, C. (2025). *ISIMIP3b tropical cyclone tracks (MIT)*
1196 [Dataset]. ISIMIP Repository. <https://doi.org/10.48364/ISIMIP.682793>

1197 Emanuel, K., Sundararajan, R., & Williams, J. (2008). Hurricanes and Global Warming: Results from
1198 Downscaling IPCC AR4 Simulations. *Bulletin of the American Meteorological Society*, 89(3), 347–
1199 368. <https://doi.org/10.1175/BAMS-89-3-347>

1200 Eyring, V., Bony, S., Meehl, G. A., Senior, C. A., Stevens, B., Stouffer, R. J., & Taylor, K. E. (2016). Overview

1201 of the Coupled Model Intercomparison Project Phase 6 (CMIP6) experimental design and
1202 organization. *Geoscientific Model Development*, 9(5), 1937–1958. [https://doi.org/10.5194/gmd-9-](https://doi.org/10.5194/gmd-9-1937-2016)
1203 1937-2016

1204 Eyring, V., Gillett, N. P., Achuta Rao, K. M., Barimalala, R., Barreiro Parrillo, M., Bellouin, N., V. Masson-
1205 Delmotte, P. Zhai, A. Pirani, S. L. Connors, C. Péan, S. Berger, & Intergovernmental Panel on Climate
1206 Change (IPCC). (2023). Human Influence on the Climate System. In *Climate Change 2021 – The*
1207 *Physical Science Basis: Working Group I Contribution to the Sixth Assessment Report of the*
1208 *Intergovernmental Panel on Climate Change* (pp. 423–552). Cambridge University Press.
1209 <https://doi.org/10.1017/9781009157896.005>

1210 Forster, P., Storelvmo, T., Armour, K., Collins, W., Dufresne, J.-L., Frame, D., Lunt, D. J., Mauritsen, T.,
1211 Palmer, Watanabe, M., Wild, M., & Zhang, H. (2021). The earth’s energy budget, climate feedbacks
1212 and climate sensitivity. In *Climate Change 2021 – The Physical Science Basis* (pp. 923–1054).
1213 Cambridge University Press. <https://doi.org/10.1017/9781009157896.009>

1214 Fosu, B., Sobel, A., Camargo, S., Tippet, M., Hemmati, M., Bowen, S., & Bloemendaal, N. (2024).
1215 Assessing future tropical cyclone risk using downscaled 1 CMIP6 projections. *Journal of Catastrophe*
1216 *Risk and Resilience*, 2(1). <https://doi.org/10.63024/dpva-2pa1>

1217 Frieler, K., Lange, S., Piontek, F., Reyer, C. P. O., Schewe, J., Warszawski, L., Zhao, F., Chini, L., Denvil, S.,
1218 Emanuel, K., Geiger, T., Halladay, K., Hurtt, G., Mengel, M., Murakami, D., Ostberg, S., Popp, A.,
1219 Riva, R., Stevanovic, M., ... Yamagata, Y. (2017). Assessing the impacts of 1.5 °C global warming –
1220 simulation protocol of the Inter-Sectoral Impact Model Intercomparison Project (ISIMIP2b).
1221 *Geoscientific Model Development*, 10(12), 4321–4345. <https://doi.org/10.5194/gmd-10-4321-2017>

1222 Frieler, K., Volkholz, J., Lange, S., Schewe, J., Mengel, M., del Rocío Rivas López, M., Otto, C., Reyer, C. P.
1223 O., Karger, D. N., & del Valle Gitta Lasslop Sarah Chadburn Eleanor Burke Angela Gallego-Sala Noah
1224 Smith Jinfeng Chang Stijn Hantson Chantelle Burton Anne Gädeke Fang Li Simon N. Gosling Hannes

1225 Müller Schmied Fred Hattermann Jida Wang Fangfang Yao Thomas Hickler Rafael Marcé Don
1226 Pierson Wim Thiery Daniel Mercado-Bettín Robert Ladwig Ana Isabel Ayala-Zamora Matthew
1227 Forrest and Michel Bechtold, J. T. M. S. T. C. M. J. L. B. C. S. H. C. M. P. T. D. E. K. O.-C. C. N. Y. R. R.
1228 A. W. C. S. X. L. R. H. D. T. O. M. M. B. T. V. T. W. F. S. I. J. S. J. K. I. V. J. J. C. M. S. R. J. K. I. D. V.
1229 (2024, January 4). *Scenario setup and forcing data for impact model evaluation and impact*
1230 *attribution within the third round of the Inter-Sectoral Model Intercomparison Project (ISIMIP3a).*
1231 Geoscientific Model Development. [https://www.google.com/url?q=https://doi.org/10.5194/gmd-](https://www.google.com/url?q=https://doi.org/10.5194/gmd-17-1-2024&sa=D&source=docs&ust=1704377607845951&usg=AOvVaw3hFVXAV75ZSOClc8itQfEs)
1232 [17-1-2024&sa=D&source=docs&ust=1704377607845951&usg=AOvVaw3hFVXAV75ZSOClc8itQfEs](https://www.google.com/url?q=https://doi.org/10.5194/gmd-17-1-2024&sa=D&source=docs&ust=1704377607845951&usg=AOvVaw3hFVXAV75ZSOClc8itQfEs)
1233 Frieler, K., Volkholz, J., Lange, S., Schewe, J., Mengel, M., Otto, C., Reyer, C. P. O., Karger, D. N., Malle, J.
1234 T., Treu, S., Menz, C., Blanchard, J. L., Harrison, C. S., Petrik, C. M., Eddy, T. D., Ortega-Cisneros, K.,
1235 Novaglio, C., Rousseau, Y., Watson, R. A., ... Bechtold, M. (2024a). Scenario setup and forcing data
1236 for impact model evaluation and impact attribution within the third round of the Inter-Sectoral
1237 Impact Model Intercomparison Project (ISIMIP3a). *Geoscientific Model Development*, 17(1), 1–51.
1238 <https://doi.org/10.5194/gmd-17-1-2024>
1239 Frieler, K., Volkholz, J., Lange, S., Schewe, J., Mengel, M., Rivas López, M. del R., Otto, C., Reyer, C. P. O.,
1240 Karger, D. N., Malle, J. T., Treu, S., Menz, C., Blanchard, J. L., Harrison, C. S., Petrik, C. M., Eddy, T.
1241 D., Ortega-Cisneros, K., Novaglio, C., Rousseau, Y., ... Bechtold, M. (2023). Scenario set-up and
1242 forcing data for impact model evaluation and impact attribution within the third round of the Inter-
1243 Sectoral Model Intercomparison Project (ISIMIP3a). In *EGUsphere*.
1244 <https://doi.org/10.5194/egusphere-2023-281>
1245 Geiger, T., Gütschow, J., Bresch, D. N., Emanuel, K., & Frieler, K. (2021). Double benefit of limiting global
1246 warming for tropical cyclone exposure. *Nature Climate Change*, 11(10), 861–866.
1247 <https://doi.org/10.1038/s41558-021-01157-9>
1248 Gennaretti, F., Sangelantoni, L., & Grenier, P. (2015). Toward daily climate scenarios for Canadian Arctic

1249 coastal zones with more realistic temperature-precipitation interdependence. *JGR: Atmospheres*,
1250 120(23), 11,862–11,877. <https://doi.org/10.1002/2015JD023890>

1251 Gillett, N. P., Shiogama, H., Funke, B., Hegerl, G., Knutti, R., Matthes, K., Santer, B. D., Stone, D., &
1252 Tebaldi, C. (2016). The detection and Attribution Model Intercomparison Project (DAMIP v1.0)
1253 contribution to CMIP6. *Geoscientific Model Development*, 9(10), 3685–3697.
1254 <https://doi.org/10.5194/gmd-9-3685-2016>

1255 Good, P., Sellar, A., Tang, Y., Rumbold, S., Ellis, R., Kelley, D., Kuhlbrodt, T., & Walton, J. (2019). *MOHC*
1256 *UKESM1.0-LL model output prepared for CMIP6 ScenarioMIP* [Dataset]. Earth System Grid
1257 Federation. <https://doi.org/10.22033/ESGF/CMIP6.1567>

1258 Gregory, J. M., Griffies, S. M., Hughes, C. W., Lowe, J. A., Church, J. A., Fukimori, I., Gomez, N., Kopp, R.
1259 E., Landerer, F., Cozannet, G. L., Ponte, R. M., Stammer, D., Tamisiea, M. E., & van de Wal, R. S. W.
1260 (2019). Concepts and terminology for sea level: Mean, variability and change, both local and global.
1261 *Surveys in Geophysics*, 40(6), 1251–1289. <https://doi.org/10.1007/s10712-019-09525-z>

1262 Grenier, P. (2018). Two Types of Physical Inconsistency to Avoid with Univariate Quantile Mapping: A
1263 Case Study over North America Concerning Relative Humidity and Its Parent Variables. *Journal of*
1264 *Applied Meteorology and Climatology*, 57(2), 347–364. <https://doi.org/10.1175/JAMC-D-17-0177.1>

1265 Haerter, J. O., Hagemann, S., Moseley, C., & Piani, C. (2011). Climate model bias correction and the role
1266 of timescales. *Hydrology and Earth System Sciences*, 15(3), 1065–1079.
1267 <https://doi.org/10.5194/hess-15-1065-2011>

1268 Hausfather, Z., & Peters, G. P. (2020, January 29). *Emissions – the “business as usual” story is misleading*.
1269 Nature Publishing Group UK. <https://doi.org/10.1038/d41586-020-00177-3>

1270 Hersbach, H., Bell, B., Berrisford, P., Hirahara, S., Horányi, A., Muñoz-Sabater, J., Nicolas, J., Peubey, C.,
1271 Radu, R., Schepers, D., Simmons, A., Soci, C., Abdalla, S., Abellan, X., Balsamo, G., Bechtold, P.,
1272 Biavati, G., Bidlot, J., Bonavita, M., ... Jean-Noël Thépaut. (2020). The ERA5 global reanalysis.

1273 *Quarterly Journal of the Royal Meteorological Society*, 146(730), 1999–2049.

1274 <https://doi.org/10.1002/qj.3803>

1275 Holland. (1980). An Analytic Model of the Wind and Pressure Profiles in Hurricanes, *Mon. Weather*

1276 *Rev*, 108, 1212–1218.

1277 Holland. (2008). A revised hurricane pressure–wind model. *Monthly Weather Review*, 136(9), 3432–

1278 3445. <https://doi.org/10.1175/2008mwr2395.1>

1279 *ISIMIP3b simulation protocol*. (2023). <https://protocol.isimip.org/>

1280 Jägermeyr, J., Müller, C., Ruane, A. C., Elliott, J., Balkovic, J., Castillo, O., Faye, B., Foster, I., Folberth, C.,

1281 Franke, J. A., Fuchs, K., Guarin, J. R., Heinke, J., Hoogenboom, G., Iizumi, T., Jain, A. K., Kelly, D.,

1282 Khabarov, N., Lange, S., ... Rosenzweig, C. (2021). Climate impacts on global agriculture emerge

1283 earlier in new generation of climate and crop models. *Nature Food*, 2(11), 873–885.

1284 <https://doi.org/10.1038/s43016-021-00400-y>

1285 John, J. G., Blanton, C., McHugh, C., Radhakrishnan, A., Rand, K., Vahlenkamp, H., Wilson, C., Zadeh, N.

1286 T., Dunne, J. P., Dussin, R., Horowitz, L. W., Krasting, J. P., Lin, P., Malyshev, S., Naik, V., Ploshay, J.,

1287 Shevliakova, E., Silvers, L., Stock, C., ... Zeng, Y. (2018). *NOAA-GFDL GFDL-ESM4 model output*

1288 *prepared for CMIP6 ScenarioMIP* [Dataset]. Earth System Grid Federation.

1289 <https://doi.org/10.22033/ESGF/CMIP6.1414>

1290 Jungclaus, J., Bittner, M., Wieners, K.-H., Wachsmann, F., Schupfner, M., Legutke, S., Giorgetta, M.,

1291 Reick, C., Gayler, V., Haak, H., de Vrese, P., Raddatz, T., Esch, M., Mauritsen, T., von Storch, J.-S.,

1292 Behrens, J., Brovkin, V., Claussen, M., Crueger, T., ... Roeckner, E. (2019). *MPI-M MPIESM1.2-HR*

1293 *model output prepared for CMIP6 CMIP* [Dataset]. Earth System Grid Federation.

1294 <https://doi.org/10.22033/ESGF/CMIP6.741>

1295 Kaplan, J. O., Koch, A., & Lau, K. H.-K. (2023). *Estimated future global lightning strokes (2010-2100)*.

1296 <https://doi.org/10.5281/zenodo.7511843>

1297 Kaplan, J. O., & Lau, K. H.-K. (2021). The WGLC global gridded lightning climatology and time series.
1298 *Earth System Science Data*, 13(7), 3219–3237. <https://doi.org/10.5194/essd-13-3219-2021>

1299 Kaplan, J. O., & Lau, K. H.-K. (2022). World Wide Lightning Location Network (WWLLN) Global Lightning
1300 Climatology (WGLC) and time series, 2022 update. *Earth System Science Data*, 14(12), 5665–5670.
1301 <https://doi.org/10.5194/essd-14-5665-2022>

1302 Krasting, J. P., John, J. G., Blanton, C., McHugh, C., Nikonov, S., Radhakrishnan, A., Rand, K., Zadeh, N. T.,
1303 Balaji, V., Durachta, J., Dupuis, C., Menzel, R., Robinson, T., Underwood, S., Vahlenkamp, H., Dunne,
1304 K. A., Gauthier, P. P. G., Ginoux, P., Griffies, S. M., ... Zhao, M. (2018). *NOAA-GFDL GFDL-ESM4*
1305 *model output prepared for CMIP6 CMIP* [Dataset]. Earth System Grid Federation.
1306 <https://doi.org/10.22033/ESGF/CMIP6.1407>

1307 Lange, S. (2017). *ISIMIP2b Bias-Correction Code*. <https://doi.org/10.5281/zenodo.1069050>

1308 Lange, S. (2018). Bias correction of surface downwelling longwave and shortwave radiation for the
1309 EWEMBI dataset. *Earth System Dynamics*, 9(2), 627–645. <https://doi.org/10.5194/esd-9-627-2018>

1310 Lange, S. (2019a). *Earth2Observe, WFDEI and ERA-interim data merged and bias-corrected for ISIMIP*
1311 *(EWEMBI)* [Dataset]. <https://doi.org/10.5880/pik.2019.004>

1312 Lange, S. (2019b). Trend-preserving bias adjustment and statistical downscaling with ISIMIP3BASD
1313 (v1.0). *Geoscientific Model Development*, 12(7), 3055–3070. [https://doi.org/10.5194/gmd-12-3055-](https://doi.org/10.5194/gmd-12-3055-2019)
1314 2019

1315 Lange, S. (2021a). *ISIMIP3BASD*. <https://doi.org/10.5281/zenodo.4686991>

1316 Lange, S. (2021b). *ISIMIP3b bias adjustment fact sheet*.
1317 https://www.isimip.org/documents/413/ISIMIP3b_bias_adjustment_fact_sheet_Gnsz7CO.pdf

1318 Lange, S., & Büchner, M. (2021). *ISIMIP3b bias-adjusted atmospheric climate input data* [Dataset]. ISIMIP
1319 Repository. <https://doi.org/10.48364/ISIMIP.842396.1>

1320 Lange, S., Menz, C., Gleixner, S., Cucchi, M., Weedon, G. P., Amici, A., Bellouin, N., Schmied, H. M.,

1321 Hersbach, H., Buontempo, C., & Cagnazzo, C. (2021). *WFDE5 over land merged with ERA5 over the*
1322 *ocean (W5E5 v2.0)* [Dataset]. ISIMIP Repository. <https://doi.org/10.48364/ISIMIP.342217>

1323 Lange, S., Quesada-Chacón, D., & Büchner, M. (2023). *Secondary ISIMIP3b bias-adjusted atmospheric*
1324 *climate input data* [Dataset]. ISIMIP Repository. <https://doi.org/10.48364/ISIMIP.581124.3>

1325 Lan, X., Tans, P., & Thoning, K. W. (2023). *Trends in globally-averaged CO2 determined from NOAA*
1326 *Global Monitoring Laboratory measurements. Version 2023-01 NOAA/GML* [Dataset].
1327 <https://gml.noaa.gov/ccgg/trends/>

1328 Large W. G., A. S. G. Y. (2004). *Diurnal to decadal global forcing for ocean and sea ice models: the data*
1329 *sets and flux climatologies* (No. NCAR/TN460+STR). CGD Division of the National Centre for
1330 Atmospheric Research (NCAR). [https://www.researchgate.net/profile/Stephen-](https://www.researchgate.net/profile/Stephen-Yeager/publication/281588002_Diurnal_to_Decadal_Global_Forcing_for_Ocean_and_Sea-Ice_Models_The_Data_Sets_and_Flux_Climatologies/links/55eede7108ae199d47bfaf41/Diurnal-to-Decadal-Global-Forcing-for-Ocean-and-Sea-Ice-Models-The-Data-Sets-and-Flux-Climatologies.pdf)
1331 [Yeager/publication/281588002_Diurnal_to_Decadal_Global_Forcing_for_Ocean_and_Sea-](https://www.researchgate.net/profile/Stephen-Yeager/publication/281588002_Diurnal_to_Decadal_Global_Forcing_for_Ocean_and_Sea-Ice_Models_The_Data_Sets_and_Flux_Climatologies/links/55eede7108ae199d47bfaf41/Diurnal-to-Decadal-Global-Forcing-for-Ocean-and-Sea-Ice-Models-The-Data-Sets-and-Flux-Climatologies.pdf)
1332 [Ice_Models_The_Data_Sets_and_Flux_Climatologies/links/55eede7108ae199d47bfaf41/Diurnal-](https://www.researchgate.net/profile/Stephen-Yeager/publication/281588002_Diurnal_to_Decadal_Global_Forcing_for_Ocean_and_Sea-Ice_Models_The_Data_Sets_and_Flux_Climatologies/links/55eede7108ae199d47bfaf41/Diurnal-to-Decadal-Global-Forcing-for-Ocean-and-Sea-Ice-Models-The-Data-Sets-and-Flux-Climatologies.pdf)
1333 [to-Decadal-Global-Forcing-for-Ocean-and-Sea-Ice-Models-The-Data-Sets-and-Flux-](https://www.researchgate.net/profile/Stephen-Yeager/publication/281588002_Diurnal_to_Decadal_Global_Forcing_for_Ocean_and_Sea-Ice_Models_The_Data_Sets_and_Flux_Climatologies/links/55eede7108ae199d47bfaf41/Diurnal-to-Decadal-Global-Forcing-for-Ocean-and-Sea-Ice-Models-The-Data-Sets-and-Flux-Climatologies.pdf)
1334 [Climatologies.pdf](https://www.researchgate.net/profile/Stephen-Yeager/publication/281588002_Diurnal_to_Decadal_Global_Forcing_for_Ocean_and_Sea-Ice_Models_The_Data_Sets_and_Flux_Climatologies/links/55eede7108ae199d47bfaf41/Diurnal-to-Decadal-Global-Forcing-for-Ocean-and-Sea-Ice-Models-The-Data-Sets-and-Flux-Climatologies.pdf)

1335 Lee, C.-Y., Camargo, S. J., Sobel, A. H., & Tippett, M. K. (2020). Statistical–Dynamical Downscaling
1336 Projections of Tropical Cyclone Activity in a Warming Climate: Two Diverging Genesis Scenarios.
1337 *Journal of Climate*, 33(11), 4815–4834. <https://doi.org/10.1175/JCLI-D-19-0452.1>

1338 Lee, C.-Y., Camargo, S. J., Sobel, A., Tippett, M. K., Quesada-Chacón, D., Büchner, M., Novak, L., & Otto,
1339 C. (2025). *ISIMIP3b tropical cyclone tracks (CHAZ)* [Dataset]. ISIMIP Repository.
1340 <https://doi.org/10.48364/ISIMIP.808980>

1341 Lee, C.-Y., Tippett, M. K., Camargo, S. J., & Sobel, A. H. (2015). Probabilistic Multiple Linear Regression
1342 Modeling for Tropical Cyclone Intensity. *Monthly Weather Review*, 143(3), 933–954.
1343 <https://doi.org/10.1175/MWR-D-14-00171.1>

1344 Lee, C.-Y., Tippett, M. K., Sobel, A. H., & Camargo, S. J. (2016). Rapid intensification and the bimodal

1345 distribution of tropical cyclone intensity. *Nature Communications*, 7, 10625.
1346 <https://doi.org/10.1038/ncomms10625>

1347 Lee, C.-Y., Tippett, M. K., Sobel, A. H., & Camargo, S. J. (2018). An environmentally forced tropical
1348 cyclone hazard model. *Journal of Advances in Modeling Earth Systems*, 10(1), 223–241.
1349 <https://doi.org/10.1002/2017ms001186>

1350 Lengaigne, M., Pang, S., Silvy, Y., Danielli, V., Gopika, S., Sadhvi, K., Dutheil, C., Rousset, C., Ethé, C.,
1351 Person, R., Madec, G., Barrier, N., Maury, O., Dalaut, L., Menkes, C., Nicol, S., Gorgues, T., Melet, A.,
1352 & Guihou, K. (2025). Vialard: An ocean modelling framework for mitigating oceanic projections
1353 from global climate models present-day biases. In *Earth future*.

1354 Liang, Y., Gillett, N. P., & Monahan, A. H. (2024). Accounting for Pacific climate variability increases
1355 projected global warming. *Nature Climate Change*, 14(6), 608–614.
1356 <https://doi.org/10.1038/s41558-024-02017-y>

1357 Li, G., Xie, S.-P., Du, Y., & Luo, Y. (2016). Effects of excessive equatorial cold tongue bias on the
1358 projections of tropical Pacific climate change. Part I: the warming pattern in CMIP5 multi-model
1359 ensemble. *Climate Dynamics*, 47(12), 3817–3831. <https://doi.org/10.1007/s00382-016-3043-5>

1360 Madec, G. (2015). NEMO ocean engine, Version 3.6 stable Note du Pole de modelisation de l'Institut
1361 Pierre-Simon Laplace, vol. 27. *IPSL, Paris: France*.

1362 Maraun, D. (2013). Bias Correction, Quantile Mapping, and Downscaling: Revisiting the Inflation Issue.
1363 *Journal of Climate*, 26(6), 2137–2143. <https://doi.org/10.1175/JCLI-D-12-00821.1>

1364 Mauritsen, T., Bader, J., Becker, T., Behrens, J., Bittner, M., Brokopf, R., Brovkin, V., Claussen, M.,
1365 Crueger, T., Esch, M., Fast, I., Fiedler, S., Fläschner, D., Gayler, V., Giorgetta, M., Goll, D. S., Haak, H.,
1366 Hagemann, S., Hedemann, C., ... Roeckner, E. (2019). Developments in the MPI-M Earth System
1367 Model version 1.2 (MPI-ESM1.2) and Its Response to Increasing CO₂. *Journal of Advances in
1368 Modeling Earth Systems*, 11(4), 998–1038. <https://doi.org/10.1029/2018MS001400>

1369 Meehl, G. A., Senior, C. A., Eyring, V., Flato, G., Lamarque, J.-F., Stouffer, R. J., Taylor, K. E., & Schlund, M.
1370 (2020). Context for interpreting equilibrium climate sensitivity and transient climate response from
1371 the CMIP6 Earth system models. *Science Advances*, 6(26), eaba1981.
1372 <https://doi.org/10.1126/sciadv.aba1981>

1373 Meiler, S., Vogt, T., Bloemendaal, N., Ciullo, A., Lee, C.-Y., Camargo, S. J., Emanuel, K., & Bresch, D. N.
1374 (2022). Intercomparison of regional loss estimates from global synthetic tropical cyclone models.
1375 *Nature Communications*, 13(1), 6156. <https://doi.org/10.1038/s41467-022-33918-1>

1376 Meinshausen, M., Nicholls, Z. R. J., Lewis, J., Gidden, M. J., Vogel, E., Freund, M., Beyerle, U., Gessner, C.,
1377 Nauels, A., Bauer, N., Canadell, J. G., Daniel, J. S., John, A., Krummel, P. B., Luderer, G.,
1378 Meinshausen, N., Montzka, S. A., Rayner, P. J., Reimann, S., ... Wang, R. H. J. (2020). The shared
1379 socio-economic pathway (SSP) greenhouse gas concentrations and their extensions to 2500.
1380 *Geoscientific Model Development*, 13(8), 3571–3605. <https://doi.org/10.5194/gmd-13-3571-2020>

1381 Meinshausen, M., Smith, S. J., Calvin, K., Daniel, J. S., Kainuma, M. L. T., Lamarque, J.-F., Matsumoto, K.,
1382 Montzka, S. A., Raper, S. C. B., Riahi, K., Thomson, A., Velders, G. J. M., & van Vuuren, D. P. P.
1383 (2011). The RCP greenhouse gas concentrations and their extensions from 1765 to 2300. *Climatic
1384 Change*, 109(1), 213. <https://doi.org/10.1007/s10584-011-0156-z>

1385 Meinshausen, M., Vogel, E., Nauels, A., Lorbacher, K., Meinshausen, N., Etheridge, D. M., Fraser, P. J.,
1386 Montzka, S. A., Rayner, P. J., Trudinger, C. M., Krummel, P. B., Beyerle, U., Canadell, J. G., Daniel, J.
1387 S., Enting, I. G., Law, R. M., Lunder, C. R., O'Doherty, S., Prinn, R. G., ... Weiss, R. (2017). Historical
1388 greenhouse gas concentrations for climate modelling (CMIP6). *Geoscientific Model Development*,
1389 10(5), 2057–2116. <https://doi.org/10.5194/gmd-10-2057-2017>

1390 Muis, S., Aerts, J. C. J. H., Á. Antolínez, J. A., Dullaart, J. C., Duong, T. M., Erikson, L., Haarsma, R. J.,
1391 Apecechea, M. I., Mengel, M., Le Bars, D., O'Neill, A., Ranasinghe, R., Roberts, M. J., Verlaan, M.,
1392 Ward, P. J., & Yan, K. (2023). Global projections of storm surges using high-resolution CMIP6

1393 climate models. *Earth's Future*, 11(9). <https://doi.org/10.1029/2023ef003479>

1394 Muis, S., Apecechea, M. I., Dullaart, J., de Lima Rego, J., Madsen, K. S., Su, J., Yan, K., & Verlaan, M.
1395 (2020). A High-Resolution Global Dataset of Extreme Sea Levels, Tides, and Storm Surges, Including
1396 Future Projections. *Frontiers in Marine Science*, 7. <https://doi.org/10.3389/fmars.2020.00263>

1397 O'Neill, B. C., Tebaldi, C., van Vuuren, D. P., Eyring, V., Friedlingstein, P., Hurtt, G., Knutti, R., Kriegler, E.,
1398 Lamarque, J.-F., Lowe, J., Meehl, G. A., Moss, R., Riahi, K., & Sanderson, B. M. (2016). The Scenario
1399 Model Intercomparison Project (ScenarioMIP) for CMIP6. *Geoscientific Model Development*, 9(9),
1400 3461–3482. <https://doi.org/10.5194/gmd-9-3461-2016>

1401 Perrette, M., & Mengel, M. (submitted 2024). *Relative sea level projections constrained by historical*
1402 *trends at tide gauge sites.*

1403 Perrette, M., & Mengel, M. (2025). *Relative sea level projections at tide-gauge locations* [Dataset].
1404 Zenodo. <https://doi.org/10.1126/sciadv.ado4506>

1405 Quesada-Chacón, D., Novak, L., Hamester, L., & Otto, C. (2025). *ISIMIP3b tropical cyclone wind and rain*
1406 *fields (MIT)* [Dataset]. ISIMIP Repository. <https://doi.org/10.48364/ISIMIP.779038>

1407 Righi, M., Andela, B., Eyring, V., Lauer, A., Predoi, V., Schlund, M., Vegas-Regidor, J., Bock, L., Brötz, B., de
1408 Mora, L., Diblen, F., Dreyer, L., Drost, N., Earnshaw, P., Hassler, B., Koldunov, N., Little, B., Loosveldt
1409 Tomas, S., & Zimmermann, K. (2020). Earth System Model Evaluation Tool (ESMValTool) v2.0 –
1410 technical overview. *Geoscientific Model Development*, 13(3), 1179–1199.
1411 <https://doi.org/10.5194/gmd-13-1179-2020>

1412 Ruosteenoja, K., Jylhä, K., Räisänen, J., & Mäkelä, A. (2017). Surface air relative humidities spuriously
1413 exceeding 100% in CMIP5 model output and their impact on future projections. *JGR Atmospheres*,
1414 122(18), 9557–9568. <https://doi.org/10.1002/2017JD026909>

1415 Ruosteenoja, K., Jylhä, K., Räisänen, J., & Mäkelä, A. (2018). Reply to comment by genthon et al. On
1416 “surface air relative humidities spuriously exceeding 100% in CMIP5 model output and their impact

1417 on future projections." *Journal of Geophysical Research*, 123(16), 8728–8734.
1418 <https://doi.org/10.1029/2018jd028680>

1419 Schupfner, M., Wieners, K.-H., Wachsmann, F., Steger, C., Bittner, M., Jungclaus, J., Früh, B., Pankatz, K.,
1420 Giorgetta, M., Reick, C., Legutke, S., Esch, M., Gayler, V., Haak, H., de Vrese, P., Raddatz, T.,
1421 Mauritsen, T., von Storch, J.-S., Behrens, J., ... Roeckner, E. (2019). *DKRZ MPI-ESM1.2-HR model*
1422 *output prepared for CMIP6 ScenarioMIP* [Dataset]. Earth System Grid Federation.
1423 <https://doi.org/10.22033/ESGF/CMIP6.2450>

1424 Séférian, R., Berthet, S., Yool, A., Palmiéri, J., Bopp, L., Tagliabue, A., Kwiatkowski, L., Aumont, O.,
1425 Christian, J., Dunne, J., Gehlen, M., Ilyina, T., John, J. G., Li, H., Long, M. C., Luo, J. Y., Nakano, H.,
1426 Romanou, A., Schwinger, J., ... Yamamoto, A. (2020). Tracking Improvement in Simulated Marine
1427 Biogeochemistry Between CMIP5 and CMIP6. *Current Climate Change Reports*, 6(3), 95–119.
1428 <https://doi.org/10.1007/s40641-020-00160-0>

1429 Sellar, A. A., Jones, C. G., Mulcahy, J. P., Tang, Y., Yool, A., Wiltshire, A., O'Connor, F. M., Stringer, M.,
1430 Hill, R., Palmieri, J., Woodward, S., Mora, L., Kuhlbrodt, T., Rumbold, S. T., Kelley, D. I., Ellis, R.,
1431 Johnson, C. E., Walton, J., Abraham, N. L., ... Zerroukat, M. (2019). UKESM1: Description and
1432 evaluation of the U.k. earth system model. *Journal of Advances in Modeling Earth Systems*, 11(12),
1433 4513–4558. <https://doi.org/10.1029/2019ms001739>

1434 Shakespeare, C. J., & Roderick, M. L. (2022). Diagnosing instantaneous forcing and feedbacks of
1435 downwelling longwave radiation at the surface: A simple methodology and its application to CMIP5
1436 models. *Journal of Climate*, 35(12), 3785–3801. <https://doi.org/10.1175/jcli-d-21-0865.1>

1437 Shiogama, H., Fujimori, S., Hasegawa, T., Hayashi, M., Hirabayashi, Y., Ogura, T., Iizumi, T., Takahashi, K.,
1438 & Takemura, T. (2023). Important distinctiveness of SSP3–7.0 for use in impact assessments. *Nature*
1439 *Climate Change*, 13(12), 1276–1278. <https://doi.org/10.1038/s41558-023-01883-2>

1440 Sobel, A. H., Lee, C.-Y., Bowen, S. G., Camargo, S. J., Cane, M. A., Clement, A., Fosu, B., Hart, M., Reed, K.

1441 A., Seager, R., & Tippet, M. K. (2021). Near-term tropical cyclone risk and coupled Earth system
1442 model biases. *Proceedings of the National Academy of Sciences of the United States of America*,
1443 *120*(33), e2209631120. <https://doi.org/10.1073/pnas.2209631120>

1444 Sobel, A. H., Lee, C.-Y., Camargo, S. J., Mandli, K. T., Emanuel, K. A., Mukhopadhyay, P., & Mahakur, M.
1445 (2019). Tropical Cyclone Hazard to Mumbai in the Recent Historical Climate. *Monthly Weather*
1446 *Review*, *147*(7), 2355–2366. <https://doi.org/10.1175/MWR-D-18-0419.1>

1447 Stewart, K. D., Kim, W. M., Urakawa, S., Hogg, A. M., Yeager, S., Tsujino, H., Nakano, H., Kiss, A. E., &
1448 Danabasoglu, G. (2020). JRA55-do-based repeat year forcing datasets for driving ocean–sea-ice
1449 models. *Ocean Modelling*, *147*, 101557. <https://doi.org/10.1016/j.ocemod.2019.101557>

1450 Swaminathan, R., Schewe, J., Walton, J., Zimmermann, K., Jones, C., Betts, R. A., Burton, C., Jones, C. D.,
1451 Mengel, M., Reyer, C. P. O., Turner, A. G., & Weigel, K. (2024). Regional impacts poorly constrained
1452 by climate sensitivity. *Earth's Future*, *12*(12). <https://doi.org/10.1029/2024ef004901>

1453 Switanek, M. B., Troch, P. A., Castro, C. L., Leuprecht, A., Chang, H.-I., Mukherjee, R., & Demaria, E. M. C.
1454 (2017). Scaled distribution mapping: a bias correction method that preserves raw climate model
1455 projected changes. *Hydrology and Earth System Sciences*, *21*(6), 2649–2666.
1456 <https://doi.org/10.5194/hess-21-2649-2017>

1457 Tagliabue, A., Kwiatkowski, L., Bopp, L., Butenschön, M., Cheung, W., Lengaigne, M., & Vialard, J. (2021).
1458 Persistent Uncertainties in Ocean Net Primary Production Climate Change Projections at Regional
1459 Scales Raise Challenges for Assessing Impacts on Ecosystem Services. *Frontiers in Climate*, *3*.
1460 <https://doi.org/10.3389/fclim.2021.738224>

1461 Tang, Y., Rumbold, S., Ellis, R., Kelley, D., Mulcahy, J., Sellar, A., Walton, J., & Jones, C. (2019). *MOHC*
1462 *UKESM1.0-LL model output prepared for CMIP6 CMIP* [Dataset]. Earth System Grid Federation.
1463 <https://doi.org/10.22033/ESGF/CMIP6.1569>

1464 Themeßl, M. J., Gobiet, A., & Heinrich, G. (2012). Empirical-statistical downscaling and error correction

1465 of regional climate models and its impact on the climate change signal. *Climatic Change*, 112(2),
1466 449–468. <https://doi.org/10.1007/s10584-011-0224-4>

1467 Thrasher, B., Maurer, E. P., McKellar, C., & Duffy, P. B. (2012). Technical Note: Bias correcting climate
1468 model simulated daily temperature extremes with quantile mapping. *Hydrology and Earth System
1469 Sciences*, 16(9), 3309–3314. <https://doi.org/10.5194/hess-16-3309-2012>

1470 Tippet, M. K., Camargo, S. J., & Sobel, A. H. (2011). A Poisson Regression Index for Tropical Cyclone
1471 Genesis and the Role of Large-Scale Vorticity in Genesis. *Journal of Climate*, 24(9), 2335–2357.
1472 <https://doi.org/10.1175/2010JCLI3811.1>

1473 Treu, S., Muis, S., Dangendorf, S., Wahl, T., Oelsmann, J., Heinicke, S., Frieler, K., & Mengel, M. (2023).
1474 Reconstruction of hourly coastal water levels and counterfactuals without sea level rise for impact
1475 attribution. In *Earth System Science Data Discussions*. <https://doi.org/10.5194/essd-2023-112>

1476 Tsujino, H., Urakawa, L. S., Griffies, S. M., Danabasoglu, G., Adcroft, A. J., Amaral, A. E., Arsouze, T.,
1477 Bentsen, M., Bernardello, R., Böning, C. W., Bozec, A., Chassignet, E. P., Danilov, S., Dussin, R.,
1478 Exarchou, E., Fogli, P. G., Fox-Kemper, B., Guo, C., Ilicak, M., ... Yu, Z. (2020). Evaluation of global
1479 ocean–sea-ice model simulations based on the experimental protocols of the Ocean Model
1480 Intercomparison Project phase 2 (OMIP-2). *Geoscientific Model Development*, 13(8), 3643–3708.
1481 <https://doi.org/10.5194/gmd-13-3643-2020>

1482 Tsujino, H., Urakawa, S., Nakano, H., Small, R. J., Kim, W. M., Yeager, S. G., Danabasoglu, G., Suzuki, T.,
1483 Bamber, J. L., Bentsen, M., Böning, C. W., Bozec, A., Chassignet, E. P., Curchitser, E., Boeira Dias, F.,
1484 Durack, P. J., Griffies, S. M., Harada, Y., Ilicak, M., ... Yamazaki, D. (2018). JRA-55 based surface
1485 dataset for driving ocean–sea-ice models (JRA55-do). *Ocean Modelling*, 130, 79–139.
1486 <https://doi.org/10.1016/j.ocemod.2018.07.002>

1487 Watanabe, M., Kang, S. M., Collins, M., Hwang, Y.-T., McGregor, S., & Stuecker, M. F. (2024). Possible
1488 shift in controls of the tropical Pacific surface warming pattern. *Nature*, 630(8016), 315–324.

1489 <https://doi.org/10.1038/s41586-024-07452-7>

1490 Weedon, G. P., Gomes, S., Viterbo, P., Österle, H., Adam, J. C., Bellouin, N., Boucher, O., & Best, M.
1491 (2010). *The watch forcing data 1958-2001: a meteorological forcing data set for land surface- and*
1492 *hydrological-models*. 41. https://publications.pik-potsdam.de/pubman/item/item_16400

1493 Woodworth-Jefcoats, P. (2022). *therMizer-FishMIP-2022-HI: Code and data for FishMIP 2022 ISIMIP 3a -*
1494 *Hawaii longline fishing ground regional model*. Github. [https://github.com/pwoodworth-](https://github.com/pwoodworth-jefcoats/therMizer-FishMIP-2022-HI)
1495 [jefcoats/therMizer-FishMIP-2022-HI](https://github.com/pwoodworth-jefcoats/therMizer-FishMIP-2022-HI)

1496 Yukimoto, S., Kawai, H., Koshiro, T., Oshima, N., Yoshida, K., Urakawa, S., Tsujino, H., Deushi, M., Tanaka,
1497 T., Hosaka, M., Yabu, S., Yoshimura, H., Shindo, E., Mizuta, R., Obata, A., Adachi, Y., & Ishii, M.
1498 (2019). The Meteorological Research Institute Earth System Model Version 2.0, MRI-ESM2.0:
1499 Description and Basic Evaluation of the Physical Component. *Journal of the Meteorological Society*
1500 *of Japan. Ser. II, 97(5)*, 931–965. <https://doi.org/10.2151/jmsj.2019-051>

1501 Yukimoto, S., Koshiro, T., Kawai, H., Oshima, N., Yoshida, K., Urakawa, S., Tsujino, H., Deushi, M., Tanaka,
1502 T., Hosaka, M., Yoshimura, H., Shindo, E., Mizuta, R., Ishii, M., Obata, A., & Adachi, Y. (2019a). *MRI*
1503 *MRI-ESM2.0 model output prepared for CMIP6 CMIP* [Dataset]. Earth System Grid Federation.
1504 <https://doi.org/10.22033/ESGF/CMIP6.621>

1505 Yukimoto, S., Koshiro, T., Kawai, H., Oshima, N., Yoshida, K., Urakawa, S., Tsujino, H., Deushi, M., Tanaka,
1506 T., Hosaka, M., Yoshimura, H., Shindo, E., Mizuta, R., Ishii, M., Obata, A., & Adachi, Y. (2019b). *MRI*
1507 *MRI-ESM2.0 model output prepared for CMIP6 ScenarioMIP* [Dataset]. Earth System Grid
1508 Federation. <https://doi.org/10.22033/ESGF/CMIP6.638>

1509 Zelinka, M. D., Myers, T. A., McCoy, D. T., Po-Chedley, S., Caldwell, P. M., Ceppi, P., Klein, S. A., & Taylor,
1510 K. E. (2020). Causes of higher climate sensitivity in CMIP6 models. *Geophysical Research Letters*,
1511 *47(1)*. <https://doi.org/10.1029/2019gl085782>

1512 Zhang, L., & Li, T. (2014). A simple analytical model for understanding the formation of sea surface

1513 temperature patterns under global warming. *Journal of Climate*, 27(22), 8413–8421.
1514 <https://doi.org/10.1175/jcli-d-14-00346.1>

1515 Zhu, L., Quiring, S. M., & Emanuel, K. A. (2013). Estimating tropical cyclone precipitation risk in Texas.
1516 *Geophysical Research Letters*, 40(23), 6225–6230. <https://doi.org/10.1002/2013gl058284>

1517 Adler, R. F., Huffman, G. J., Chang, A., Ferraro, R., Xie, P.-P., Janowiak, J., Rudolf, B., Schneider, U., Curtis,
1518 S., Bolvin, D., Gruber, A., Susskind, J., Arkin, P., & Nelkin, E. (2003). The Version-2 Global
1519 Precipitation Climatology Project (GPCP) Monthly Precipitation Analysis (1979–Present). *Journal of*
1520 *Hydrometeorology*, 4(6), 1147–1167. [https://doi.org/10.1175/1525-](https://doi.org/10.1175/1525-7541(2003)004<1147:TVGPCP>2.0.CO;2)
1521 [7541\(2003\)004<1147:TVGPCP>2.0.CO;2](https://doi.org/10.1175/1525-7541(2003)004<1147:TVGPCP>2.0.CO;2)

1522 Andela, B., Broetz, B., de Mora, L., Drost, N., Eyring, V., Koldunov, N., Lauer, A., Mueller, B., Predoi, V.,
1523 Righi, M., Schlund, M., Vegas-Regidor, J., Zimmermann, K., Adeniyi, K., Arnone, E., Bellprat, O., Berg,
1524 P., Bock, L., Caron, L.-P., ... Weigel, K. (2020). ESMValTool. <https://doi.org/10.5281/zenodo.3970975>

1525 Andela, B., Broetz, B., de Mora, L., Drost, N., Eyring, V., Koldunov, N., Lauer, A., Predoi, V., Righi, M.,
1526 Schlund, M., Vegas-Regidor, J., Zimmermann, K., Bock, L., Diblen, F., Dreyer, L., Earnshaw, P.,
1527 Hassler, B., Little, B., & Loosveldt-Tomas, S. (2020). ESMValCore.
1528 <https://doi.org/10.5281/zenodo.3952695>

1529 Barrier, N., Lengaigne, M., Rault, J., Person, R., Ethé, C., Aumont, O., & Maury, O. (2023). Mechanisms
1530 underlying the epipelagic ecosystem response to ENSO in the equatorial Pacific ocean. *Progress in*
1531 *Oceanography*, 213, 103002. <https://doi.org/10.1016/j.pocean.2023.103002>

1532 Bock, L., Lauer, A., Schlund, M., Barreiro, M., Bellouin, N., Jones, C., Meehl, G. A., Predoi, V., Roberts, M.
1533 J., & Eyring, V. (2020). Quantifying progress across different CMIP phases with the ESMValTool.
1534 *Journal of Geophysical Research*, 125(21). <https://doi.org/10.1029/2019jd032321>

1535 Boucher, O., Denvil, S., Levvasseur, G., Cozic, A., Caubel, A., Foujols, M.-A., Meurdesoif, Y., Cadule, P.,

1536 Devilliers, M., Dupont, E., & Lurton, T. (2019). IPSL IPSL-CM6A-LR model output prepared for CMIP6
1537 ScenarioMIP [Dataset]. Earth System Grid Federation. <https://doi.org/10.22033/ESGF/CMIP6.1532>

1538 Boucher, O., Denvil, S., Levavasseur, G., Cozic, A., Caubel, A., Foujols, M.-A., Meurdesoif, Y., Cadule, P.,
1539 Devilliers, M., Ghattas, J., Lebas, N., Lurton, T., Mellul, L., Musat, I., Mignot, J., & Cheruy, F. (2018).
1540 IPSL IPSL-CM6A-LR model output prepared for CMIP6 CMIP [Dataset]. Earth System Grid
1541 Federation. <https://doi.org/10.22033/ESGF/CMIP6.1534>

1542 Boucher, O., Servonnat, J., Albright, A. L., Aumont, O., Balkanski, Y., Bastrikov, V., Bekki, S., Bonnet, R.,
1543 Bony, S., Bopp, L., Braconnot, P., Brockmann, P., Cadule, P., Caubel, A., Cheruy, F., Codron, F., Cozic,
1544 A., Cugnet, D., D'Andrea, F., ... Vuichard, N. (2020). Presentation and evaluation of the IPSL-CM6A-
1545 LR climate model. *Journal of Advances in Modeling Earth Systems*, 12(7).
1546 <https://doi.org/10.1029/2019ms002010>

1547 Büchner, M., & Reyer, C. (2022). ISIMIP3b atmospheric composition input data [Dataset]. ISIMIP
1548 Repository. <https://doi.org/10.48364/ISIMIP.482153.1>

1549 Buck, A. L. (1981). New Equations for Computing Vapor Pressure and Enhancement Factor. *Journal of*
1550 *Applied Meteorology and Climatology*, 20(12), 1527–1532. [https://doi.org/10.1175/1520-0450\(1981\)020<1527:NEFCVP>2.0.CO;2](https://doi.org/10.1175/1520-0450(1981)020<1527:NEFCVP>2.0.CO;2)

1552 Camargo, S. J., Tippett, M. K., Sobel, A. H., Vecchi, G. A., & Zhao, M. (2014). Testing the Performance of
1553 Tropical Cyclone Genesis Indices in Future Climates Using the HiRAM Model. *Journal of Climate*,
1554 27(24), 9171–9196. <https://doi.org/10.1175/JCLI-D-13-00505.1>

1555 Cannon, A. J. (2018). Multivariate quantile mapping bias correction: an N-dimensional probability
1556 density function transform for climate model simulations of multiple variables. *Climate Dynamics*,
1557 50(1), 31–49. <https://doi.org/10.1007/s00382-017-3580-6>

1558 Cecil, D. (2006). LIS/OTD 0.5 Degree High Resolution Monthly Climatology (HRMC) [Dataset]. NASA
1559 Global Hydrometeorology Resource Center DAAC. <https://doi.org/10.5067/LIS/LIS-OTD/DATA303>

1560 Cucchi, M., Weedon, G. P., Amici, A., Bellouin, N., Lange, S., Müller Schmied, H., Hersbach, H., &
1561 Buontempo, C. (2020). WFDE5: bias-adjusted ERA5 reanalysis data for impact studies. *Earth System
1562 Science Data*, 12(3), 2097–2120. <https://doi.org/10.5194/essd-12-2097-2020>

1563 Dunne, J. P., Horowitz, L. W., Adcroft, A. J., Ginoux, P., Held, I. M., John, J. G., Krasting, J. P., Malyshev, S.,
1564 Naik, V., Paulot, F., Shevliakova, E., Stock, C. A., Zadeh, N., Balaji, V., Blanton, C., Dunne, K. A.,
1565 Dupuis, C., Durachta, J., Dussin, R., ... Zhao, M. (2020). The GFDL earth system model version 4.1
1566 (GFDL-ESM 4.1): Overall coupled model description and simulation characteristics. *Journal of
1567 Advances in Modeling Earth Systems*, 12(11). <https://doi.org/10.1029/2019ms002015>

1568 Durack, P. J. (n.d.). CMIP6 source_id values. Retrieved January 16, 2023, from [https://wcrp-
1569 cmip.github.io/CMIP6_CVs/docs/CMIP6_source_id.html](https://wcrp-cmip.github.io/CMIP6_CVs/docs/CMIP6_source_id.html)

1570 Eddy, T. D., Heneghan, R. F., Bryndum-Buchholz, A., Fulton, E. A., Harrison, C. S., Tittensor, D. P., Lotze,
1571 H. K., Ortega-Cisneros, K., Novaglio, C., Bianchi, D., Büchner, M., Bulman, C., Cheung, W. W. L.,
1572 Christensen, V., Coll, M., Everett, J. D., Fierro-Arcos, D., Galbraith, E. D., Gascuel, D., ... Blanchard, J.
1573 L. (2025). Global and regional marine ecosystem models reveal key uncertainties in climate change
1574 projections. *Earth's Future*, 13(3). <https://doi.org/10.1029/2024ef005537>

1575 Emanuel, K., DesAutels, C., Holloway, C., & Korty, R. (2004). Environmental Control of Tropical Cyclone
1576 Intensity. *Journal of the Atmospheric Sciences*, 61(7), 843–858. [https://doi.org/10.1175/1520-
0469\(2004\)061<0843:ECOTCI>2.0.CO;2](https://doi.org/10.1175/1520-
1577 0469(2004)061<0843:ECOTCI>2.0.CO;2)

1578 Emanuel, K., Sundararajan, R., & Williams, J. (2008). Hurricanes and Global Warming: Results from
1579 Downscaling IPCC AR4 Simulations. *Bulletin of the American Meteorological Society*, 89(3), 347–
1580 368. <https://doi.org/10.1175/BAMS-89-3-347>

1581 Eyring, V., Bony, S., Meehl, G. A., Senior, C. A., Stevens, B., Stouffer, R. J., & Taylor, K. E. (2016). Overview
1582 of the Coupled Model Intercomparison Project Phase 6 (CMIP6) experimental design and
1583 organization. *Geoscientific Model Development*, 9(5), 1937–1958. [78](https://doi.org/10.5194/gmd-9-</p></div><div data-bbox=)

1584 1937-2016

1585 Eyring, V., Gillett, N. P., Achuta Rao, K. M., Barimalala, R., Barreiro Parrillo, M., Bellouin, N., V. Masson-
1586 Delmotte, P. Zhai, A. Pirani, S. L. Connors, C. Péan, S. Berger, & Intergovernmental Panel on Climate
1587 Change (IPCC). (2023). Human Influence on the Climate System. In *Climate Change 2021 – The*
1588 *Physical Science Basis: Working Group I Contribution to the Sixth Assessment Report of the*
1589 *Intergovernmental Panel on Climate Change* (pp. 423–552). Cambridge University Press.
1590 <https://doi.org/10.1017/9781009157896.005>

1591 Fosu, B., Sobel, A., Camargo, S., Tippett, M., Hemmati, M., Bowen, S., & Bloemendaal, N. (2024).
1592 Assessing future tropical cyclone risk using downscaled 1 CMIP6 projections. *Journal of Catastrophe*
1593 *Risk and Resilience*, 2(1). <https://doi.org/10.63024/dpva-2pa1>

1594 Frieler, K. (submitted 2023). Scenario Set-up and the new CMIP6-based climate-related forcings
1595 provided within the third round of the Inter-Sectoral Model Intercomparison Project (ISIMIP3b,
1596 group I and II). *Geoscientific Model Development*.

1597 Frieler, K., Lange, S., Piontek, F., Reyer, C. P. O., Schewe, J., Warszawski, L., Zhao, F., Chini, L., Denvil, S.,
1598 Emanuel, K., Geiger, T., Halladay, K., Hurtt, G., Mengel, M., Murakami, D., Ostberg, S., Popp, A.,
1599 Riva, R., Stevanovic, M., ... Yamagata, Y. (2017). Assessing the impacts of 1.5 °C global warming –
1600 simulation protocol of the Inter-Sectoral Impact Model Intercomparison Project (ISIMIP2b).
1601 *Geoscientific Model Development*, 10(12), 4321–4345. <https://doi.org/10.5194/gmd-10-4321-2017>

1602 Frieler, K., Volkholz, J., Lange, S., Schewe, J., Mengel, M., del Rocío Rivas López, M., Otto, C., Reyer, C. P.
1603 O., Karger, D. N., & del Valle Gitta Lasslop Sarah Chadburn Eleanor Burke Angela Gallego-Sala Noah
1604 Smith Jinfeng Chang Stijn Hantson Chantelle Burton Anne Gädeke Fang Li Simon N. Gosling Hannes
1605 Müller Schmied Fred Hattermann Jida Wang Fangfang Yao Thomas Hickler Rafael Marcé Don
1606 Pierson Wim Thiery Daniel Mercado-Bettín Robert Ladwig Ana Isabel Ayala-Zamora Matthew
1607 Forrest and Michel Bechtold, J. T. M. S. T. C. M. J. L. B. C. S. H. C. M. P. T. D. E. K. O.-C. C. N. Y. R. R.

1608 A. W. C. S. X. L. R. H. D. T. O. M. M. B. T. V. T. W. F. S. I. J. S. J. K. I. V. J. J. C. M. S. R. J. K. I. D. V.
1609 (2024, January 4). Scenario setup and forcing data for impact model evaluation and impact
1610 attribution within the third round of the Inter-Sectoral Model Intercomparison Project (ISIMIP3a).
1611 Geoscientific Model Development. [https://www.google.com/url?q=https://doi.org/10.5194/gmd-](https://www.google.com/url?q=https://doi.org/10.5194/gmd-17-1-2024&sa=D&source=docs&ust=1704377607845951&usg=AOvVaw3hFVXAV75ZSOClc8itQfEs)
1612 [17-1-2024&sa=D&source=docs&ust=1704377607845951&usg=AOvVaw3hFVXAV75ZSOClc8itQfEs](https://www.google.com/url?q=https://doi.org/10.5194/gmd-17-1-2024&sa=D&source=docs&ust=1704377607845951&usg=AOvVaw3hFVXAV75ZSOClc8itQfEs)
1613 Frieler, K., Volkholz, J., Lange, S., Schewe, J., Mengel, M., del Rocío Rivas López, M., Otto, C., Reyer, C. P.
1614 O., Karger, D. N., Malle, J. T., Treu, S., Menz, C., Blanchard, J. L., Harrison, C. S., Petrik, C. M., Eddy,
1615 T. D., Ortega-Cisneros, K., Novaglio, C., Rousseau, Y., ... Bechtold, M. (2024). Scenario setup and
1616 forcing data for impact model evaluation and impact attribution within the third round of the Inter-
1617 Sectoral Impact Model Intercomparison Project (ISIMIP3a). Geoscientific Model Development,
1618 17(1), 1–51. <https://doi.org/10.5194/gmd-17-1-2024>
1619 Frieler, K., Volkholz, J., Lange, S., Schewe, J., Mengel, M., Rivas López, M. del R., Otto, C., Reyer, C. P. O.,
1620 Karger, D. N., Malle, J. T., Treu, S., Menz, C., Blanchard, J. L., Harrison, C. S., Petrik, C. M., Eddy, T.
1621 D., Ortega-Cisneros, K., Novaglio, C., Rousseau, Y., ... Bechtold, M. (2023). Scenario set-up and
1622 forcing data for impact model evaluation and impact attribution within the third round of the Inter-
1623 Sectoral Model Intercomparison Project (ISIMIP3a). In EGU sphere.
1624 <https://doi.org/10.5194/egusphere-2023-281>
1625 Geiger, T., Gütschow, J., Bresch, D. N., Emanuel, K., & Frieler, K. (2021). Double benefit of limiting global
1626 warming for tropical cyclone exposure. *Nature Climate Change*, 11(10), 861–866.
1627 <https://doi.org/10.1038/s41558-021-01157-9>
1628 Gennaretti, F., Sangelantoni, L., & Grenier, P. (2015). Toward daily climate scenarios for Canadian Arctic
1629 coastal zones with more realistic temperature-precipitation interdependence. *JGR: Atmospheres*,
1630 120(23), 11,862–11,877. <https://doi.org/10.1002/2015JD023890>
1631 Gillett, N. P., Shiogama, H., Funke, B., Hegerl, G., Knutti, R., Matthes, K., Santer, B. D., Stone, D., &

1632 Tebaldi, C. (2016). The detection and Attribution Model Intercomparison Project (DAMIP v1.0)
1633 contribution to CMIP6. *Geoscientific Model Development*, 9(10), 3685–3697.
1634 <https://doi.org/10.5194/gmd-9-3685-2016>

1635 Good, P., Sellar, A., Tang, Y., Rumbold, S., Ellis, R., Kelley, D., Kuhlbrodt, T., & Walton, J. (2019). MOHC
1636 UKESM1.0-LL model output prepared for CMIP6 ScenarioMIP [Dataset]. Earth System Grid
1637 Federation. <https://doi.org/10.22033/ESGF/CMIP6.1567>

1638 Grenier, P. (2018). Two Types of Physical Inconsistency to Avoid with Univariate Quantile Mapping: A
1639 Case Study over North America Concerning Relative Humidity and Its Parent Variables. *Journal of*
1640 *Applied Meteorology and Climatology*, 57(2), 347–364. <https://doi.org/10.1175/JAMC-D-17-0177.1>

1641 Haerter, J. O., Hagemann, S., Moseley, C., & Piani, C. (2011). Climate model bias correction and the role
1642 of timescales. *Hydrology and Earth System Sciences*, 15(3), 1065–1079.
1643 <https://doi.org/10.5194/hess-15-1065-2011>

1644 Hausfather, Z., & Peters, G. P. (2020, January 29). Emissions – the “business as usual” story is misleading.
1645 Nature Publishing Group UK. <https://doi.org/10.1038/d41586-020-00177-3>

1646 Hersbach, H., Bell, B., Berrisford, P., Hirahara, S., Horányi, A., Muñoz-Sabater, J., Nicolas, J., Peubey, C.,
1647 Radu, R., Schepers, D., Simmons, A., Soci, C., Abdalla, S., Abellan, X., Balsamo, G., Bechtold, P.,
1648 Biavati, G., Bidlot, J., Bonavita, M., ... Jean-Noël Thépaut. (2020). The ERA5 global reanalysis.
1649 *Quarterly Journal of the Royal Meteorological Society*, 146(730), 1999–2049.
1650 <https://doi.org/10.1002/qj.3803>

1651 Holland. (1980). An Analytic Model of the Wind and Pressure Profiles in Hurricanes, *Mon. Mon. Weather*
1652 *Rev*, 108, 1212–1218.

1653 Holland. (2008). A revised hurricane pressure–wind model. *Monthly Weather Review*, 136(9), 3432–
1654 3445. <https://doi.org/10.1175/2008mwr2395.1>

1655 ISIMIP3b simulation protocol. (2023). <https://protocol.isimip.org/>

1656 Jägermeyr, J., Müller, C., Ruane, A. C., Elliott, J., Balkovic, J., Castillo, O., Faye, B., Foster, I., Folberth, C.,
1657 Franke, J. A., Fuchs, K., Guarin, J. R., Heinke, J., Hoogenboom, G., Iizumi, T., Jain, A. K., Kelly, D.,
1658 Khabarov, N., Lange, S., ... Rosenzweig, C. (2021). Climate impacts on global agriculture emerge
1659 earlier in new generation of climate and crop models. *Nature Food*, 2(11), 873–885.
1660 <https://doi.org/10.1038/s43016-021-00400-y>

1661 John, J. G., Blanton, C., McHugh, C., Radhakrishnan, A., Rand, K., Vahlenkamp, H., Wilson, C., Zadeh, N.
1662 T., Dunne, J. P., Dussin, R., Horowitz, L. W., Krasting, J. P., Lin, P., Malyshev, S., Naik, V., Ploshay, J.,
1663 Shevliakova, E., Silvers, L., Stock, C., ... Zeng, Y. (2018). NOAA-GFDL GFDL-ESM4 model output
1664 prepared for CMIP6 ScenarioMIP [Dataset]. Earth System Grid Federation.
1665 <https://doi.org/10.22033/ESGF/CMIP6.1414>

1666 Jungclaus, J., Bittner, M., Wieners, K.-H., Wachsmann, F., Schupfner, M., Legutke, S., Giorgetta, M.,
1667 Reick, C., Gayler, V., Haak, H., de Vrese, P., Raddatz, T., Esch, M., Mauritsen, T., von Storch, J.-S.,
1668 Behrens, J., Brovkin, V., Claussen, M., Crueger, T., ... Roeckner, E. (2019). MPI-M MPIESM1.2-HR
1669 model output prepared for CMIP6 CMIP [Dataset]. Earth System Grid Federation.
1670 <https://doi.org/10.22033/ESGF/CMIP6.741>

1671 Kaplan, J. O., Koch, A., & Lau, K. H.-K. (2023). Estimated future global lightning strokes (2010-2100).
1672 <https://doi.org/10.5281/zenodo.7511843>

1673 Kaplan, J. O., & Lau, K. H.-K. (2021). The WGLC global gridded lightning climatology and time series.
1674 *Earth System Science Data*, 13(7), 3219–3237. <https://doi.org/10.5194/essd-13-3219-2021>

1675 Kaplan, J. O., & Lau, K. H.-K. (2022). World Wide Lightning Location Network (WWLLN) Global Lightning
1676 Climatology (WGLC) and time series, 2022 update. *Earth System Science Data*, 14(12), 5665–5670.
1677 <https://doi.org/10.5194/essd-14-5665-2022>

1678 Krasting, J. P., John, J. G., Blanton, C., McHugh, C., Nikonov, S., Radhakrishnan, A., Rand, K., Zadeh, N. T.,
1679 Balaji, V., Durachta, J., Dupuis, C., Menzel, R., Robinson, T., Underwood, S., Vahlenkamp, H., Dunne,

1680 K. A., Gauthier, P. P. G., Ginoux, P., Griffies, S. M., ... Zhao, M. (2018). NOAA-GFDL GFDL-ESM4
1681 model output prepared for CMIP6 CMIP [Dataset]. Earth System Grid Federation.
1682 <https://doi.org/10.22033/ESGF/CMIP6.1407>

1683 Lange, S. (2017). ISIMIP2b Bias-Correction Code. <https://doi.org/10.5281/zenodo.1069050>

1684 Lange, S. (2018). Bias correction of surface downwelling longwave and shortwave radiation for the
1685 EWEMBI dataset. *Earth System Dynamics*, 9(2), 627–645. <https://doi.org/10.5194/esd-9-627-2018>

1686 Lange, S. (2019a). Earth2Observe, WFDEI and ERA-interim data merged and bias-corrected for ISIMIP
1687 (EWEMBI) [Dataset]. <https://doi.org/10.5880/pik.2019.004>

1688 Lange, S. (2019b). Trend-preserving bias adjustment and statistical downscaling with ISIMIP3BASD
1689 (v1.0). *Geoscientific Model Development*, 12(7), 3055–3070. [https://doi.org/10.5194/gmd-12-](https://doi.org/10.5194/gmd-12-3055-2019)
1690 [3055-2019](https://doi.org/10.5194/gmd-12-3055-2019)

1691 Lange, S. (2021a). ISIMIP3BASD. <https://doi.org/10.5281/zenodo.4686991>

1692 Lange, S. (2021b). ISIMIP3b bias adjustment fact sheet.
1693 https://www.isimip.org/documents/413/ISIMIP3b_bias_adjustment_fact_sheet_Gnsz7CO.pdf

1694 Lange, S., Menz, C., Gleixner, S., Cucchi, M., Weedon, G. P., Amici, A., Bellouin, N., Schmied, H. M.,
1695 Hersbach, H., Buontempo, C., & Cagnazzo, C. (2021). WFDE5 over land merged with ERA5 over the
1696 ocean (W5E5 v2.0) [Dataset]. ISIMIP Repository. <https://doi.org/10.48364/ISIMIP.342217>

1697 Lange, S., Quesada-Chacón, D., & Büchner, M. (2023). Secondary ISIMIP3b bias-adjusted atmospheric
1698 climate input data [Dataset]. ISIMIP Repository. <https://doi.org/10.48364/ISIMIP.581124.3>

1699 Lan, X., Tans, P., & Thoning, K. W. (2023). Trends in globally-averaged CO2 determined from NOAA
1700 Global Monitoring Laboratory measurements. Version 2023-01 NOAA/GML [Dataset].
1701 <https://gml.noaa.gov/ccgg/trends/>

1702 Large W. G., A. S. G. Y. (2004). Diurnal to decadal global forcing for ocean and sea ice models: the data
1703 sets and flux climatologies (No. NCAR/TN460+STR). CGD Division of the National Centre for

1704 Atmospheric Research (NCAR). <https://www.researchgate.net/profile/Stephen->
1705 [Yeager/publication/281588002_Diurnal_to_Decadal_Global_Forcing_for_Ocean_and_Sea-](https://www.researchgate.net/publication/281588002_Diurnal_to_Decadal_Global_Forcing_for_Ocean_and_Sea-)
1706 [Ice_Models_The_Data_Sets_and_Flux_Climatologies/links/55eede7108ae199d47bfaf41/Diurnal-](https://www.researchgate.net/publication/281588002_Diurnal_to_Decadal_Global_Forcing_for_Ocean_and_Sea-Ice_Models_The_Data_Sets_and_Flux_Climatologies/links/55eede7108ae199d47bfaf41/Diurnal-)
1707 [to-Decadal-Global-Forcing-for-Ocean-and-Sea-Ice-Models-The-Data-Sets-and-Flux-](https://www.researchgate.net/publication/281588002_Diurnal_to_Decadal_Global_Forcing_for_Ocean_and_Sea-Ice_Models_The_Data_Sets_and_Flux-)
1708 [Climatologies.pdf](https://www.researchgate.net/publication/281588002_Diurnal_to_Decadal_Global_Forcing_for_Ocean_and_Sea-Ice_Models_The_Data_Sets_and_Flux-)

1709 Lee, C.-Y., Camargo, S. J., Sobel, A. H., & Tippett, M. K. (2020). Statistical–Dynamical Downscaling
1710 Projections of Tropical Cyclone Activity in a Warming Climate: Two Diverging Genesis Scenarios.
1711 *Journal of Climate*, 33(11), 4815–4834. <https://doi.org/10.1175/JCLI-D-19-0452.1>

1712 Lee, C.-Y., Tippett, M. K., Camargo, S. J., & Sobel, A. H. (2015). Probabilistic Multiple Linear Regression
1713 Modeling for Tropical Cyclone Intensity. *Monthly Weather Review*, 143(3), 933–954.
1714 <https://doi.org/10.1175/MWR-D-14-00171.1>

1715 Lee, C.-Y., Tippett, M. K., Sobel, A. H., & Camargo, S. J. (2016). Rapid intensification and the bimodal
1716 distribution of tropical cyclone intensity. *Nature Communications*, 7, 10625.
1717 <https://doi.org/10.1038/ncomms10625>

1718 Lee, C.-Y., Tippett, M. K., Sobel, A. H., & Camargo, S. J. (2018). An environmentally forced tropical
1719 cyclone hazard model. *Journal of Advances in Modeling Earth Systems*, 10(1), 223–241.
1720 <https://doi.org/10.1002/2017ms001186>

1721 Lengaigne, M., Pang, S., Silvy, Y., Danielli, V., Gopika, S., Sadhvi, K., Dutheil, C., Rousset, C., Ethé, C.,
1722 Person, R., Madec, G., Barrier, N., Maury, O., Dalaut, L., Menkes, C., Nicol, S., Gorgues, T., Melet, A.,
1723 & Guihou, K. (2025). Vialard: An ocean modelling framework for mitigating oceanic projections
1724 from global climate models present-day biases. In *Earth future*.

1725 Li, G., Xie, S.-P., Du, Y., & Luo, Y. (2016). Effects of excessive equatorial cold tongue bias on the
1726 projections of tropical Pacific climate change. Part I: the warming pattern in CMIP5 multi-model
1727 ensemble. *Climate Dynamics*, 47(12), 3817–3831. <https://doi.org/10.1007/s00382-016-3043-5>

1728 Madec, G. (2015). NEMO ocean engine, Version 3.6 stable Note du Pole de modelisation de l'Institut
1729 Pierre-Simon Laplace, vol. 27. IPSL, Paris: France.

1730 Maraun, D. (2013). Bias Correction, Quantile Mapping, and Downscaling: Revisiting the Inflation Issue.
1731 Journal of Climate, 26(6), 2137–2143. <https://doi.org/10.1175/JCLI-D-12-00821.1>

1732 Mauritsen, T., Bader, J., Becker, T., Behrens, J., Bittner, M., Brokopf, R., Brovkin, V., Claussen, M.,
1733 Crueger, T., Esch, M., Fast, I., Fiedler, S., Fläschner, D., Gayler, V., Giorgetta, M., Goll, D. S., Haak, H.,
1734 Hagemann, S., Hedemann, C., ... Roeckner, E. (2019). Developments in the MPI-M Earth System
1735 Model version 1.2 (MPI-ESM1.2) and Its Response to Increasing CO₂. Journal of Advances in
1736 Modeling Earth Systems, 11(4), 998–1038. <https://doi.org/10.1029/2018MS001400>

1737 Meehl, G. A., Senior, C. A., Eyring, V., Flato, G., Lamarque, J.-F., Stouffer, R. J., Taylor, K. E., & Schlund, M.
1738 (2020). Context for interpreting equilibrium climate sensitivity and transient climate response from
1739 the CMIP6 Earth system models. Science Advances, 6(26), eaba1981.
1740 <https://doi.org/10.1126/sciadv.aba1981>

1741 Meiler, S., Vogt, T., Bloemendaal, N., Ciullo, A., Lee, C.-Y., Camargo, S. J., Emanuel, K., & Bresch, D. N.
1742 (2022). Intercomparison of regional loss estimates from global synthetic tropical cyclone models.
1743 Nature Communications, 13(1), 6156. <https://doi.org/10.1038/s41467-022-33918-1>

1744 Meinshausen, M., Nicholls, Z. R. J., Lewis, J., Gidden, M. J., Vogel, E., Freund, M., Beyerle, U., Gessner, C.,
1745 Nauels, A., Bauer, N., Canadell, J. G., Daniel, J. S., John, A., Krummel, P. B., Luderer, G.,
1746 Meinshausen, N., Montzka, S. A., Rayner, P. J., Reimann, S., ... Wang, R. H. J. (2020). The shared
1747 socio-economic pathway (SSP) greenhouse gas concentrations and their extensions to 2500.
1748 Geoscientific Model Development, 13(8), 3571–3605. <https://doi.org/10.5194/gmd-13-3571-2020>

1749 Meinshausen, M., Smith, S. J., Calvin, K., Daniel, J. S., Kainuma, M. L. T., Lamarque, J.-F., Matsumoto, K.,
1750 Montzka, S. A., Raper, S. C. B., Riahi, K., Thomson, A., Velders, G. J. M., & van Vuuren, D. P. P.
1751 (2011). The RCP greenhouse gas concentrations and their extensions from 1765 to 2300. Climatic

1752 Change, 109(1), 213. <https://doi.org/10.1007/s10584-011-0156-z>

1753 Meinshausen, M., Vogel, E., Nauels, A., Lorbacher, K., Meinshausen, N., Etheridge, D. M., Fraser, P. J.,
1754 Montzka, S. A., Rayner, P. J., Trudinger, C. M., Krummel, P. B., Beyerle, U., Canadell, J. G., Daniel, J.
1755 S., Enting, I. G., Law, R. M., Lunder, C. R., O'Doherty, S., Prinn, R. G., ... Weiss, R. (2017). Historical
1756 greenhouse gas concentrations for climate modelling (CMIP6). *Geoscientific Model Development*,
1757 10(5), 2057–2116. <https://doi.org/10.5194/gmd-10-2057-2017>

1758 Muis, S., Aerts, J. C. J. H., Á. Antolínez, J. A., Dullaart, J. C., Duong, T. M., Erikson, L., Haarsma, R. J.,
1759 Apecechea, M. I., Mengel, M., Le Bars, D., O'Neill, A., Ranasinghe, R., Roberts, M. J., Verlaan, M.,
1760 Ward, P. J., & Yan, K. (2023). Global projections of storm surges using high-resolution CMIP6
1761 climate models. *Earth's Future*, 11(9). <https://doi.org/10.1029/2023ef003479>

1762 Muis, S., Apecechea, M. I., Dullaart, J., de Lima Rego, J., Madsen, K. S., Su, J., Yan, K., & Verlaan, M.
1763 (2020). A High-Resolution Global Dataset of Extreme Sea Levels, Tides, and Storm Surges, Including
1764 Future Projections. *Frontiers in Marine Science*, 7. <https://doi.org/10.3389/fmars.2020.00263>

1765 Perrette, M., & Mengel, M. (submitted 2024). Relative sea level projections constrained by historical
1766 trends at tide gauge sites.

1767 Righi, M., Andela, B., Eyring, V., Lauer, A., Predoi, V., Schlund, M., Vegas-Regidor, J., Bock, L., Brötz, B., de
1768 Mora, L., Diblen, F., Dreyer, L., Drost, N., Earnshaw, P., Hassler, B., Koldunov, N., Little, B., Loosveldt
1769 Tomas, S., & Zimmermann, K. (2020). Earth System Model Evaluation Tool (ESMValTool) v2.0 –
1770 technical overview. *Geoscientific Model Development*, 13(3), 1179–1199.
1771 <https://doi.org/10.5194/gmd-13-1179-2020>

1772 Ruosteenoja, K., Jylhä, K., Räisänen, J., & Mäkelä, A. (2017). Surface air relative humidities spuriously
1773 exceeding 100% in CMIP5 model output and their impact on future projections. *JGR Atmospheres*,
1774 122(18), 9557–9568. <https://doi.org/10.1002/2017JD026909>

1775 Ruosteenoja, K., Jylhä, K., Räisänen, J., & Mäkelä, A. (2018). Reply to comment by genthon et al. On

1776 “surface air relative humidities spuriously exceeding 100% in CMIP5 model output and their impact
1777 on future projections.” *Journal of Geophysical Research*, 123(16), 8728–8734.
1778 <https://doi.org/10.1029/2018jd028680>

1779 Schupfner, M., Wieners, K.-H., Wachsmann, F., Steger, C., Bittner, M., Jungclaus, J., Früh, B., Pankatz, K.,
1780 Giorgetta, M., Reick, C., Legutke, S., Esch, M., Gayler, V., Haak, H., de Vrese, P., Raddatz, T.,
1781 Mauritsen, T., von Storch, J.-S., Behrens, J., ... Roeckner, E. (2019). DKRZ MPI-ESM1.2-HR model
1782 output prepared for CMIP6 ScenarioMIP [Dataset]. Earth System Grid Federation.
1783 <https://doi.org/10.22033/ESGF/CMIP6.2450>

1784 Sférian, R., Berthet, S., Yool, A., Palmiéri, J., Bopp, L., Tagliabue, A., Kwiatkowski, L., Aumont, O.,
1785 Christian, J., Dunne, J., Gehlen, M., Ilyina, T., John, J. G., Li, H., Long, M. C., Luo, J. Y., Nakano, H.,
1786 Romanou, A., Schwinger, J., ... Yamamoto, A. (2020). Tracking Improvement in Simulated Marine
1787 Biogeochemistry Between CMIP5 and CMIP6. *Current Climate Change Reports*, 6(3), 95–119.
1788 <https://doi.org/10.1007/s40641-020-00160-0>

1789 Sellar, A. A., Jones, C. G., Mulcahy, J. P., Tang, Y., Yool, A., Wiltshire, A., O’Connor, F. M., Stringer, M.,
1790 Hill, R., Palmieri, J., Woodward, S., Mora, L., Kuhlbrodt, T., Rumbold, S. T., Kelley, D. I., Ellis, R.,
1791 Johnson, C. E., Walton, J., Abraham, N. L., ... Zerroukat, M. (2019). UKESM1: Description and
1792 evaluation of the U.k. earth system model. *Journal of Advances in Modeling Earth Systems*, 11(12),
1793 4513–4558. <https://doi.org/10.1029/2019ms001739>

1794 Shiogama, H., Fujimori, S., Hasegawa, T., Hayashi, M., Hirabayashi, Y., Ogura, T., Iizumi, T., Takahashi, K.,
1795 & Takemura, T. (2023). Important distinctiveness of SSP3–7.0 for use in impact assessments. *Nature*
1796 *Climate Change*, 13(12), 1276–1278. <https://doi.org/10.1038/s41558-023-01883-2>

1797 Sobel, A. H., Lee, C.-Y., Bowen, S. G., Camargo, S. J., Cane, M. A., Clement, A., Fosu, B., Hart, M., Reed, K.
1798 A., Seager, R., & Tippett, M. K. (2021). Near-term tropical cyclone risk and coupled Earth system
1799 model biases. *Proceedings of the National Academy of Sciences of the United States of America*,

1800 120(33), e2209631120. <https://doi.org/10.1073/pnas.2209631120>

1801 Sobel, A. H., Lee, C.-Y., Camargo, S. J., Mandli, K. T., Emanuel, K. A., Mukhopadhyay, P., & Mahakur, M.
1802 (2019). Tropical Cyclone Hazard to Mumbai in the Recent Historical Climate. *Monthly Weather*
1803 *Review*, 147(7), 2355–2366. <https://doi.org/10.1175/MWR-D-18-0419.1>

1804 Stewart, K. D., Kim, W. M., Urakawa, S., Hogg, A. M., Yeager, S., Tsujino, H., Nakano, H., Kiss, A. E., &
1805 Danabasoglu, G. (2020). JRA55-do-based repeat year forcing datasets for driving ocean–sea-ice
1806 models. *Ocean Modelling*, 147, 101557. <https://doi.org/10.1016/j.ocemod.2019.101557>

1807 Switanek, M. B., Troch, P. A., Castro, C. L., Leuprecht, A., Chang, H.-I., Mukherjee, R., & Demaria, E. M. C.
1808 (2017). Scaled distribution mapping: a bias correction method that preserves raw climate model
1809 projected changes. *Hydrology and Earth System Sciences*, 21(6), 2649–2666.
1810 <https://doi.org/10.5194/hess-21-2649-2017>

1811 Tagliabue, A., Kwiatkowski, L., Bopp, L., Butenschön, M., Cheung, W., Lengaigne, M., & Vialard, J. (2021).
1812 Persistent Uncertainties in Ocean Net Primary Production Climate Change Projections at Regional
1813 Scales Raise Challenges for Assessing Impacts on Ecosystem Services. *Frontiers in Climate*, 3.
1814 <https://doi.org/10.3389/fclim.2021.738224>

1815 Tang, Y., Rumbold, S., Ellis, R., Kelley, D., Mulcahy, J., Sellar, A., Walton, J., & Jones, C. (2019). MOHC
1816 UKESM1.0-LL model output prepared for CMIP6 CMIP [Dataset]. Earth System Grid Federation.
1817 <https://doi.org/10.22033/ESGF/CMIP6.1569>

1818 Themeßl, M. J., Gobiet, A., & Heinrich, G. (2012). Empirical-statistical downscaling and error correction
1819 of regional climate models and its impact on the climate change signal. *Climatic Change*, 112(2),
1820 449–468. <https://doi.org/10.1007/s10584-011-0224-4>

1821 Thrasher, B., Maurer, E. P., McKellar, C., & Duffy, P. B. (2012). Technical Note: Bias correcting climate
1822 model simulated daily temperature extremes with quantile mapping. *Hydrology and Earth System*
1823 *Sciences*, 16(9), 3309–3314. <https://doi.org/10.5194/hess-16-3309-2012>

1824 Tippett, M. K., Camargo, S. J., & Sobel, A. H. (2011). A Poisson Regression Index for Tropical Cyclone
1825 Genesis and the Role of Large-Scale Vorticity in Genesis. *Journal of Climate*, 24(9), 2335–2357.
1826 <https://doi.org/10.1175/2010JCLI3811.1>

1827 Treu, S., Muis, S., Dangendorf, S., Wahl, T., Oelsmann, J., Heinicke, S., Frieler, K., & Mengel, M. (2023).
1828 Reconstruction of hourly coastal water levels and counterfactuals without sea level rise for impact
1829 attribution. In *Earth System Science Data Discussions*. <https://doi.org/10.5194/essd-2023-112>

1830 Tsujino, H., Urakawa, L. S., Griffies, S. M., Danabasoglu, G., Adcroft, A. J., Amaral, A. E., Arsouze, T.,
1831 Bentsen, M., Bernardello, R., Böning, C. W., Bozec, A., Chassignet, E. P., Danilov, S., Dussin, R.,
1832 Exarchou, E., Fogli, P. G., Fox-Kemper, B., Guo, C., Ilicak, M., ... Yu, Z. (2020). Evaluation of global
1833 ocean–sea-ice model simulations based on the experimental protocols of the Ocean Model
1834 Intercomparison Project phase 2 (OMIP-2). *Geoscientific Model Development*, 13(8), 3643–3708.
1835 <https://doi.org/10.5194/gmd-13-3643-2020>

1836 Weedon, G. P., Gomes, S., Viterbo, P., Österle, H., Adam, J. C., Bellouin, N., Boucher, O., & Best, M.
1837 (2010). The watch forcing data 1958-2001: a meteorological forcing data set for land surface- and
1838 hydrological-models. 41. https://publications.pik-potsdam.de/pubman/item/item_16400

1839 Woodworth-Jefcoats, P. (2022). therMizer-FishMIP-2022-HI: Code and data for FishMIP 2022 ISIMIP 3a -
1840 Hawaii longline fishing ground regional model. Github. [https://github.com/pwoodworth-](https://github.com/pwoodworth-jefcoats/therMizer-FishMIP-2022-HI)
1841 [jefcoats/therMizer-FishMIP-2022-HI](https://github.com/pwoodworth-jefcoats/therMizer-FishMIP-2022-HI)

1842 Yukimoto, S., Kawai, H., Koshiro, T., Oshima, N., Yoshida, K., Urakawa, S., Tsujino, H., Deushi, M., Tanaka,
1843 T., Hosaka, M., Yabu, S., Yoshimura, H., Shindo, E., Mizuta, R., Obata, A., Adachi, Y., & Ishii, M.
1844 (2019). The Meteorological Research Institute Earth System Model Version 2.0, MRI-ESM2.0:
1845 Description and Basic Evaluation of the Physical Component. *Journal of the Meteorological Society*
1846 of Japan. Ser. II, 97(5), 931–965. <https://doi.org/10.2151/jmsj.2019-051>

1847 Yukimoto, S., Koshiro, T., Kawai, H., Oshima, N., Yoshida, K., Urakawa, S., Tsujino, H., Deushi, M., Tanaka,

1848 T., Hosaka, M., Yoshimura, H., Shindo, E., Mizuta, R., Ishii, M., Obata, A., & Adachi, Y. (2019a). MRI
1849 MRI-ESM2.0 model output prepared for CMIP6 CMIP [Dataset]. Earth System Grid Federation.
1850 <https://doi.org/10.22033/ESGF/CMIP6.621>

1851 Yukimoto, S., Koshiro, T., Kawai, H., Oshima, N., Yoshida, K., Urakawa, S., Tsujino, H., Deushi, M., Tanaka,
1852 T., Hosaka, M., Yoshimura, H., Shindo, E., Mizuta, R., Ishii, M., Obata, A., & Adachi, Y. (2019b). MRI
1853 MRI-ESM2.0 model output prepared for CMIP6 ScenarioMIP [Dataset]. Earth System Grid
1854 Federation. <https://doi.org/10.22033/ESGF/CMIP6.638>

1855 Zhu, L., Quiring, S. M., & Emanuel, K. A. (2013). Estimating tropical cyclone precipitation risk in Texas.
1856 *Geophysical Research Letters*, 40(23), 6225–6230. <https://doi.org/10.1002/2013gl058284>

1857 ISIMIP data repository: ISIMIP [data set], <https://data.isimip.org/>, last access: 28 April 2025.
1858 ISIMIP Input data table: ISIMIP [data set], [https://www.isimip.org/gettingstarted/input-data-bias-
1859 adjustment/](https://www.isimip.org/gettingstarted/input-data-bias-adjustment/), last access: 28 April 2025.

1860 ISIMIP terms of use: <https://www.isimip.org/gettingstarted/terms-of-use/>, last access: 28 April
1861 2025.

1862